

ADVANCEMENT OF ROTORDYNAMIC TOPICS

A Thesis

presented to

the Faculty of California Polytechnic State University,

San Luis Obispo

In Partial Fulfillment

of the Requirements for the Degree

Master of Science in Mechanical Engineering

by

Cameron Naugle

April 2018

© 2018

Cameron Naugle

ALL RIGHTS RESERVED

## COMMITTEE MEMBERSHIP

TITLE: Advancement of Rotordynamic topics

AUTHOR: Cameron Naugle

DATE SUBMITTED: April 2018

COMMITTEE CHAIR: Xi (Julia) Wu, Ph.D.

Professor of Mechanical Engineering

COMMITTEE MEMBER: Mohammad Noori

Professor of Mechanical Engineering

COMMITTEE MEMBER: Hemanth Porumamilla

Professor of Mechanical Engineering

COMMITTEE MEMBER: Peter Schuster

Professor of Mechanical Engineering

## ABSTRACT

Advancement of Rotordynamic topics

Cameron Naugle

In this thesis a basis for creating valuable rotordynamic models is formed. Theoretical models are formulated from the kinematic constraints to form a robust finite element model suited well for expansion. Analysis techniques for multiple degrees of freedom models with arbitrary damping are derived and demonstrated. These techniques include eigenvector and eigenvalue analysis of the complex state space equations. Furthermore, analysis techniques are developed for analyzing experimental data and comparing to theoretical models. All of the material is here to create a finite element model, compare its results to experimental results, and fine tune the design using stability analysis.

## ACKNOWLEDGMENTS

Thanks to:

•

## TABLE OF CONTENTS

	Page
LIST OF TABLES . . . . .	viii
LIST OF FIGURES . . . . .	ix
<b>CHAPTER</b>	
1 Finite Element Method For Rotordynamic systems . . . . .	1
1.1 Beam Element FE Equation . . . . .	1
1.1.1 Timoshenko Beam Finite Element . . . . .	1
1.1.1.1 Kinematic Relationships . . . . .	2
1.1.1.2 Internal Constitutive Relationship . . . . .	4
1.1.1.3 Differential Equations of Motion . . . . .	7
1.1.1.4 Shape Functions . . . . .	11
1.1.1.5 Finite Equations of Motion . . . . .	16
1.1.1.6 Rotating Internal Damping . . . . .	16
1.1.1.7 Beam Element in Complex Coordinates . . . . .	19
1.2 Disk Nodal Equations . . . . .	20
1.2.1 Disk in complex coordinates . . . . .	22
1.3 Bearing Nodal Equations . . . . .	22
1.3.1 Bearing in Complex Coordinates . . . . .	23
1.4 Assembly of the Global Systems of Equations . . . . .	23
1.4.1 In the Real Coordinate System . . . . .	24
1.4.2 In the Complex Coordinate System . . . . .	24
1.5 Model Analysis . . . . .	24
1.5.1 State Space Representation and the Eigenvalue Problem . . . . .	26
1.5.2 Unbalance Response . . . . .	27
1.5.3 Roots Locus and Stability Analysis . . . . .	29
1.5.4 Shapes . . . . .	32
1.5.5 Campbell . . . . .	33
2 Experimental Analysis . . . . .	36
2.1 Data Collection and Analysis . . . . .	36

2.1.1	Amplitude . . . . .	39
2.1.2	Frequency Spectrum . . . . .	39
2.1.3	Phase Angle . . . . .	40
2.1.3.1	Time Domain Approach . . . . .	40
2.1.3.2	Frequency Domain Approach . . . . .	41
2.2	Experimental Plots . . . . .	41
2.2.1	Bode . . . . .	42
2.2.2	Cascade . . . . .	42
2.2.3	Orbit . . . . .	43
2.2.4	Filtering . . . . .	45
3	Synthesis in Example of a Magnetic Bearing on an Overhung Rotor . . . . .	48
3.1	Physical System . . . . .	48
3.2	Experimental Results . . . . .	49
3.3	Theoretical Model . . . . .	50
3.3.1	Active Magnetic Bearing . . . . .	53
3.3.1.1	Proportional Derivative Control . . . . .	56
3.4	Addition of Magnetic Bearing to the Rotor Model . . . . .	57
	BIBLIOGRAPHY . . . . .	62
	APPENDICES	
.1	Bernoulli-Euler Beam equation . . . . .	65

## LIST OF TABLES

Table	Page
1.1 Properties of disks, shaft elements, and bearings of the example problem. . . . .	26
3.1 Geometric parameters of the overhung rotor system. . . . .	49
3.2 Properties of disks, shaft elements, and bearings of the theoretical model. . . . .	51
3.3 Active Magnetic Bearing Parameters. . . . .	59

## LIST OF FIGURES

Figure	Page
1.1 Beam Element with nodal displacements. . . . .	2
1.2 Timoshenko beam section with degrees of freedom at some point $x$ along beam axis. . . . .	3
1.3 Beam differential element with generalized forces. . . . .	8
1.4 Beam Element with nodal displacements. . . . .	12
1.5 Shape Functions as they vary with $\zeta$ using two different ratios of length to radius of beam element. . . . .	15
1.6 Depiction of skew angle $\chi$ . . . . .	21
1.7 Diagram of Two disk model example problem. . . . .	25
1.8 Frequency response of the second disk subject to an unbalance at the second disk. . . . .	28
1.9 Bode diagram of the second disk subject to an unbalance at the second disk. . . . .	28
1.10 Roots Locus of the example problem with an internal damping coefficient of 0.0002. Red circles represent positive frequencies, while blue dots represent negative ones. . . . .	30
1.11 Roots Locus of the example problem in 3-D with an internal damping coefficient of 0.0002. Red circles represent positive frequencies, while blue dots represent negative ones. . . . .	31
1.12 length to radius ratio of 1. . . . .	32
1.13 Damping ratio vs. spin speed with indication of threshold of stability. . . . .	32
1.14 Modal shapes of the example problem. . . . .	34
1.15 Campbell Diagram of the example problem. . . . .	35
2.1 Position of the rotor shaft over a certain timespan. . . . .	37
2.3 A window in time of the transient vibration signal in orthogonal directions. . . . .	38
2.4 Bode diagram of the experimental system described in §2.2. Red is horizontal plane, and blue is vertical. . . . .	43
2.5 Cascade of the experimental system described in §2.2. . . . .	44
2.6 3DOrbit of the experimental system described in §2.2. . . . .	45

2.7	Orbits of the experimental example. Spin speed is counterclockwise.	46
2.8	Cascade of the experimental system with a synchronous filter applied.	47
3.1	Overhung rotor system diagram.	48
3.2	3D Orbit of the experimental overhung rotor system.	49
3.3	Cascade of the experimental overhung rotor system.	50
3.4	Bode diagram of the experimental overhung rotor filtered to 1X.	50
3.6	Damping ratio vs. spin speed with indication of threshold of stability.	52
3.7	Damping ratio vs. spin speed with indication of threshold of stability.	53
3.8	Damping ratio vs. spin speed with indication of threshold of stability.	54
3.11	Roots locus of Overhung rotor system with varying $k_v$ .	60
3.12	Bode diagram at node 6 comparing the rotor without AMB(solid) and with AMB(dashed).	61
3.13	Bode diagram at node 6 comparing the rotor without AMB(solid) and with AMB(dashed) for complete levitation at node 4.	61
.14	Free body diagram of a beam section in planar bending.	66

# Chapter 1

## FINITE ELEMENT METHOD FOR ROTORDYNAMIC SYSTEMS

In this chapter the Finite Element Method(FEM) will be employed in the simulation of rotordynamic systems. There are many advantages to using this discretizing method to solve problems of rotating machines. One of which is the generic form that the equation, and its parts take. The method lends itself to being able to easily create new matrices that can insert right into your equations of motion. Another, is the ability to move components around in space without the need to reevaluate the physics. Finally, the analysis techniques for Multiple Degree Of Freedom (MDOF) systems is wide reaching, and will serve to richly enhance our understanding of a complex system made of simple parts.

First, the beam element commonly referred to as the Timoshenko Beam Element will be derived from the kinematic and constitutive constraints. Then the solution to the resulting equation of motion will be discretized and variables separated in position and time to give the finite element equations of motion. Further, an extension to the beam element model is presented that will consider the viscous damping effects in the beam element. Equations for disks, bearings, and complex versions of all equations will be presented. Finally, the assembly and analysis of the model will result in intuitive figures that will be shown to compare well to experimental data.

### 1.1 Beam Element FE Equation

#### 1.1.1 Timoshenko Beam Finite Element

The Timoshenko beam element allows for the beam cross section plane at any axis location to differ from normal with the axis of the beam. In other words, the element

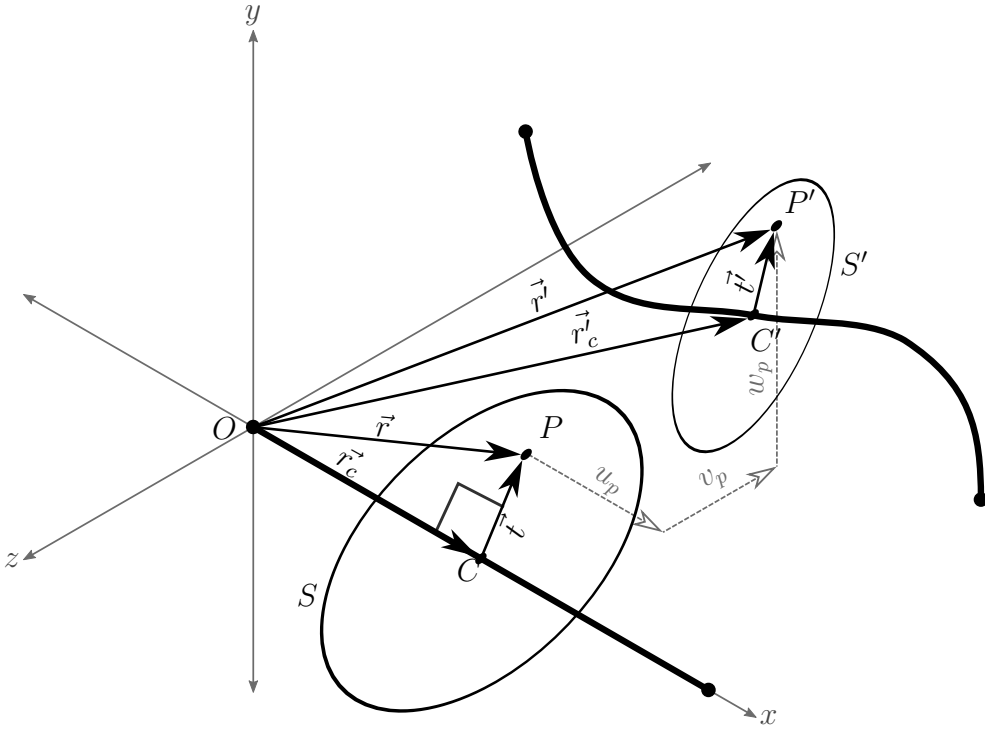


**Figure 1.1: Beam Element with nodal displacements.**

allows for shear stresses. This element often also includes the effects of rotary inertia and gyroscopic moments, as it will in this derivation. Generalized displacements used are assumed to be variable in both time and space. The element has six degrees of freedom. Three translation and three rotations all defined on the beam axis. So then all displacements are functions of time,  $t$ , and the axial spacial coordinate,  $x$ .

#### 1.1.1.1 Kinematic Relationships

In order to develop the stresses and strains internal to the beam, and subsequently the equations of motion, the motion of some arbitrary point on the beam must be defined in terms of the generalized coordinates. Motion of two points is taken into consideration to assist in dividing the motion into a translation and a rotation. These points are shown in Figure 1.1. The first point,  $C$ , falls on the beam axis at location

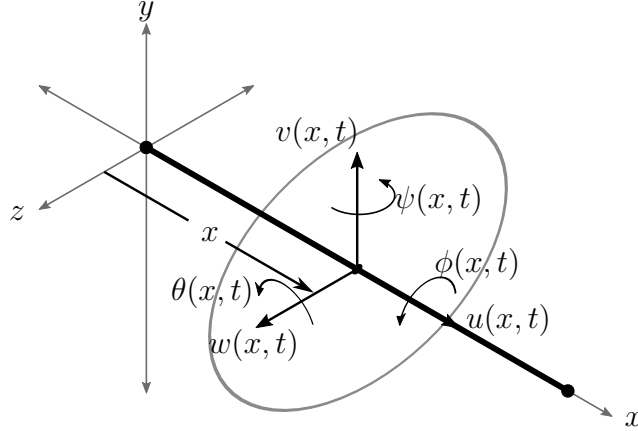


**Figure 1.2:** Timoshenko beam section with degrees of freedom at some point  $x$  along beam axis.

$x$ , and in the undeformed configuration, the vector  $\vec{r}_c = \overrightarrow{OC}$  forms a right angle with the surface of the cross section. The second point,  $P$  is at some arbitrary  $(y, z)$  location on the cross section. The vector  $\vec{t} = \overrightarrow{CP}$  points from the beam axis to the point along the cross section. If we follow this point  $P$  we will be able to define the motion of the cross section as a whole, or more succinctly, to define the displacements  $u_p, v_p, w_p$  in terms of the coordinates  $u, v, w, \psi, \theta$ , &  $\phi$ . The motion of point  $P$  is split into translation and rotation, where  $\vec{t}$  is rotated and  $\vec{r}_c$  is translated to point to the deformed location  $P'$ . The vector pointing to  $P$  in the undeformed state is defined as

$$\vec{r} = \vec{r}_c + \vec{t} \quad (1.1)$$

Rotations are represented with a rotation transformation matrix,

$$\vec{t}' = \underline{R}\vec{t} \quad (1.2)$$

The linearized first order rotational matrix for small angles is represented by

$$\underline{R} = \begin{bmatrix} 1 & -\theta & \psi \\ \theta & 1 & -\phi \\ -\psi & \phi & 1 \end{bmatrix} \quad (1.3)$$

and the translation with a displacement vector

$$\vec{r}'_c = \vec{r}_c + \vec{u} \quad (1.4)$$

Combined motion from  $P$  to  $P'$  can be defined by

$$\vec{u}_p = \vec{r}' - \vec{r} \quad (1.5)$$

where  $\vec{u}_p$  is the vector containing  $u_p$ ,  $v_p$ , &  $w_p$ . The vector definitions for  $\vec{r}'$  and  $\vec{r}$  are substituted to the above equation to obtain

$$\vec{u}_p = \vec{r}'_c + \vec{t}' - \vec{r}_c + \vec{t} \quad (1.6)$$

and now using the definition for  $\vec{u}$  and  $\vec{t}'$  leads to the simplified expression for the motion of  $P$

$$\vec{u}_p = \vec{u} + (\underline{R} - \underline{I})\vec{t} \quad (1.7)$$

expanding matrices reveals the equation

$$\vec{u}_p = \begin{Bmatrix} u_p \\ v_p \\ w_p \end{Bmatrix} = \begin{Bmatrix} u \\ v \\ w \end{Bmatrix} + \begin{bmatrix} 0 & -\theta & \psi \\ \theta & 0 & -\phi \\ -\psi & \phi & 0 \end{bmatrix} \begin{Bmatrix} 0 \\ y \\ z \end{Bmatrix} \quad (1.8)$$

Therefore, the motion of any point on the beam may be approximated with

$$\vec{u}_p = \begin{Bmatrix} u - \theta y + \psi z \\ v - \phi z \\ w + \phi y \end{Bmatrix} \quad (1.9)$$

### 1.1.1.2 Internal Constitutive Relationship

Stresses are assumed to exist in the beam in the axial direction, and in shear on the face of the beam section. Stresses in the transverse, or the  $y$  and  $z$ , directions are assumed negligible. Shear stresses out of the plane section are assumed to be vanishing as the differential element shrinks. Internal damping is to be considered independently from this material constitutive relationship. Written out, these stresses

are represented by the matrix

$$\sigma_{ij} = \begin{bmatrix} \sigma_{xx} & \sigma_{xy} & \sigma_{xz} \\ \sigma_{xy} & 0 & 0 \\ \sigma_{xz} & 0 & 0 \end{bmatrix} \quad (1.10)$$

using the Hooke's Law for a linear elastic isotropic material, expressed as

$$\epsilon_{ij} = \frac{1}{E}[(1 + \nu)\sigma_{ij} - \nu\delta_{ij}\sigma_{kk}] \quad (1.11)$$

allows the determination of the stress strain relationship in engineering notation as

$$\begin{Bmatrix} \sigma_{xx} \\ \sigma_{xy} \\ \sigma_{xz} \end{Bmatrix} = \begin{bmatrix} E & 0 & 0 \\ 0 & 2G & 0 \\ 0 & 0 & 2G \end{bmatrix} \begin{Bmatrix} \epsilon_{xx} \\ \epsilon_{xy} \\ \epsilon_{xz} \end{Bmatrix} \quad (1.12)$$

where,  $G = \frac{E}{2(1+\nu)}$ . Strains are derived from displacements of equation (1.9) using a linear strain-displacement relationship for infinitesimal strains:  $2\epsilon_{ij} = u_{i,j} + u_{j,i}$ .

$$\begin{cases} \epsilon_{xx} = u' - \theta'y + \psi'z \\ \epsilon_{xy} = \frac{1}{2}(v' - \phi'z - \theta) \\ \epsilon_{xz} = \frac{1}{2}(w' + \phi'y + \psi) \end{cases} \quad (1.13)$$

Note that in the case of the Euler-Bernoulli beam derivation the slope in a transverse direction displacement is equal to the rotation angle about the orthogonal transverse axis, i.e.,  $v' = \theta$  and  $w' = \psi$ . Application of those would reduce the system to the Euler-Bernoulli beam.

It will be proven useful to introduce generalized strains that group strain contributions above as axial, bending, torsion, and shear, represented by the symbols  $\varepsilon$ ,  $\rho$ ,

$\varphi, \gamma$ , respectively.

$$\begin{cases} \varepsilon = u' \\ \rho_y = -\theta' \\ \rho_z = \psi' \\ \varphi = \phi' \\ \gamma_y = v' - \theta \\ \gamma_z = w' + \psi \end{cases} \quad (1.14)$$

allowing the representation of the strains from eq (1.13) using the generalized strains as:

$$\begin{cases} \epsilon_{xx} = \varepsilon + \rho_y y + \rho_z z \\ \epsilon_{xy} = \frac{1}{2}(\gamma_y - \varphi z) \\ \epsilon_{xz} = \frac{1}{2}(\gamma_z + \varphi y) \end{cases} \quad (1.15)$$

Now the stresses in equation (1.12) can be represented with the displacements as

$$\begin{Bmatrix} \sigma_{xx} \\ \sigma_{xy} \\ \sigma_{xz} \end{Bmatrix} = \begin{Bmatrix} E(u' - \theta' y + \psi' z) \\ G(v' - \phi' z - \theta) \\ G(w' + \phi' y + \psi) \end{Bmatrix} = \begin{Bmatrix} E(\varepsilon + \rho_y y + \rho_z z) \\ G(\gamma_y - \varphi z) \\ G(\gamma_z + \varphi y) \end{Bmatrix} \quad (1.16)$$

$$U = \int_V \sigma_{ij} \epsilon_{ij} dV \quad (1.17)$$

Now the inner product of the total virtual strain energy can be expanded

$$U = \int_V [\sigma_{xx} \epsilon_{xx} + 2\sigma_{xy} \epsilon_{xy} + 2\sigma_{xz} \epsilon_{xz}] dV \quad (1.18)$$

Then expand virtual strains into the generalized strains corresponding to the degrees of freedom of the beam element and collect terms on generalized strains

$$U = \int_V [\sigma_{xx} \varepsilon + \sigma_{xx} y \rho_y + \sigma_{xx} z \rho_z + \sigma_{xy} \gamma_y + \sigma_{xz} \gamma_z + (\sigma_{xz} y - \sigma_{xy} z) \varphi] dV \quad (1.19)$$

this internal mechanical energy expression allows us to recognize stresses conjugate with each generalized strain as the corresponding stress for that phenomena. Integration allows the determination of the forces and moments related to each generalized

strain as

$$\left\{ \begin{array}{lll} N = \int_A \sigma_{xx} dA & = E(A\varepsilon + S_y \rho_y + S_z \rho_z) \\ M_y = \int_A \sigma_{xx} z dA & = E(S_z \varepsilon + I_{xy} \rho_y + I_y \rho_z) \\ M_z = \int_A \sigma_{xx} y dA & = E(S_y \varepsilon + I_z \rho_y + I_{xy} \rho_z) \\ Q_y = \int_A \sigma_{xy} dA & = \kappa G(A\gamma_y - S_z \varphi) \\ Q_z = \int_A \sigma_{xz} dA & = \kappa G(A\gamma_z + S_y \varphi) \\ M_x = \int_A (\sigma_{xz} y - \sigma_{xy} z) dA & = \kappa G(A_y \gamma_z - A_z \gamma_y + J_x \varphi) \end{array} \right. \quad (1.20)$$

where,  $\left\{ \begin{array}{ll} \kappa = \frac{6(1+\nu)}{7+6\nu}, \text{for circular cross sections.} \\ A = \int_A dA \quad S_y = \int_A y dA \\ S_z = \int_A z dA \quad I_y = \int_A z^2 dA \\ I_z = \int_A y^2 dA \quad J_x = I_y + I_z \end{array} \right.$

$\kappa$  is the shear coefficient which attempts to correct for the fact that the shear strain is not constant over the beam cross section. Assuming the central axis of the beam is coincident with the shear center, then  $A_y = A_z = I_{xy} = 0$ . Which simplifies the conjugate forces to

$$\left\{ \begin{array}{ll} N = EA\varepsilon & = EAu' \\ M_y = EI_y \rho_z & = EI_y \psi' \\ M_z = EI_z \rho_y & = -EI_z \theta' \\ Q_y = \kappa G A \gamma_y & = \kappa G A (v' - \theta) \\ Q_z = \kappa G A \gamma_z & = \kappa G A (w' + \psi) \\ M_x = \kappa G J_x \varphi & = \kappa G J_x \phi' \end{array} \right. \quad (1.21)$$

### 1.1.1.3 Differential Equations of Motion

Now the equations of motion are derived for the Timoshenko beam element. External forces are not included in this derivation. Though they may easily be added to the

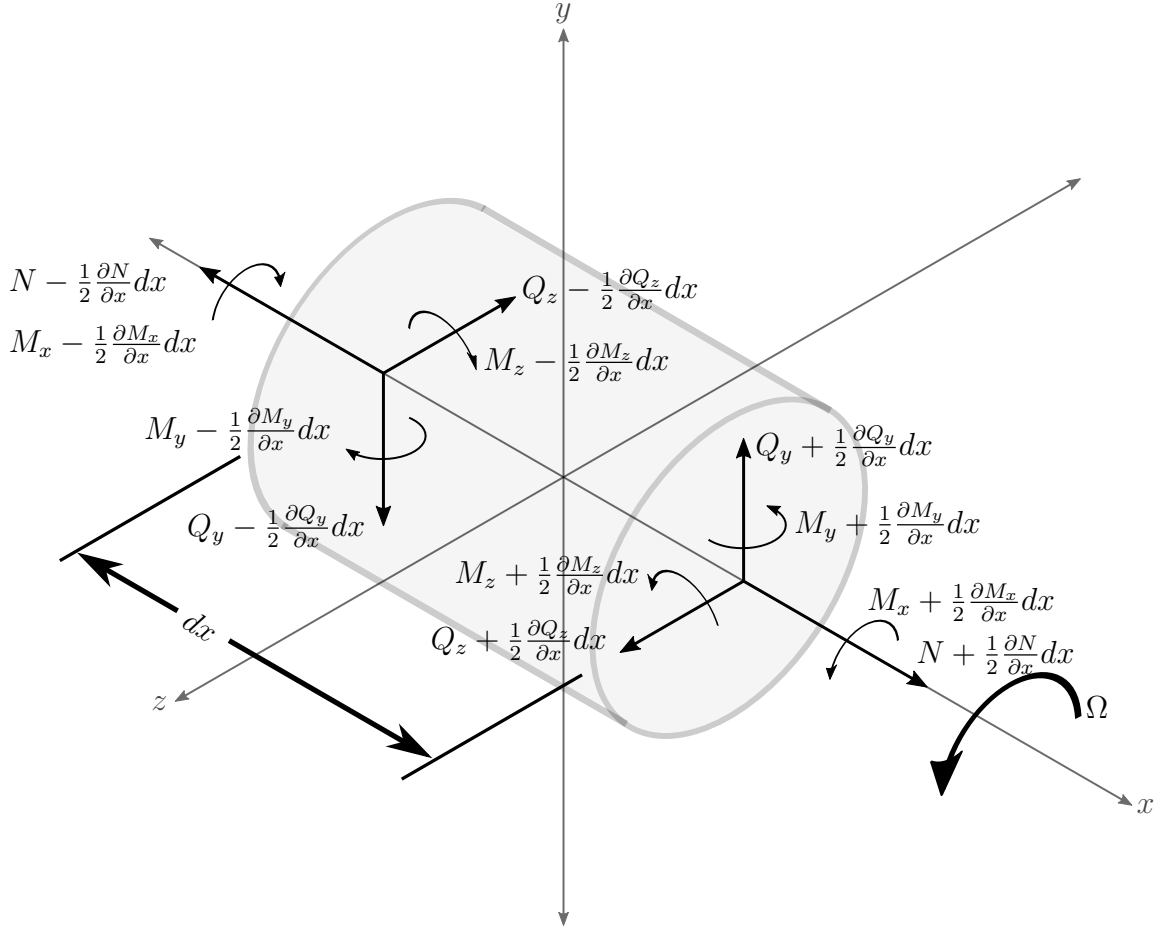


**Figure 1.3: Beam differential element with generalized forces.**

diagram of figure 1.3 and included in the analysis. It is also assumed that the cross section remains planar during deformation and the material properties are homogeneous through time and space. The derivation is the same as for a Euler-Bernoulli beam with the exception of the constitutive relations used at the end and the inclusion of torsion and axial degrees of freedom. Using conservation of momentum and conservation of the moment of momentum a relationship between inertia and internal forces is developed. Applying summation of forces in the  $x$ -direction

$$(N + \frac{1}{2} \frac{\partial N}{\partial x} dx) - (N - \frac{1}{2} \frac{\partial N}{\partial x} dx) = \rho Adx \frac{\partial^2 u}{\partial x^2} \quad (1.22)$$

by Simplifying the above equation, and performing the same steps for the other directions and moments we get

$$\left\{ \begin{array}{l} \frac{\partial N}{\partial x} = \rho A \frac{\partial^2 u}{\partial x^2} \\ \frac{\partial Q_y}{\partial x} = \rho A \frac{\partial^2 v}{\partial x^2} \\ \frac{\partial Q_z}{\partial x} = \rho A \frac{\partial^2 w}{\partial x^2} \\ \frac{\partial M_y}{\partial x} - Q_z = \rho I_y \frac{\partial^2 \psi}{\partial x^2} + \rho J_x \Omega \frac{\partial \theta}{\partial x} \\ \frac{\partial M_z}{\partial x} + Q_y = \rho I_z \frac{\partial^2 \theta}{\partial x^2} - \rho J_x \Omega \frac{\partial \psi}{\partial x} \\ \frac{\partial M_x}{\partial x} = \rho J_x \frac{\partial^2 \phi}{\partial x^2} \end{array} \right. \quad (1.23)$$

Gyroscopic moments have been explicitly added to the summations in the appropriate equations. The generalized forces of equation (1.21) are substituted in the equilibrium equations (1.23)

$$\left\{ \begin{array}{l} EAu'' = \rho A \ddot{u} \\ \kappa GA(v'' - \theta') = \rho A \ddot{v} \\ \kappa GA(w'' + \psi') = \rho A \ddot{w} \\ EI_y \psi'' - \kappa GA(w' + \psi) = \rho I_y \ddot{\psi} + \rho J_x \Omega \dot{\theta} \\ EI_z \theta'' + \kappa GA(v' - \theta) = \rho I_z \ddot{\theta} - \rho J_x \Omega \dot{\psi} \\ \kappa G J_x \phi'' = \rho J_x \ddot{\phi} \end{array} \right. \quad \begin{array}{l} (1.24a) \\ (1.24b) \\ (1.24c) \\ (1.24d) \\ (1.24e) \\ (1.24f) \end{array}$$

In matrix form, this system of equations can be represented by this equation

$$\underline{\mathcal{M}}^e \ddot{\vec{\mathbf{u}}} + \Omega \underline{\mathcal{G}}^e \dot{\vec{\mathbf{u}}} - \left( \frac{\partial(\cdot)}{\partial x} \underline{\mathcal{S}}^e - \underline{\mathcal{P}}^e \underline{\mathcal{S}}^e \right) \vec{\mathbf{u}} = 0 \quad (1.25)$$

where,

$$\left\{ \begin{array}{l} \underline{\mathcal{M}}^e = \begin{bmatrix} \rho A & 0 & 0 & 0 & 0 & 0 \\ 0 & \rho A & 0 & 0 & 0 & 0 \\ 0 & 0 & \rho I_y & 0 & 0 & 0 \\ 0 & 0 & 0 & \rho I_z & 0 & 0 \\ 0 & 0 & 0 & 0 & \rho A & 0 \\ 0 & 0 & 0 & 0 & 0 & \rho J_x \end{bmatrix} \quad \underline{\mathcal{G}}^e = \begin{bmatrix} 0 & 0 & 0 & 0 & 0 & 0 \\ 0 & 0 & 0 & 0 & 0 & 0 \\ 0 & 0 & 0 & \rho J_x & 0 & 0 \\ 0 & 0 & -\rho J_x & 0 & 0 & 0 \\ 0 & 0 & 0 & 0 & 0 & 0 \\ 0 & 0 & 0 & 0 & 0 & 0 \end{bmatrix} \\ \\ \underline{\mathcal{P}}^e = \begin{bmatrix} 0 & 0 & 0 & 0 & 0 & 0 \\ 0 & 0 & 0 & 0 & 0 & 0 \\ 0 & 1 & 0 & 0 & 0 & 0 \\ -1 & 0 & 0 & 0 & 0 & 0 \\ 0 & 0 & 0 & 0 & 0 & 0 \\ 0 & 0 & 0 & 0 & 0 & 0 \end{bmatrix} \quad \underline{\mathcal{S}}^e = \begin{bmatrix} \kappa G A \frac{\partial()}{\partial x} & 0 & 0 & -\kappa G A & 0 & 0 \\ 0 & \kappa G A \frac{\partial()}{\partial x} & \kappa G A & 0 & 0 & 0 \\ 0 & 0 & E I_y \frac{\partial()}{\partial x} & 0 & 0 & 0 \\ 0 & 0 & 0 & E I_z \frac{\partial()}{\partial x} & 0 & 0 \\ 0 & 0 & 0 & 0 & E A \frac{\partial()}{\partial x} & 0 \\ 0 & 0 & 0 & 0 & 0 & \kappa G J_x \frac{\partial()}{\partial x} \end{bmatrix} \end{array} \right. \quad (1.26)$$

and  $\vec{\mathbf{u}} = [v, w, \psi, \theta, u, \phi]^\top$ . The principle of virtual displacements is utilized on the equations of motion to obtain the weak form of the equations of motion and integrated over the length of the beam.

$$\int_0^l \delta \vec{\mathbf{u}}^\top \underline{\mathcal{M}}^e \ddot{\vec{\mathbf{u}}} dx + \int_0^l \delta \vec{\mathbf{u}}^\top \Omega \underline{\mathcal{G}}^e \dot{\vec{\mathbf{u}}} - \int_0^l \delta \vec{\mathbf{u}}^\top \frac{\partial()}{\partial x} \underline{\mathcal{S}}^e \vec{\mathbf{u}} dx + \int_0^l \delta \vec{\mathbf{u}}^\top \underline{\mathcal{P}} \underline{\mathcal{S}}^e \vec{\mathbf{u}} dx = 0 \quad (1.27)$$

integration by parts on the third term and replacing  $\underline{\mathcal{S}}$  with  $\underline{\mathcal{D}} \underline{\mathcal{B}}$ , and making use of the Identity matrix,  $\underline{\mathbf{I}}$  where  $\frac{\partial()}{\partial x} \underline{\mathbf{I}}$  is interpreted here as if the partial was a scalar

$$\int_0^l \delta \vec{\mathbf{u}}^\top \underline{\mathcal{M}}^e \ddot{\vec{\mathbf{u}}} dx + \Omega \int_0^l \delta \vec{\mathbf{u}}^\top \underline{\mathcal{G}}^e \dot{\vec{\mathbf{u}}} + \int_0^l \delta \vec{\mathbf{u}}^\top \left( \frac{\partial()}{\partial x} \underline{\mathbf{I}} + \underline{\mathcal{P}} \right) \underline{\mathcal{D}}^e \underline{\mathcal{B}} \vec{\mathbf{u}} dx = 0 \quad (1.28)$$

$$\underline{\mathcal{D}}^e = \begin{bmatrix} \kappa G A & 0 & 0 & 0 & 0 & 0 \\ 0 & \kappa G A & 0 & 0 & 0 & 0 \\ 0 & 0 & E I_y & 0 & 0 & 0 \\ 0 & 0 & 0 & E I_z & 0 & 0 \\ 0 & 0 & 0 & 0 & E A & 0 \\ 0 & 0 & 0 & 0 & 0 & \kappa G J_x \end{bmatrix} \quad \& \quad \underline{\mathcal{B}} = \begin{bmatrix} \frac{\partial()}{\partial x} & 0 & 0 & -1 & 0 & 0 \\ 0 & \frac{\partial()}{\partial x} & 1 & 0 & 0 & 0 \\ 0 & 0 & \frac{\partial()}{\partial x} & 0 & 0 & 0 \\ 0 & 0 & 0 & \frac{\partial()}{\partial x} & 0 & 0 \\ 0 & 0 & 0 & 0 & \frac{\partial()}{\partial x} & 0 \\ 0 & 0 & 0 & 0 & 0 & \frac{\partial()}{\partial x} \end{bmatrix} \quad (1.29)$$

Notice that  $\frac{\partial()}{\partial x} \underline{\mathbf{I}} + \underline{\mathcal{P}} = \underline{\mathcal{B}}^\top$  so the equation of motion becomes

$$\int_0^l \delta \vec{\mathbf{u}}^\top \underline{\mathcal{M}}^e \ddot{\vec{\mathbf{u}}} dx + \Omega \int_0^l \delta \vec{\mathbf{u}}^\top \underline{\mathcal{G}}^e \dot{\vec{\mathbf{u}}} + \int_0^l \delta \vec{\mathbf{u}}^\top \underline{\mathcal{B}}^\top \underline{\mathcal{D}}^e \underline{\mathcal{B}} \vec{\mathbf{u}} dx = 0 \quad (1.30)$$

$\underline{\mathcal{M}}^e$  is the inertia of the element,  $\underline{\mathcal{G}}^e$  is the rotating inertia,  $\underline{\mathcal{D}}^e$  is the material stress-strain relationship, and  $\underline{\mathcal{B}}^e$  is the strain-displacement operator. The solution of this differential system motivates a separation of variables that will be discussed in the next section.

#### 1.1.1.4 Shape Functions

The displacements thus far have been assumed to be functions of both position and time. Now the total displacement is separated into functions that depend on time and functions that depend on position. This is a fundamental part of the discretization of the beam element, and the use the finite element method.

$$\begin{cases} \vec{\mathbf{u}}(x, t) = \underline{\mathbf{N}}(x)\vec{\mathbf{q}}(t) \\ \dot{\vec{\mathbf{u}}}(x, t) = \underline{\mathbf{N}}(x)\dot{\vec{\mathbf{q}}}(t) \\ \ddot{\vec{\mathbf{u}}}(x, t) = \underline{\mathbf{N}}(x)\ddot{\vec{\mathbf{q}}}(t) \\ \delta\vec{\mathbf{u}}(x, t) = \underline{\mathbf{N}}(x)\delta\vec{\mathbf{q}}(t) \end{cases} \quad (1.31)$$

where,  $\vec{\mathbf{u}} = [v, w, -\psi, \theta, u, \phi]^\top$  &  $\vec{\mathbf{q}} = [v_1, w_1, -\psi_1, \theta_1, v_2, w_2, -\psi_2, \theta_2, u_1, \phi_1, u_2, \phi_2]^\top$ . This specific order of  $\vec{\mathbf{q}}$  is chosen with  $u$  and  $\phi$  at the end to ease the condensation of the axial and torsional degrees of freedom out of the system if their use is not necessary for the system of interest.  $\psi$  angles are defined as negative to allow for the same stiffness matrix to define the motion in both planes, and more importantly, to allow for the use of the complex plane to simplify the problem. The shape functions  $\underline{\mathbf{N}}(x)$  interpolate the displacements between the beam ends. These functions must solve the static portion of the differential equations (1.24). These shape functions are chosen as polynomials that satisfy the boundary nodal displacements and rotations at the ends of a beam element. These nodal degrees of freedom, depicted in Figure 1.4 are considered to be interpolated through the beam element by the shape functions. Interpolation functions chosen are listed in Equation (1.32). Axial displacement,  $u$ , and torsional rotation,  $\phi$  are independent, so their shape functions are

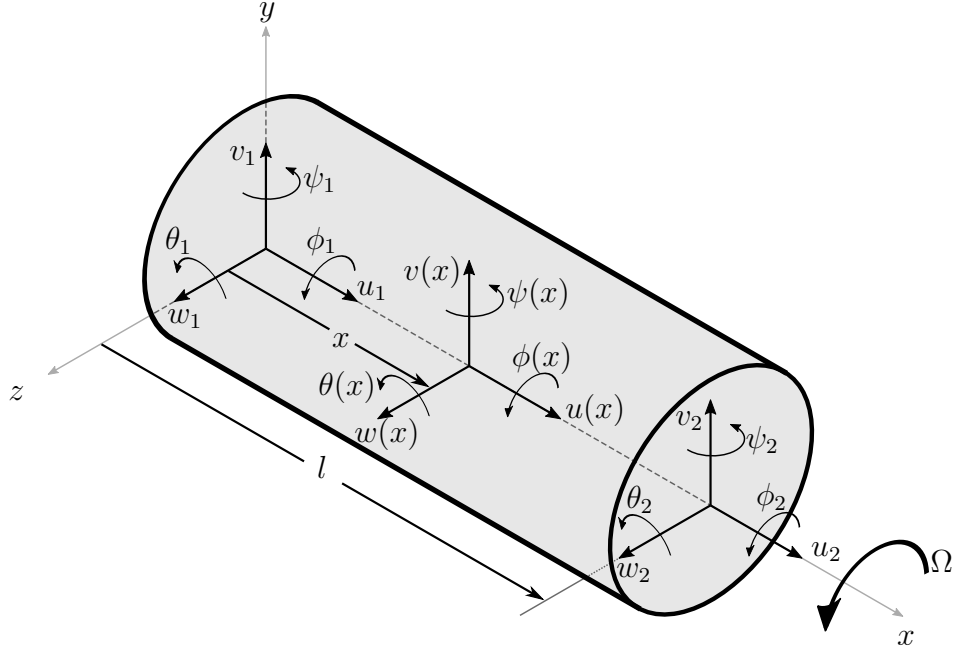


**Figure 1.4: Beam Element with nodal displacements.**

chosen as polynomials that satisfy the differential equation. Conversely, transverse displacements,  $v$  &  $w$ , and bending rotations,  $\psi$  &  $\theta$  are coupled. Coupling of the shape functions has been proven to reduce some negative effects of linearly interpolated elements [25]. Polynomial functions are chosen for  $v$  &  $w$  and their rotational counterparts are derived using the differential relations.

$$\left\{ \begin{array}{l} u = c_1 + c_2 x \\ v = c_3 + c_4 x + c_5 x^2 + c_6 x^3 \\ w = c_7 + c_8 x + c_9 x^2 + c_{10} x^3 \\ \phi = c_{11} + c_{12} x \end{array} \right. \quad (1.32a)$$

$$(1.32b)$$

$$(1.32c)$$

$$(1.32d)$$

$c_{1,2,\dots}$  are the unknown constants of the polynomial solutions. Using transverse displacement of equations (1.32b) & (1.32c) in the differential equations (1.24b), (1.24c),

(1.24d), (1.24e) the interpolation functions of bending rotations are derived as:

$$\left\{ \begin{array}{l} \psi = K_y c_{10} - c_8 - 2c_9 x - 3c_{10} x^2 \\ \theta = K_z c_6 + c_4 + 2c_5 x + 3c_6 x^2 \end{array} \right. \quad (1.33a)$$

$$\left\{ \begin{array}{l} \psi = K_y c_{10} - c_8 - 2c_9 x - 3c_{10} x^2 \\ \theta = K_z c_6 + c_4 + 2c_5 x + 3c_6 x^2 \end{array} \right. \quad (1.33b)$$

where,  $K_y = \frac{6EI_y}{\kappa GA}$  &  $K_z = \frac{6EI_z}{\kappa GA}$  Boundary Conditions Boundary conditions for the interpolation polynomials of equations (1.32) & (1.33) are defined as the components of the vector  $\vec{\mathbf{q}} u_j = u(x_j)$  and similarly for other degrees of freedom. Where,  $j = 1, 2$  and defines the two states. In this derivation,  $x_1 = 0$  and  $x_2 = l$ . Application of these boundary condition results in this relation between the polynomial constants and the boundary conditions.

$$\left\{ \begin{array}{l} u_1 \\ u_2 \\ v_1 \\ v_2 \\ w_1 \\ w_2 \\ \psi_1 \\ \psi_2 \\ \theta_1 \\ \theta_2 \\ \phi_1 \\ \phi_2 \end{array} \right\} = \left[ \begin{array}{cccccccccccc} 1 & 0 & 0 & 0 & 0 & 0 & 0 & 0 & 0 & 0 & 0 & 0 \\ 1 & l & 0 & 0 & 0 & 0 & 0 & 0 & 0 & 0 & 0 & 0 \\ 0 & 0 & 1 & 0 & 0 & 0 & 0 & 0 & 0 & 0 & 0 & 0 \\ 0 & 0 & 1 & l & l^2 & l^3 & 0 & 0 & 0 & 0 & 0 & 0 \\ 0 & 0 & 0 & 0 & 0 & 0 & 1 & 0 & 0 & 0 & 0 & 0 \\ 0 & 0 & 0 & 0 & 0 & 0 & 0 & 1 & l & l^2 & l^3 & 0 \\ 0 & 0 & 0 & 0 & 0 & 0 & 0 & -1 & 0 & -K_y & 0 & 0 \\ 0 & 0 & 0 & 0 & 0 & 0 & 0 & -1 & -2l & -K_y - 3l^2 & 0 & 0 \\ 0 & 0 & 0 & 1 & 0 & K_z & 0 & 0 & 0 & 0 & 0 & 0 \\ 0 & 0 & 0 & 1 & 2l & K_z + 3l^2 & 0 & 0 & 0 & 0 & 0 & 0 \\ 0 & 0 & 0 & 0 & 0 & 0 & 0 & 0 & 0 & 0 & 1 & 0 \\ 0 & 0 & 0 & 0 & 0 & 0 & 0 & 0 & 0 & 0 & 1 & l \end{array} \right] \left\{ \begin{array}{l} c_1 \\ c_2 \\ c_3 \\ c_4 \\ c_5 \\ c_6 \\ c_7 \\ c_8 \\ c_9 \\ c_{10} \\ c_{11} \\ c_{12} \end{array} \right\} \quad (1.34)$$

Inversion of this matrix results in a system of equations defining the constant  $c_1$  through  $c_{12}$ . These constants are then substituted in to the polynomial expressions

(1.32) & (1.33) giving the interpolations as functions of the nodal displacements.

$$\begin{cases} u = N_1 u_1 + N_2 u_2 \\ v = T_{t_1y} v_1 + T_{t_2y} v_2 + T_{r_1y} \theta_1 + T_{r_2y} \theta_2 \\ w = T_{t_1z} w_1 + T_{t_2z} w_2 + T_{r_1z} \psi_1 + T_{r_2z} \psi_2 \\ \psi = R_{t_1z} w_1 + R_{t_2z} w_2 + R_{r_1z} \psi_1 + R_{r_2z} \psi_2 \\ \theta = R_{t_1y} v_1 + R_{t_2y} v_2 + R_{r_1y} \theta_1 + R_{r_2y} \theta_2 \\ \phi = N_1 \phi_1 + N_2 \phi_2 \end{cases} \quad (1.35)$$

with;

$$\begin{cases} N_1 = 1 - \zeta & N_2 = \zeta \\ T_{t_1y,z} = \frac{1}{1+\alpha_{y,z}}(2\zeta^3 - 3\zeta^2 - \alpha_{y,z}\zeta + 1 + \alpha_{y,z}) & T_{t_2y,z} = \frac{1}{1+\alpha_{y,z}}(-2\zeta^3 + 3\zeta^2 + \alpha_{y,z}\zeta) \\ T_{r_1y,z} = \frac{l}{1+\alpha_{y,z}}[\zeta^3 - (2 + \frac{1}{2}\alpha_{y,z})\zeta^2 + (1 + \frac{1}{2}\alpha_{y,z})\zeta] & T_{r_2y,z} = \frac{l}{1+\alpha_{y,z}}[\zeta^3 - (1 - \frac{1}{2}\alpha_{y,z})\zeta^2 - \frac{1}{2}\alpha_{y,z}\zeta] \\ R_{t_1y,z} = \frac{6/l}{1+\alpha_{y,z}}(\zeta^2 - \zeta) & R_{t_2y,z} = \frac{6/l}{1+\alpha_{y,z}}(-\zeta^2 + \zeta) \\ R_{r_1y,z} = \frac{1}{1+\alpha_{y,z}}(3\zeta^2 - (4 + \alpha_{y,z})\zeta + 1 + \alpha_{y,z}) & R_{r_2y,z} = \frac{1}{1+\alpha_{y,z}}(3\zeta^2 - (2 - \alpha_{y,z})\zeta) \end{cases} \quad (1.36)$$

where,  $\alpha_y = 2K_y/l^2 = \frac{12EI_y}{\kappa Gal^2}$ ,  $\alpha_z = 2K_z/l^2 = \frac{12EI_z}{\kappa Gal^2}$ , &  $\zeta = x/l$ . (1.35) is expressed in matrix form as it appears in (1.31) where

$$\mathbf{N}(x) = \begin{bmatrix} T_{t_1y} & 0 & 0 & T_{r_1y} & T_{t_2y} & 0 & 0 & T_{r_2y} & 0 & 0 & 0 & 0 \\ 0 & T_{t_1z} & T_{r_1z} & 0 & 0 & T_{t_2z} & T_{r_2z} & 0 & 0 & 0 & 0 & 0 \\ 0 & R_{t_1z} & R_{r_1z} & 0 & 0 & R_{t_2z} & R_{r_2z} & 0 & 0 & 0 & 0 & 0 \\ R_{t_1y} & 0 & 0 & R_{r_1y} & R_{t_2y} & 0 & 0 & R_{r_2y} & 0 & 0 & 0 & 0 \\ 0 & 0 & 0 & 0 & 0 & 0 & 0 & 0 & N_1 & 0 & N_2 & 0 \\ 0 & 0 & 0 & 0 & 0 & 0 & 0 & 0 & N_1 & 0 & N_2 & 0 \end{bmatrix} \quad (1.37)$$

still with the generalized displacement vector  $\vec{\mathbf{q}} = [v_1, w_1, -\psi_1, \theta_1, v_2, w_2, -\psi_2, \theta_2, u_1, \phi_1, u_2, \phi_2]^T$

Shape functions depend on the term  $\alpha$  which is sometimes called the shear correction factor. This shear correction factor is proportional to the square of the ratio of radius to length of the beam element. So, as the length increases relative to the radius,  $\alpha$  tends to zero. It will be evident in the following section that as  $\alpha$  approaches

zero, the equations of motion approach the equations of the Bernoulli-Euler beam. A spatial representation of the shape functions of equation (1.36) is given in figure 1.5. Shape functions plotted with respect to the non-dimensional length lend a visu-

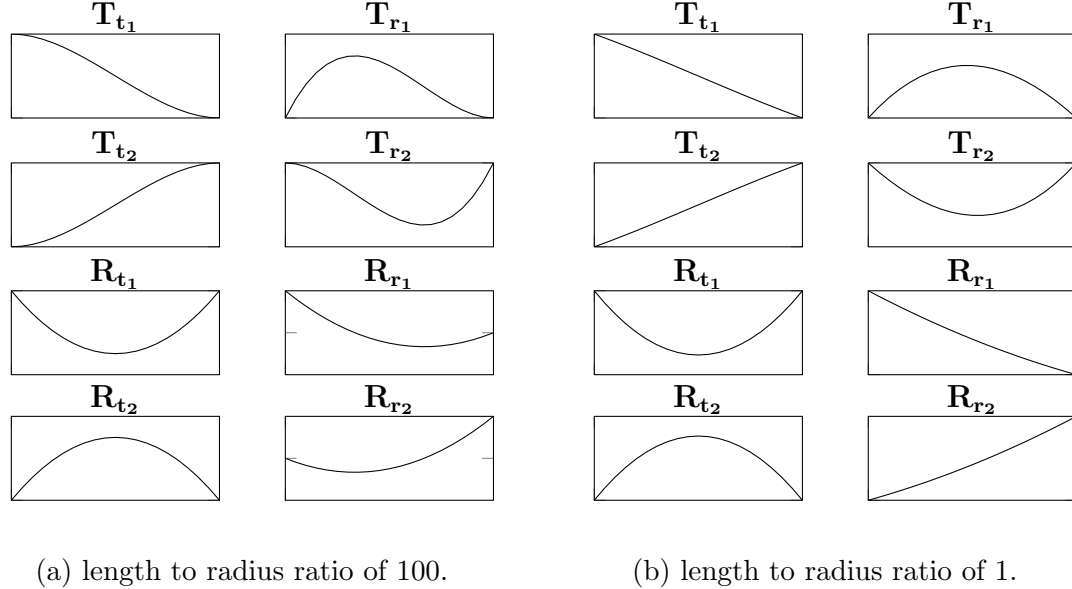


**Figure 1.5: Shape Functions as they vary with  $\zeta$  using two different ratios of length to radius of beam element.**

alization to the contribution of each shape function. Shape functions for axial and torsion are omitted since they are just linear polynomials. Each individual plot can be interpreted as a transformation from the input, being the coordinate multiplied to it, to the output of the variable function. For instance, the first shape function plot is the output of  $v(x)$  with an input of  $v_1$  while all other coordinates are zero. The shape makes sense under this interpretation, as the translation starts at some value,  $v_1$  and decreases to zero at the end since  $v_2$  is zero. Also, the expected shape breaks as the radius approaches the length as in Figure 1.5b. All shapes this beam will make in the model is a linear combination of the shapes shown here.

### 1.1.1.5 Finite Equations of Motion

To obtain the equations of motion in terms of the generalized coordinates,  $\vec{q}$ , displacement variables  $\vec{u}$  are replaced with definitions in equation 1.31.

$$\int_0^l \underline{\mathbf{N}}^\top \delta \vec{q}^\top \underline{\mathcal{M}}^e \underline{\mathbf{N}} \ddot{\vec{q}} dx + \Omega \int_0^l \underline{\mathbf{N}}^\top \delta \vec{q}^\top \underline{\mathcal{G}}^e \underline{\mathbf{N}} \dot{\vec{q}} dx + \int_0^l \underline{\mathbf{N}}^\top \delta \vec{q}^\top \underline{\mathcal{B}}^\top \underline{\mathcal{D}}^e \underline{\mathcal{B}} \underline{\mathbf{N}} \vec{q} dx = 0 \quad (1.38)$$

Note that  $\vec{q}$  is not dependent on  $x$  so it, and its derivatives, may be pulled out of the integrals. Define  $\underline{\mathbf{B}} = \underline{\mathcal{B}} \underline{\mathbf{N}}$  and substitute in, noting that  $\underline{\mathbf{B}}$  interpolates strains from discrete displacements  $\vec{q}$ . The motion equations are then

$$\int_0^l \underline{\mathbf{N}}^\top \underline{\mathcal{M}}^e \underline{\mathbf{N}} dx \ddot{\vec{q}} + \Omega \int_0^l \underline{\mathbf{N}}^\top \underline{\mathcal{G}}^e \underline{\mathbf{N}} dx \dot{\vec{q}} + \int_0^l \underline{\mathbf{B}}^\top \underline{\mathcal{D}}^e \underline{\mathbf{B}} dx \vec{q} = 0 \quad (1.39)$$

Define

$$\left\{ \begin{array}{l} \underline{\mathbf{M}}^e = \int_0^l \underline{\mathbf{N}}^\top \underline{\mathcal{M}}^e \underline{\mathbf{N}} dx \\ \underline{\mathbf{G}}^e = \int_0^l \underline{\mathbf{N}}^\top \underline{\mathcal{G}}^e \underline{\mathbf{N}} dx \end{array} \right. \quad (1.40a)$$

$$\left\{ \begin{array}{l} \underline{\mathbf{K}}^e = \int_0^l \underline{\mathbf{B}}^\top \underline{\mathcal{D}}^e \underline{\mathbf{B}} dx \end{array} \right. \quad (1.40b)$$

$$\left\{ \begin{array}{l} \underline{\mathbf{M}}^e = \int_0^l \underline{\mathbf{N}}^\top \underline{\mathcal{M}}^e \underline{\mathbf{N}} dx \\ \underline{\mathbf{G}}^e = \int_0^l \underline{\mathbf{N}}^\top \underline{\mathcal{G}}^e \underline{\mathbf{N}} dx \\ \underline{\mathbf{K}}^e = \int_0^l \underline{\mathbf{B}}^\top \underline{\mathcal{D}}^e \underline{\mathbf{B}} dx \end{array} \right. \quad (1.40c)$$

so that, the general equations of motion for the timoshenko beam element are

$$\underline{\mathbf{M}}^e \ddot{\vec{q}} + \Omega \underline{\mathbf{G}}^e \dot{\vec{q}} + \underline{\mathbf{K}}^e \vec{q} = 0 \quad (1.41)$$

Notwithstanding the inclusion of viscous and hysteretic internal damping phenomena. Derivations, and inclusion of these phenomena in the equations of motion are to be included in the following section.

### 1.1.1.6 Rotating Internal Damping

Rotating damping is the main cause of instability in rotating machines. Non-rotating damping, such as the damping contributions from bearing supports, introduce a stabilizing effect. But, as rotating damping is dependent on rotation, its direction of force

can contribute to destabilization. Typically, friction components such as bearings with shrink fits or oil bearings are responsible for this destabilizing force. Due to the inherent complexity of modeling loose bearing components, or shrink fit dynamics, the analysis of the internal damping in the shaft elements is considered alone. This will allow for the study of the destabilizing effect in general, and the factors that may contribute stability such as structural damping and anisotropy of supports. Another area of interest is the design of components for specific rotor geometry to maximize the stability in the system. This stability analysis is only possible with the inclusion of some destabilizing force, [16],[15],[22],[36].

To motivate understanding of this force a simple derivation is provided with a rotating damping whose force is proportional to the flex of rate of change of the flex of the shaft. Obviously this is easier to define in the rotating reference frame, as the variables in this coordinate system directly represent the flex of the shaft from its neutral position. This relationship is as follows:

$$\vec{F}_{\xi\eta} = -c_r \begin{Bmatrix} \dot{\xi}_c \\ \dot{\eta}_c \end{Bmatrix} \quad (1.42)$$

Now to translate this force back to the stationary reference frame, we will see the rotation transformation matrix

$$\underline{\mathcal{R}} = \begin{bmatrix} \cos \Omega t & \sin \Omega t \\ -\sin \Omega t & \cos \Omega t \end{bmatrix} \quad (1.43)$$

transforms stationary into rotating coordinates

$$\begin{cases} \begin{Bmatrix} \xi_c \\ \eta_c \end{Bmatrix} = \underline{\mathcal{R}} \begin{Bmatrix} y_c \\ z_c \end{Bmatrix} \\ \begin{Bmatrix} \dot{\xi}_c \\ \dot{\eta}_c \end{Bmatrix} = \underline{\mathcal{R}} \begin{Bmatrix} \dot{y}_c \\ \dot{z}_c \end{Bmatrix} + \dot{\underline{\mathcal{R}}} \begin{Bmatrix} y_c \\ z_c \end{Bmatrix} \end{cases} \quad (1.44)$$

where,

$$\dot{\underline{\mathcal{R}}} = \Omega \begin{bmatrix} -\sin \Omega t & \cos \Omega t \\ -\cos \Omega t & -\sin \Omega t \end{bmatrix} \quad (1.45)$$

substituting the second equation in 1.44 for the velocities in 1.42

$$\vec{\mathcal{F}}_{xy} = -c_r \begin{Bmatrix} \dot{y}_c \\ \dot{z}_c \end{Bmatrix} - c_r \Omega \begin{bmatrix} 0 & 1 \\ -1 & 0 \end{bmatrix} \begin{Bmatrix} y_c \\ z_c \end{Bmatrix} \quad (1.46)$$

From the equation (1.46) we see a dependence on both velocity and position. The portion dependent on the velocity is inherently stable as it pulls opposite the motion. Conversely, the portion dependent on position cross couples the two displacements. This causes a destabilizing effect that grows as  $\Omega$  increases. A net destabilizing force is produced once the latter portion of the exceeds the former. Without the presence of other structural damping forces, the system will destabilize.

For the beam element, the constitutive relationship[36] is comprised of both viscous and hysteretic forms of damping,  $\eta_v$  &  $\eta_h$  respectively.

$$\sigma_{xx} = E \left\{ \frac{\epsilon_{xx}}{\sqrt{1 + \eta_h^2}} + \left( \eta_v + \frac{\eta_h}{\omega \sqrt{1 + \eta_h^2}} \right) \dot{\epsilon}_{xx} \right\} \quad (1.47)$$

through the use of kinematics to obtain strain-displacement relations,

$$\begin{cases} \epsilon_{xx} = -r \cos(\Omega - \omega)t \frac{\partial^2 R}{\partial x^2} \\ \dot{\epsilon}_{xx} = (\Omega - \omega)r \sin(\Omega - \omega)t \frac{\partial^2 R}{\partial x^2} - r \cos(\Omega - \omega)t \frac{\partial}{\partial t} \frac{\partial^2 R}{\partial x^2} \end{cases} \quad (1.48)$$

and inspection to obtain moment equations,

$$\begin{cases} M_y = \int_0^{2\pi} \int_0^a [w + r \sin \Omega t] \sigma_{xx} dr (rd(\Omega t)) \\ M_z = \int_0^{2\pi} \int_0^a [-v + r \cos \Omega t] \sigma_{xx} dr (rd(\Omega t)) \end{cases} \quad (1.49)$$

we can complete a moment bending relationship to be used in the equations of motion

$$\begin{Bmatrix} M_y \\ M_z \end{Bmatrix} = EI \begin{bmatrix} \eta_a & \Omega \eta_v + \eta_b \\ \Omega \eta_v + \eta_b & -\eta_a \end{bmatrix} \begin{Bmatrix} v'' \\ w'' \end{Bmatrix} + EI \begin{bmatrix} \eta_v & 0 \\ 0 & -\eta_v \end{bmatrix} \begin{Bmatrix} \dot{v}'' \\ \dot{w}'' \end{Bmatrix} \quad (1.50)$$

where,  $\eta_a = \frac{1+\eta_h}{\sqrt{1+\eta_h^2}}$  &  $\eta_b = \frac{\eta_h}{\sqrt{1+\eta_h^2}}$

Now use the same strategy followed when solving for the weak form of the beam differential equations using the Principle of Virtual Displacements starting at equation (1.27). Then use the separation of variables of defined by equation (1.31) to arrive at the total beam element equations of motion including internal damping as

$$\underline{\mathbf{M}}^e \ddot{\vec{\mathbf{q}}} + (\eta_v \underline{\mathbf{K}}^e + \Omega \underline{\mathbf{G}}^e) \dot{\vec{\mathbf{q}}} + [\eta_a \underline{\mathbf{K}}^e + (\Omega \eta_v + \eta_b) \underline{\mathbf{C}}^e] \vec{\mathbf{q}} = 0 \quad (1.51)$$

where,

$$\underline{\mathcal{I}} = \begin{bmatrix} 0 & 1 & 0 & 0 & 0 & 0 \\ -1 & 0 & 0 & 0 & 0 & 0 \\ 0 & 0 & 0 & 1 & 0 & 0 \\ 0 & 0 & -1 & 0 & 0 & 0 \\ 0 & 0 & 0 & 0 & 0 & 0 \\ 0 & 0 & 0 & 0 & 0 & 0 \end{bmatrix} \quad \& \quad \underline{\mathbf{C}}^e = \int_0^l \underline{\mathbf{B}}^T \underline{\mathcal{I}} \underline{\mathcal{D}} \underline{\mathbf{B}} dx \quad (1.52)$$

$\underline{\mathbf{C}}^e$  is the “Circulation matrix”, or the skew symmetric stiffness matrix.

#### 1.1.1.7 Beam Element in Complex Coordinates

Complex coordinates collapse the equations of each plane into one set of equations. This lends properties to axisymmetric rotor systems that will be exploited in the analysis of the model. For the complex analysis in this body of work, the system is assumed to be axisymmetric and the torsional and axial degrees of freedom are omitted. Since the contributions from axial and torsional degrees of freedom are uncoupled from the system, their condensation has no effect on the remainder of system matrices. Complex coordinates used here are defined as:

$$\vec{\mathbf{s}} = \begin{Bmatrix} \vec{r} \\ \vec{p} \end{Bmatrix} = \begin{Bmatrix} v + iw \\ \theta - i\psi \end{Bmatrix} \quad (1.53)$$

Because the element is axisymmetric, and the special form of coordinates is used, symmetric beam equations in one plane hold for the complex plane and skew symmetric matrices become complex versions of the same matrix. Elemental matrices

can be formed using the collapsed version of the shape functions matrix

$$\underline{\mathbf{N}}^c = \begin{bmatrix} T_{t_1y} & T_{r_1y} & T_{t_2y} & T_{r_2y} \\ R_{t_1} & R_{r_1} & R_{t_2} & R_{r_2} \end{bmatrix} \quad (1.54)$$

in

$$\vec{s} = \underline{\mathbf{N}}^c \vec{\mathbf{q}}^c \quad (1.55)$$

where  $\vec{\mathbf{q}}^c = [\vec{s}_1, \vec{s}_2]^\top$ .

To convince this property of the system in the complex plane, a proof for the elemental equations of motion will be made. Taking equation (1.24b), adding equation (1.24c) multiplied by the imaginary unit  $i$  and using the definition for complex variables  $\vec{p}$  and  $\vec{r}$  leads to the transverse equation of motion in the complex plane

$$\kappa G A (\vec{r}'' - \vec{p}') = \rho A \ddot{\vec{r}} \quad (1.56)$$

and taking equation (1.24e) and subtracting equation (1.24d) multiplied by  $i$  gives the rotation equation in the complex plane

$$EI\vec{p}'' - \kappa G A (\vec{r}' - \vec{p}) = \rho I \ddot{\vec{p}} + i\rho J \Omega \dot{\vec{p}} \quad (1.57)$$

which by inspection of both of these equations it is evident that the form is the same as equations (1.24b) and (1.24e) except for the imaginary unit on the cross coupled parts of the equation. Now that this idea is motivated, the finite element equations of motion analogous to equation (1.51) are

$$\underline{\mathbf{M}}^{ec} \ddot{\vec{\mathbf{q}}}^c + (\eta_v \underline{\mathbf{K}}^{ec} - i\Omega \underline{\mathbf{G}}^{ec}) \dot{\vec{\mathbf{q}}}^c + [\eta_a \underline{\mathbf{K}}^{ec} - i(\Omega\eta_v + \eta_b) \underline{\mathbf{C}}^{ec}] \vec{\mathbf{q}}^c = 0 \quad (1.58)$$

## 1.2 Disk Nodal Equations

Since the beam element has been discretized into nodal degrees of freedom, so long as the locations of disks in the model are chosen to coincide with one of these nodal locations, the expressions for stiffness and inertia can be directly combined with the

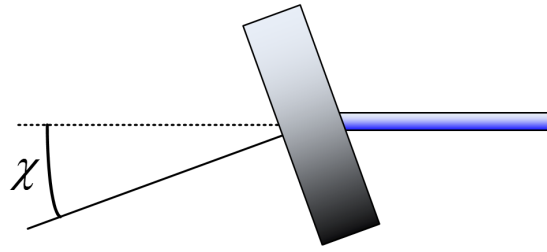


**Figure 1.6: Depiction of skew angle  $\chi$**

global matrices at that node. The mass element is considered as a body at a point with inertia, gyroscopic moments, and unbalance considered as external forces.

$$\underline{\mathbf{M}}^d \ddot{\vec{\mathbf{q}}}_k + \Omega \underline{\mathbf{G}}^d \dot{\vec{\mathbf{q}}}_k = \Omega^2 \vec{\mathbf{F}}^d \quad (1.59)$$

the superscript  $d$  represents that the matrix or array is for a disk, and the subscript  $k$  on the displacement array indicates the array is only displacements for a single node, written out as:  $\vec{\mathbf{q}}_k = [v, w, -\psi, \theta, u, \phi]^T$ . The matrices and forcing array of (3.6) are as follows,

$$\left\{ \begin{array}{l} \underline{\mathbf{M}}^d = \begin{bmatrix} \rho Al & 0 & 0 & 0 & 0 & 0 \\ 0 & \rho Al & 0 & 0 & 0 & 0 \\ 0 & 0 & \rho I_z & 0 & 0 & 0 \\ 0 & 0 & 0 & \rho I_y & 0 & 0 \\ 0 & 0 & 0 & 0 & \rho Al & 0 \\ 0 & 0 & 0 & 0 & 0 & \rho J_x \end{bmatrix} \quad \underline{\mathbf{G}} = \begin{bmatrix} 0 & 0 & 0 & 0 & 0 & 0 \\ 0 & 0 & 0 & 0 & 0 & 0 \\ 0 & 0 & 0 & \rho J_x & 0 & 0 \\ 0 & 0 & -\rho J_x & 0 & 0 & 0 \\ 0 & 0 & 0 & 0 & 0 & 0 \\ 0 & 0 & 0 & 0 & 0 & 0 \end{bmatrix} \\ \vec{\mathbf{F}}^d = \begin{Bmatrix} \rho Al \epsilon \cos(\Omega t + \delta_\epsilon) \\ \rho Al \epsilon \sin(\Omega t + \delta_\epsilon) \\ -\rho(I_y - J_x)\chi \sin(\Omega t) \\ \rho(I_z - J_x)\chi \cos(\Omega t) \\ 0 \\ 0 \end{Bmatrix} \end{array} \right. \quad (1.60)$$

Disk unbalance is caused by an eccentricity, or a geometrical distance between the axis of rotation and the center of mass of the disk. Eccentricity is represented here

as  $\epsilon$  and is equivalent to that geometric distance. The moment unbalance forces, the third and fourth equations of  $\vec{\mathbf{F}}^d$  in (1.60), are caused by the skew angle,  $\chi$ , which is the angle the disk major axis forms with the axis of rotation as in Figure 1.6. The major axis is the axis normal from the disk face from which the polar moment of inertia,  $J_x$  is defined.

### 1.2.1 Disk in complex coordinates

Disk equations of motion (3.6) are converted to the complex plane in the same manner the beam element was derived in §1.1.1.7

$$\underline{\mathbf{M}}^{dc} \ddot{\underline{\mathbf{q}}}^c_k - i\Omega \underline{\mathbf{G}}^{dc} \dot{\underline{\mathbf{q}}}^c_k = \Omega^2 \vec{\mathbf{F}}^{dc} \quad (1.61)$$

where,

$$\underline{\mathbf{M}}^{dc} = \begin{bmatrix} \rho Al & 0 \\ 0 & \rho I \end{bmatrix}, \quad \underline{\mathbf{G}}^{dc} = \begin{bmatrix} 0 & 0 \\ 0 & \rho J_x \end{bmatrix}, \quad \vec{\mathbf{F}}^{dc} = \begin{cases} \rho Al\epsilon e^{i\delta_\epsilon} e^{i\Omega t} \\ \rho(I - J_x)\chi e^{i\Omega t} \end{cases}$$

## 1.3 Bearing Nodal Equations

Bearings in this work are to be considered massless points of stiffness and damping acting at a node. Represented by the local equations of motion

$$\underline{\mathbf{D}}^b \dot{\underline{\mathbf{q}}}_k + \underline{\mathbf{K}}^b \vec{\mathbf{q}}_k = 0 \quad (1.62)$$

The superscript  $b$  indicates the matrix is for a bearing. A simple model for the stiffness and damping is used. Structural damping of the bearing is considered to be proportional to the stiffness, Raleigh Damping for the local bearing system. The

stiffness matrix is comprised of only transverse stiffness terms, as

$$\underline{\mathbf{K}}^b = \begin{bmatrix} k_{yy} & k_{yz} & 0 & 0 & 0 & 0 \\ k_{zy} & k_{zz} & 0 & 0 & 0 & 0 \\ 0 & 0 & 0 & 0 & 0 & 0 \\ 0 & 0 & 0 & 0 & 0 & 0 \\ 0 & 0 & 0 & 0 & 0 & 0 \\ 0 & 0 & 0 & 0 & 0 & 0 \end{bmatrix} \quad \underline{\mathbf{D}}^b = a\underline{\mathbf{K}}^b \quad (1.63)$$

The stiffness is typically simplified further to represent an orthotropic bearing, where  $k_{yz} = k_{zy} = 0$  or further yet as a isotropic bearing, where  $k_{yz} = k_{zy} = 0$  &  $k_{yy} = k_{zz} = k$ . Generally, these unknown parameters of stiffness are determined by changing the values to achieve the correct natural frequencies of the system.

### 1.3.1 Bearing in Complex Coordinates

Following the same methodology as sections §1.1.1.7 & §1.2.1, the equation of motion in the complex plane is

$$\underline{\mathbf{D}}^{bc} \dot{\underline{\mathbf{q}}}^c_k + \underline{\mathbf{K}}^{bc} \underline{\mathbf{q}}^c_k = 0 \quad (1.64)$$

where,

$$\underline{\mathbf{K}}^{bc} = \begin{bmatrix} k & 0 \\ 0 & k \end{bmatrix}, \quad \underline{\mathbf{D}}^{bc} = a\underline{\mathbf{K}}^{bc}$$

$k$  is the isotropic bearing stiffness. It is possible to define the complex system with anisotropic terms of stiffness, but the complexity added to the system outweighs the benefit of using the complex plane in the first place.

## 1.4 Assembly of the Global Systems of Equations

The matrices in the global system of equations are determined using the direct approach of taking the summation of the inertia, damping, stiffness, or force at each degree of freedom.

### 1.4.1 In the Real Coordinate System

$$\underline{\mathbf{M}}\ddot{\underline{\mathbf{q}}} + \underline{\mathbf{G}}\dot{\underline{\mathbf{q}}} + \underline{\mathbf{K}}\underline{\mathbf{q}} = \Omega^2 \vec{\mathbf{F}} \quad (1.65)$$

Each summation is defined as

$$\begin{cases} \underline{\mathbf{M}} = \underline{\mathbf{M}}_G^e + \underline{\mathbf{M}}_G^b + \underline{\mathbf{M}}_G^d & \underline{\mathbf{D}} = \eta_v \underline{\mathbf{K}}_G^e + \Omega \underline{\mathbf{G}}_G^e + \Omega \underline{\mathbf{G}}_G^d + \underline{\mathbf{D}}_G^b \\ \underline{\mathbf{K}} = \eta_a \underline{\mathbf{K}}_G^e + (\Omega \eta_v + \eta_b) \underline{\mathbf{C}}_G^e + \underline{\mathbf{K}}_G^b & \vec{\mathbf{F}} = \vec{\mathbf{F}}_G^d \end{cases}$$

Subscript  $G$  indicates the matrix is in the global coordinate system that contains all of the degrees of freedom. Care must be taken here to associate the correct degrees of freedom, and recognize that some of the matrices are elemental and others are nodal.

### 1.4.2 In the Complex Coordinate System

$$\underline{\mathbf{M}}\ddot{\underline{\mathbf{q}}}^c + \underline{\mathbf{D}}\dot{\underline{\mathbf{q}}}^c + \underline{\mathbf{K}}\underline{\mathbf{q}}^c = \Omega^2 \vec{\mathbf{F}} \quad (1.66)$$

where,

$$\begin{cases} \underline{\mathbf{M}} = \underline{\mathbf{M}}_G^{ec} + \underline{\mathbf{M}}_G^{dc} + \underline{\mathbf{M}}_G^{bc} & \underline{\mathbf{D}} = \eta_v \underline{\mathbf{K}}_G^{ec} - i\Omega(\underline{\mathbf{G}}_G^{ec} + \underline{\mathbf{G}}_G^{dc}) + \underline{\mathbf{D}}_G^{bc} \\ \underline{\mathbf{K}} = \eta_a \underline{\mathbf{K}}_G^{ec} - i(\Omega \eta_v + \eta_b) \underline{\mathbf{C}}_G^{ec} + \underline{\mathbf{K}}_G^{bc} & \vec{\mathbf{F}} = \vec{\mathbf{F}}_G^{dc} \end{cases}$$

## 1.5 Model Analysis

The benefit of the finite element model is the general linear ordinary differential equation that is left to solve in equations (1.65), & (1.66). Many techniques exist to provide frequency and time domain information on the solution to this system of equations. In rotordynamic analysis many of the analyses are interested in the dependence of the system on the spin speed  $\Omega$ . The inclusion of this parameter as a time dependent variable would make the solutions to the system much more difficult. In this work, the spin speed is considered to be constant in each operation taken in a series of operation as the value is changed. In this way, the effect of spin acceleration

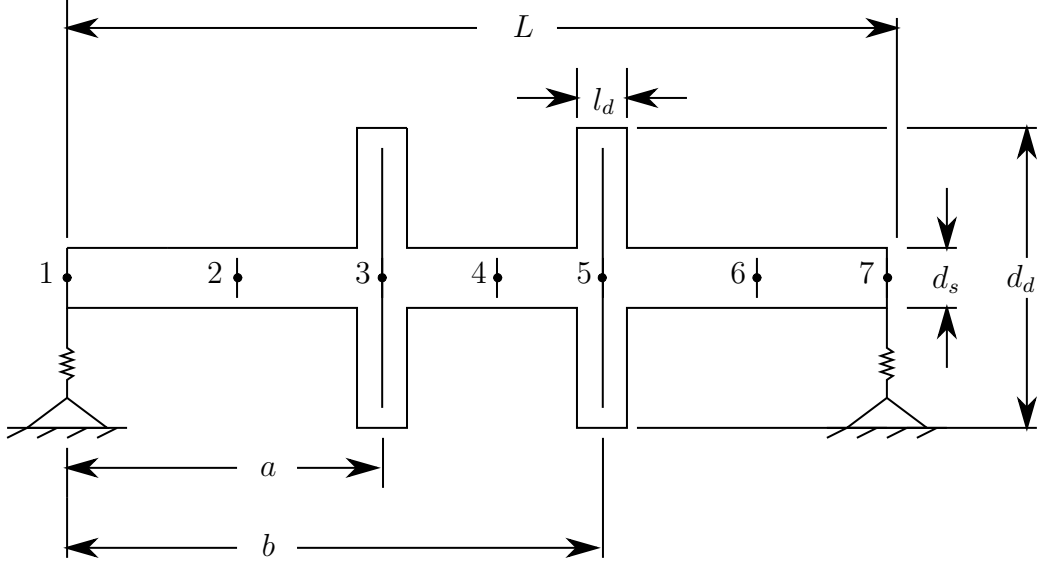


**Figure 1.7: Diagram of Two disk model example problem.**

is not taken into account, but the dependence on spin speed is approximated. For the vast majority of rotordynamic systems this approximation is sufficiently accurate. For a simple critical speed computation without dependence on spin speed,  $\Omega$ , the homogeneous solution, using  $\vec{q} = e^{i\Omega t}$  while neglecting all damping and forcing, will provide the free whirling dynamic equation. In the case that the critical speeds need to be calculated with the inclusion of spin speed, like in the Campbell diagram, a solution of the form  $\vec{q}_0 e^{i\omega t}$  is used so that the spin speed and whirl speed can vary freely. Unbalance response is calculated using the particular integral as well.

Details of the different analyses to follow will be accompanied by an example problem to demonstrate the results. The problem of interest is a simple two disk rotor system depicted in Figure 1.7. The geometry and material properties are listed in Table 1.1. The Beam is discretized as in figure 1.7 with 6 elements. With geometry of  $L = 1.8[m]$ ,  $a = \frac{1}{3}L$ , &  $b = \frac{2}{3}L$  and bearing located at the ends of the shaft.

**Table 1.1: Properties of disks, shaft elements, and bearings of the example problem.**

	$\rho \left[ \frac{kg}{m^3} \right]$	$r[m]$	$\nu$	$E[Pa]$	$\eta_v[s]$	$\eta_h$
<b>Shaft</b>	7850	0.5	0.3	$210 \times 10^9$	0.0002	0
	$\rho \left[ \frac{kg}{m^3} \right]$	$r[m]$	$l[m]$			
<b>Disks</b>	7850	0.3	0.1			
	$k_x \left[ \frac{N}{m} \right]$	$k_y \left[ \frac{N}{m} \right]$	$c_x \left[ \frac{Ns}{m} \right]$	$c_y \left[ \frac{Ns}{m} \right]$		
<b>Bearings</b>	$1 \times 10^7$	$1 \times 10^7$	100		100	

### 1.5.1 State Space Representation and the Eigenvalue Problem

The system can be represented in state space where,

$$\dot{\vec{z}} = \underline{\mathbf{A}}\vec{z} + \underline{\mathbf{B}}\vec{w}, \quad \vec{z} = \begin{Bmatrix} \dot{\vec{q}} \\ \vec{q} \end{Bmatrix} \quad (1.67)$$

$\underline{\mathbf{B}}\vec{w}$  is an input into the system, which here will represent the forces due to unbalance.

Solving for  $\underline{\mathbf{A}}$  &  $\underline{\mathbf{B}}\vec{w}$

$$\underline{\mathbf{A}} = \begin{bmatrix} -\underline{\mathbf{M}}^{-1}\underline{\mathbf{D}} & -\underline{\mathbf{M}}^{-1}\underline{\mathbf{K}} \\ \mathbf{I} & \mathbf{0} \end{bmatrix} \quad \& \quad \underline{\mathbf{B}}\vec{w} = \Omega^2 \begin{Bmatrix} \underline{\mathbf{M}}^{-1}\vec{F} \\ 0 \end{Bmatrix} \quad (1.68)$$

This equation is valid in both the complex and real coordinate plane. With the use of complex coordinates, the state vector is represented by  $\vec{z} = [\dot{\vec{q}}^c, \vec{q}^c]^\top$ .  $\mathbf{I}$  &  $\mathbf{0}$  are appropriately sized to match the matrices in the system of choice.  $\underline{\mathbf{A}}$  is the dynamic matrix of the system, which represents the dynamics in a single expression. Now in the form of a first order linear differential equation, numerical integration and many other numerical analysis techniques may be applied.

Using equation (1.67) and assuming a solution of  $\vec{z} = \vec{\Theta}e^{st}$  leads to the eigenvalue problem

$$(\underline{\mathbf{A}} - s)\vec{\Theta} = \mathbf{0} \quad (1.69)$$

$\vec{\Theta}$  is the vector containing the eigenvectors. Since the state in which these equations are defined is the combination of displacement and velocity, the eigenvectors are defined as a set corresponding to both displacement and velocity. This effectively duplicates the set as

$$\vec{\Theta} = \begin{Bmatrix} \vec{\theta}_{\dot{\vec{q}}} \\ \vec{\theta}_{\vec{q}} \end{Bmatrix} = \begin{Bmatrix} s\vec{\theta}_{\vec{q}} \\ \vec{\theta}_{\vec{q}} \end{Bmatrix}$$

### 1.5.2 Unbalance Response

The unbalance response of the dynamic system can be achieved by substituting the particular integral  $\vec{q} = \vec{q}_0 e^{i\Omega t}$  into the equation of motion (1.65),(1.66).

$$\vec{q}_0 = (-\Omega^2 \underline{\mathbf{M}} + i\Omega \underline{\mathbf{D}} + \underline{\mathbf{K}})^{-1} \Omega^2 \vec{\mathbf{F}} \quad (1.70)$$

where the matrix in the parenthesis is called the dynamic response of the system. The dynamic response acts as a transfer matrix that converts inputs,  $\vec{\mathbf{F}}$  into outputs  $\vec{q}_0$ . The result is complex with the absolute part of the result representing the magnitude of the response, and the angle of the result as representing the phase delay of the response from the input. If the input phase is known in terms of shaft angle, then the phase delay of the response angle can be interpreted as a shaft angle.

The Unbalance response can also be calculated using the particular integral  $\vec{q} = \vec{q}_0 e^{i\omega t}$  where  $\omega$  is the independent whirl frequency. Then the response is found as the transfer response of the oscillation  $e^{i(\Omega-\omega)t}$ .

For the example problem defined in §1.5 the unbalance response to a disk b unbalance of  $2 \times 10^{-5} [m]$  is depicted in Figure 1.8. We may enhance the frequency response figure by associating a plot of the phase angle with the response. This is called the Bode diagram and is presented in figure 1.9

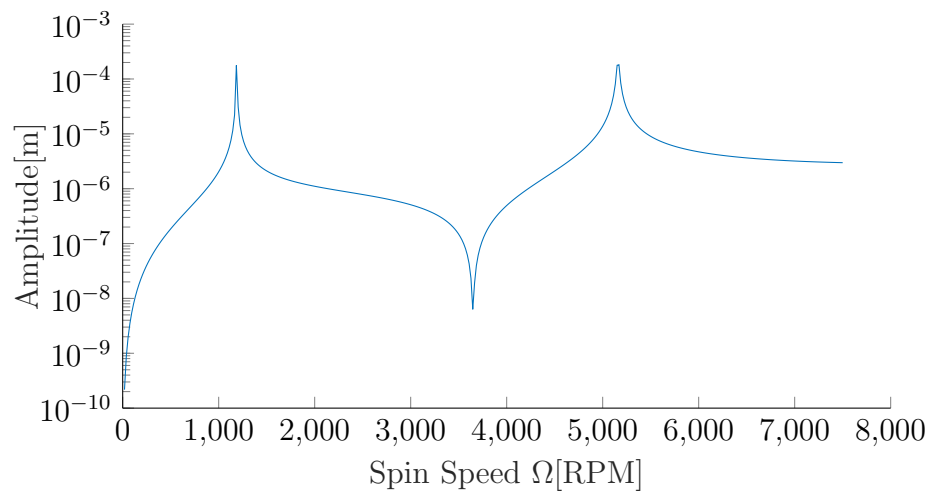


**Figure 1.8:** Frequency response of the second disk subject to an unbalance at the second disk.

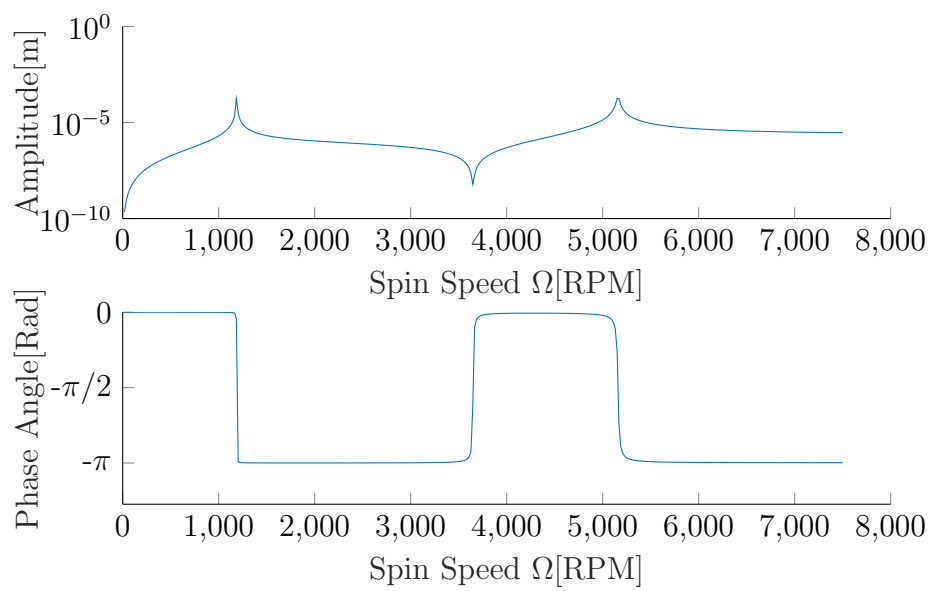


**Figure 1.9:** Bode diagram of the second disk subject to an unbalance at the second disk.

### 1.5.3 Roots Locus and Stability Analysis

One of the most valuable facets of a rotordynamic model is its ability to predict instability. Unstable operation can lead to rotor failures and unsafe operating conditions. Before the advent of modern mathematical models for rotating machinery, it was not common to operate a machine above the first critical speed. Internal damping and other rotating damping can cause a subsynchronous whirl when operating above the first critical speed. This effect is worse for machines with stiff bending modes, and is often instigated by loose fittings, shrink fits, and couplings. As mentioned in §1.1.1.6, the effect of external damping sources will not be investigated here. Rather, the stability will be tested by modeling the internal damping of the rotor due to viscous heat production during loading and unloading of the beam in bending. See §1.1.1.6 for a more detailed explanation and derivation.

Roots Locus is the plot of the eigenvalues on the  $\Re - \Im$  plane as some value they are dependent on changes. In rotordynamic analysis the dependent variable is often the spin speed  $\Omega$ . In this plane, the eigenvalues  $s$  represent the complex set of which the real part is the damping and the imaginary is the damped natural frequency. The roots locus is useful in determining stability of the system, and which mode is responsible for the instability. Using the eigenvalues  $s$  of the eigenvalue problem defined in equation (1.69) on the example problem defined in §1.5 a plot of the roots locus can be found as in figure 1.10. Internal damping coefficient,  $\eta_v$ , is added to the system at the value of  $0.0002[s]$ . The first three modes are presented with the negative complex couple joining each positive mode of vibration. In completely symmetric systems, the eigenvalue problem It is evident by looking at figure 1.10 that the system becomes unstable at some point, as many of the eigenvalues are in the positive real region of the plane. Since this example system is symmetric about the axis, the positive and negative pairs for each mode start at the same point when

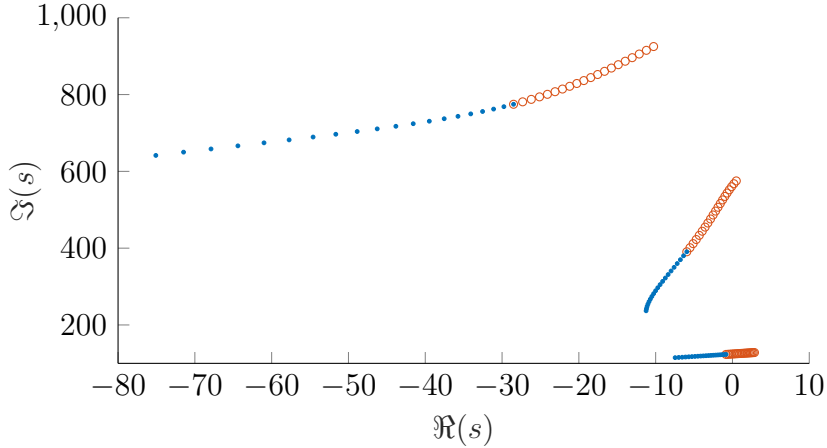


**Figure 1.10: Roots Locus of the example problem with an internal damping coefficient of 0.0002. Red circles represent positive frequencies, while blue dots represent negative ones.**

the spin speed is zero. The positive modes then move in the positive real direction—becoming more unstable. On the other hand, the negative frequencies move in the negative real direction—becoming more stable. This phenomena of the positive modes becoming more unstable and the negative becoming more stable is a general trend, but not a rule, and the rotating damping assists defined in §1.1.1.6 assists in this trend. Also, Gyroscopic effects tend to increase the whirl frequency (Imaginary part of eigenvalue) of the positive mode, while the opposite effect is seen in the negative mode.

The Roots Locus for the example problem is also presented in three dimensions to lend in the understanding of the relationship with spin speed. This can be seen in Figure 1.11. A direct method of measuring the stability of the system is to observe the real part of the eigenvalues of the dynamic matrix. Since the solution was assumed to be of the form  $\vec{z} = \vec{\Theta}e^{st}$ , then the eigenvalues represent the values of the complex exponent  $s$ . Splitting  $s$  into its real and complex components as  $s = \sigma + i\omega_d$ , and plugging into  $\vec{z}$  gives:  $\vec{z} = \vec{\Theta}e^{\sigma+i\omega_d t}$ . By inspection, it is evident that when the real part is positive, the response will grow without bound—an unstable system.

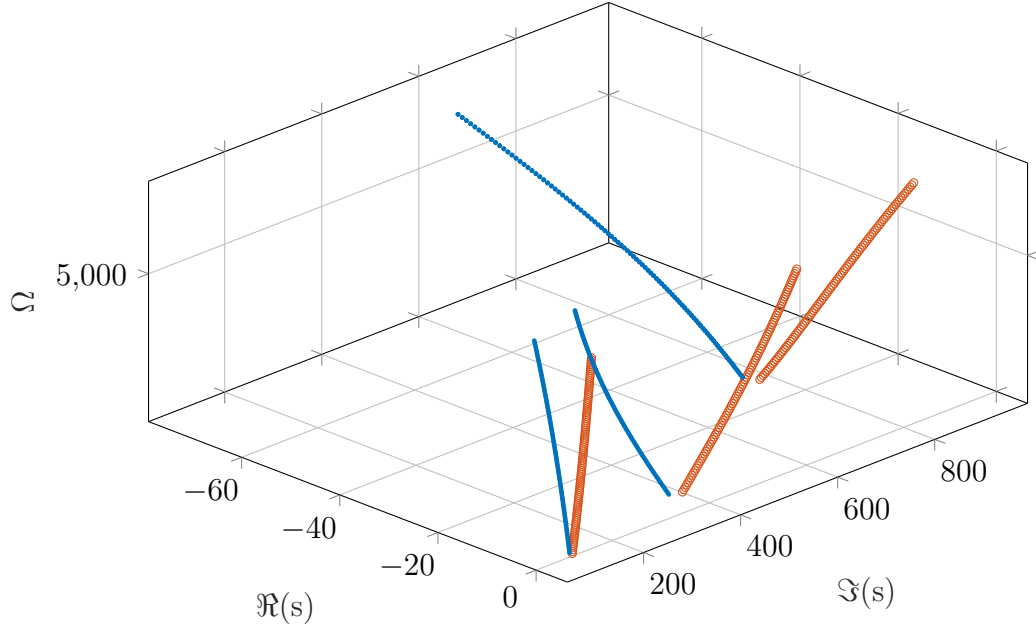


**Figure 1.11: Roots Locus of the example problem in 3-D with an internal damping coefficient of 0.0002. Red circles represent positive frequencies, while blue dots represent negative ones.**

Damping is commonly represented as a the ratio of the real part of the eigenvalue to the natural frequency as

$$\zeta = \frac{-\sigma}{\omega_n}, \quad \omega_n = \sqrt{\sigma^2 + \omega_d^2} \quad (1.71)$$

where  $\zeta$  is the damping ratio, and  $\omega_n$  is the natural frequency. The stability margin, or the range of speeds through which the system remains stable can be determined by plotting the maximum real part,  $\Re(s)$ , of the set against spin speed. The point at which  $\Re(s)$ , or  $\sigma$ , crosses the real axis is the threshold of stability. The plot which represents this is termed the Stability Margin plot, and is shown in 1.12 for the example problem defined in §1.5.

Finally, the stability can be analyzed using the damping coefficients( $\zeta$ ) plotted against speed. This figure, shown in 1.13, indicates instability as when  $\zeta$  drops below zero.

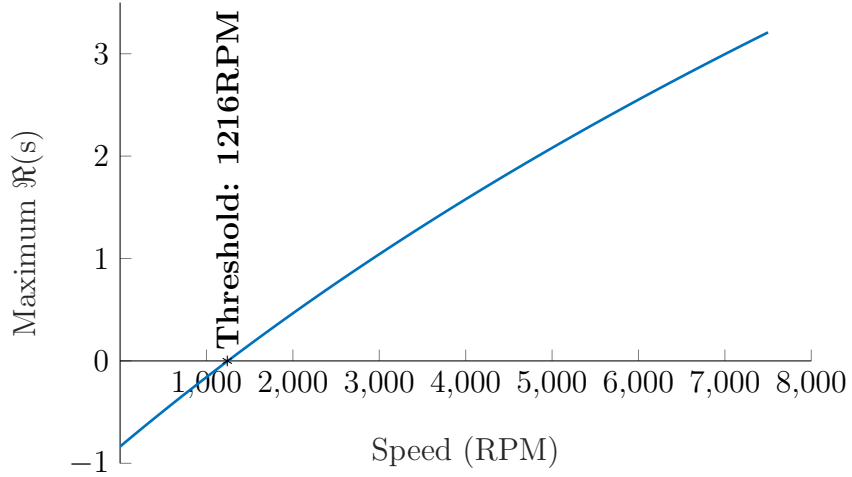


**Figure 1.12:** length to radius ratio of 1.

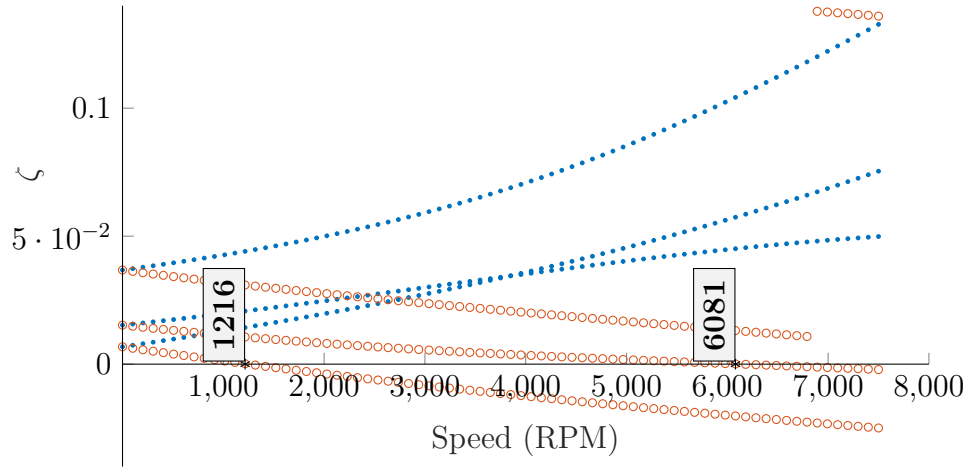


**Figure 1.13:** Damping ratio vs. spin speed with indication of threshold of stability.

#### 1.5.4 Shapes

Deformed shape can be predicted using the eigenvectors of the eigenvalue problem 1.69. Eigenvectors contain displacement arrangement that corresponds to a natural frequency; this includes phase and relative amplitude of the generalized displacements from one another. For a simple model to conceptualize this idea, consider a rigid rod that can only translate in one plane at each end. The eigenvectors will contain all linearly independent combinations of the movement of the left side relative to the

right. This would be in general; opposite left to right (one up, one down), and same left and right(both up, or both down). The bending modes of the beam operate in a similar manner but scaled up, and just like in the simple case, including the same number of modes as there are degrees of freedom in the system. Since the state space representation used for eigenanalysis contains  $\dot{\vec{q}}$ , &  $\vec{q}$  the eigenvector will contain  $2N$  modes. For a general  $i$ th mode of vibration, the eigenvector  $\vec{\Theta}_i$  contains the displacement information. But, since the portion of  $\vec{\Theta}_i$  pertaining to velocities,  $\vec{\theta}_{\dot{\vec{q}}_i}$ , is a linear combination of  $\vec{\theta}_{\vec{q}_i}$ , all of the information is contained in one of these arrays. Therefore, the interpolation of displacements for the  $i$ th mode is given by

$$\vec{u}_i = \underline{\mathbf{N}} \vec{\theta}_{\vec{q}_i} \quad (1.72)$$

where, the value of  $\vec{u}_i$  is now a function of  $x$ . So, through the choice of an array of positions that span the length of the beam element the displacement, and phase angle distribution of the  $i$ th mode of vibration is determined. Phase angle and amplitude of an transverse pair may be used to for an orbit of a beam axis location  $x$ .

Shape figures for the first 3 modes of the example problem are presented in Figures 1.14a, 1.14b, and 1.14c. Note that the real and imaginary parts of the eigenvalues are listed along with the shapes. Also, note that the speed is chosen to coincide with the damped natural frequency so that this is the critical speed bending shape.

### 1.5.5 Campbell

The Campbell diagram correlates the spin speed and the whirl speed. The whirl speed is calculated as the imaginary part of the complex eigenvalue of the dynamic matrix (1.67). Spin speed is varied while calculating all of the critical speeds at each step of spin speed. The campbell diagram for the example problem is given in figure 1.15. This diagram can be used to diserne the critical speeds of the system. As can be seen in figure 1.15 the  $\omega = \Omega$  synchronous line passes through 3 different complex modes

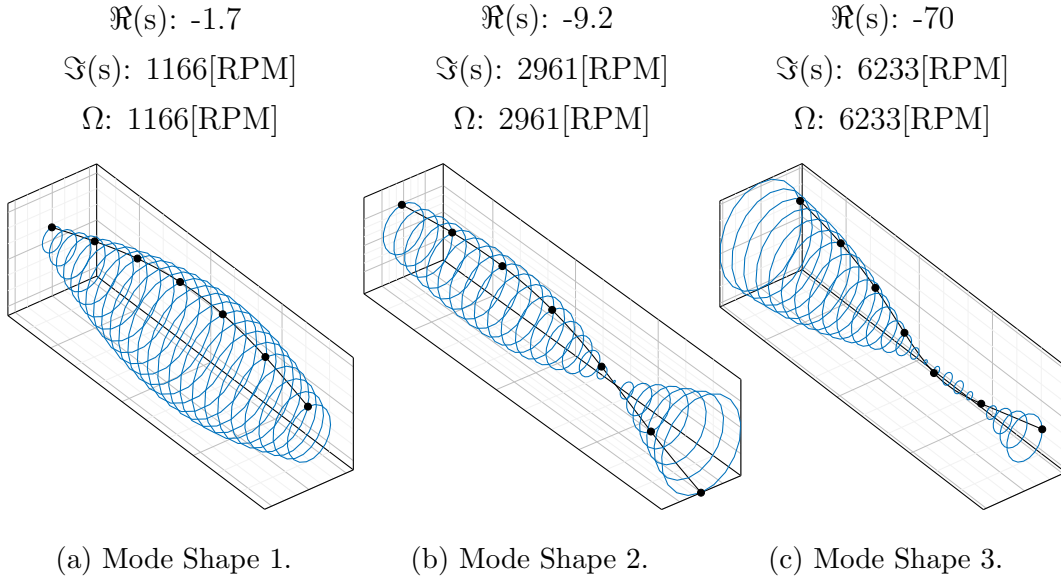


**Figure 1.14: Modal shapes of the example problem.**

in this speed range. Note: with the large influence of the gyroscopic effect in the example problem presented here, the positive and negative frequencies for the second and third modes diverge from one another rather quickly. A physical interpretation of the selective effect of the gyroscopic moments can be presented by taking the mode shapes into account. Recall that the disks in the example are mounted at nodal locations 2 & 3. In figure 1.14 it is evident that in the first mode, Figure 1.14a, both disks are translating together. As a matter of fact, most of all the points of the system are translating in sync. This type of mode is called a cylindrical mode for the fact that as the whirl is traced, as it is in 1.14a, it forms a cylinder. The consequence of this type of motion is limiting on the transverse rotation angle of the mass elements. Since the gyroscopic moments are proportional to these angles, their magnitude is very low compared to transverse effects. On the contrary, in mode 2 & 3 of figures 1.14b & 1.14c respectively, the angle of the disks and other mass elements is changing significantly through rotation. Because of this, large gyroscopic moments induce an out of phase force that stiffens positive whirl and softens negative whirl tendencies. Gyroscopic moments are larger in these types of modes where there is

a point of inflection on the beam, commonly called an antinode of vibration. This mode is called a conical mode, as analogous with the cylindrical mode, the shape of the path forms one or many cones.

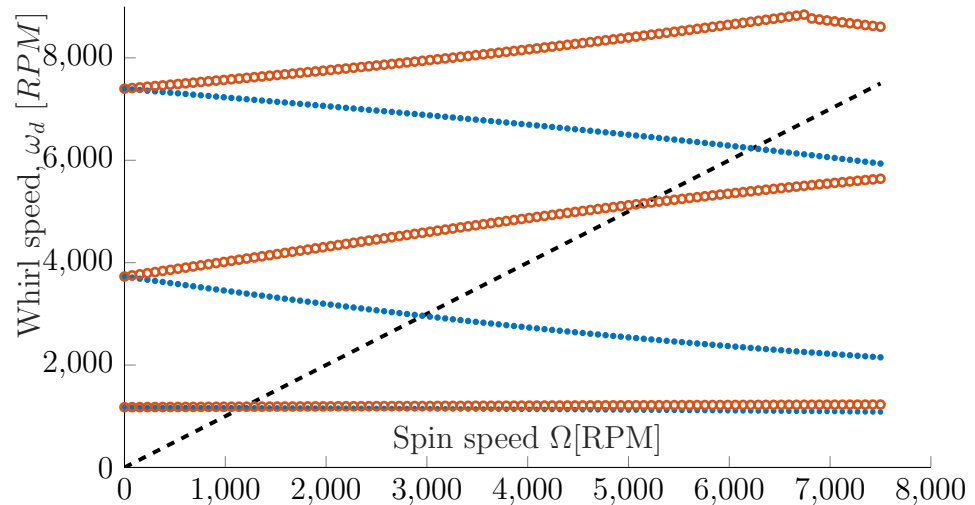


**Figure 1.15: Campbell Diagram of the example problem.**

## Chapter 2

### EXPERIMENTAL ANALYSIS

#### 2.1 Data Collection and Analysis

The most important measurement to be made in order to perform significant analysis is the vibration signal. Improvements on this would be to collect some speed information and preferably some reference point on a turn of the shaft in the system. This is often performed using a once per turn reference mark on the shaft. Additionally, a spin speed measurement independent of the spin speed and with more time precision will aid in filtering and providing accuracy of frequency spectrum. An orthogonal vibration signal can help in characterizing non-symmetric systems, and allow for the visualization of the shaft centerline orbit path. For the correct characterization of the signals mentioned thus far, it is important to also retain the sampling rates of the various signals.

There are two main figures that form the basis for other rotordynamic analysis techniques and figures. These are the Bode diagram and the Frequency Spectrum. The Bode diagram plots the amplitude of vibration against speed alongside the phase angle against speed. Frequency spectrum plots encapsulate frequency domain information gathered from the time domain amplitude data. A derivation of the Bode diagram, the Polar plot, plots the amplitude and phase of the signal as a vector on the polar plane as speed changes. Finally, the cascade plot cascades frequency spectrum plots as speed changes.

A difficulty in rotordynamic analysis arises in the change of speed of the system forcing much of the analysis to be performed in a short window in time. The window is typically made small enough to where the operation performed would be the same

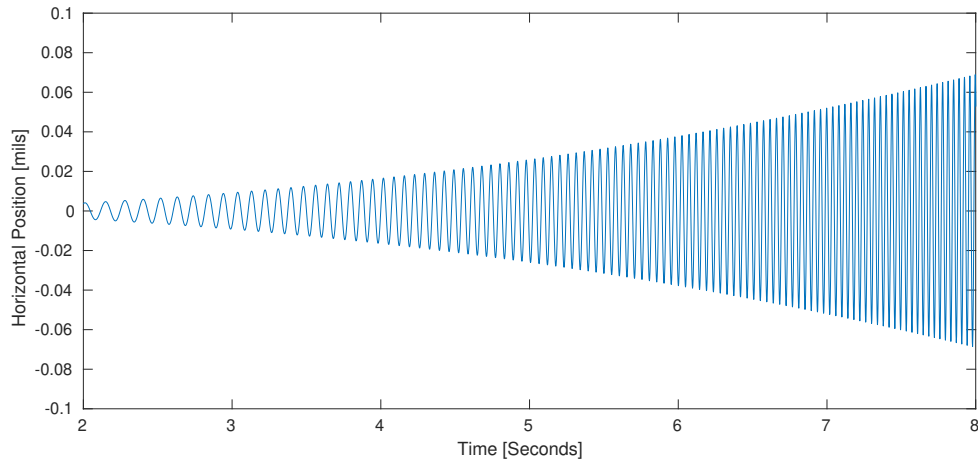
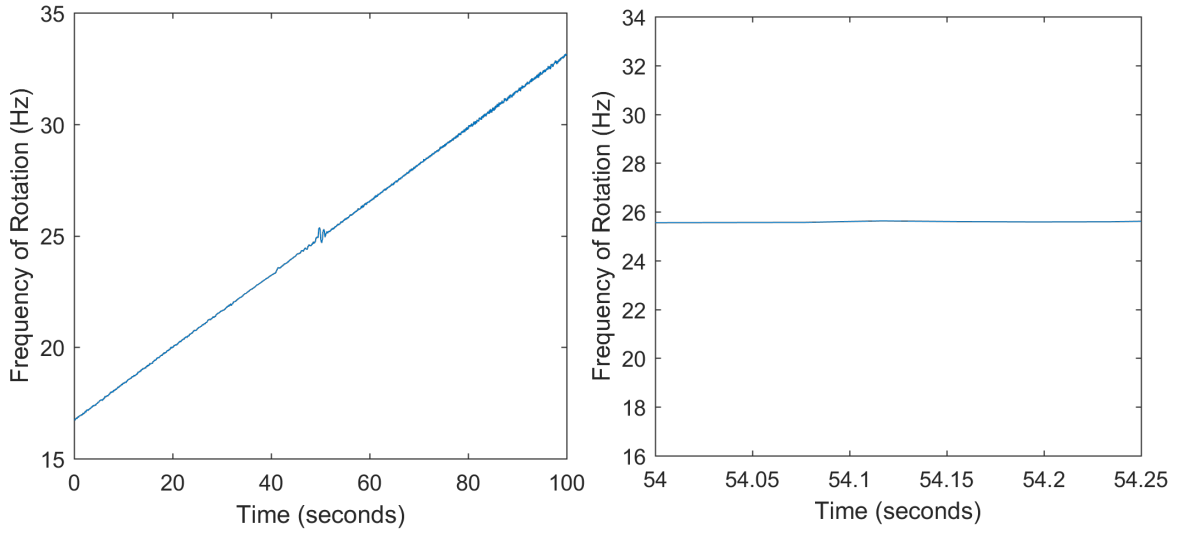


**Figure 2.1: Position of the rotor shaft over a certain timespan.**

or similar if it had been performed on a stationary system. A generic ramping of speed, and inherently vibration, is depicted in Figure 2.1. The time domain signals will be represented as  $v(t)$  &  $w(t)$  for an orthogonal set of transducers.

To combat the dynamic nature of the system, a windowing approach is taken as depicted in figures 2.2a and 2.2b. Approaching the problem this way Inside of a window of vibration, as the one shown in Figure 2.3, the Speed, Amplitude and Phase all approach constant the smaller the window gets. The Frequency Response has a twofold proportionality to window size; as the window gets smaller the frequency content of the signal itself approaches constant, but the resolution of the transform to approximate those frequencies decreases.

The variables  $v(t)$  &  $w(t)$  will now take the form  $v(n)$  &  $w(n)$  inside the window in fig. 2.3, where  $n$  is sample number. All of the plots to be presented here will be functions of two or more of the following variables: Amplitude[mils], Phase[Rad], Frequency Spectrum[mils], and Rotation Speed[RPM]. The Speed comes from the system so no analysis is necessary. Amplitude, Phase, and Frequency Spectrum must be calculated in windows of the data. Amplitude, Phase and speed are often combined into an array of vectors where speed is the index and Amplitude and Phase are the magnitude and



(a) Rotor speed change over time during a ramp up.  
(b) Rotor speed change over time during a ramp up.

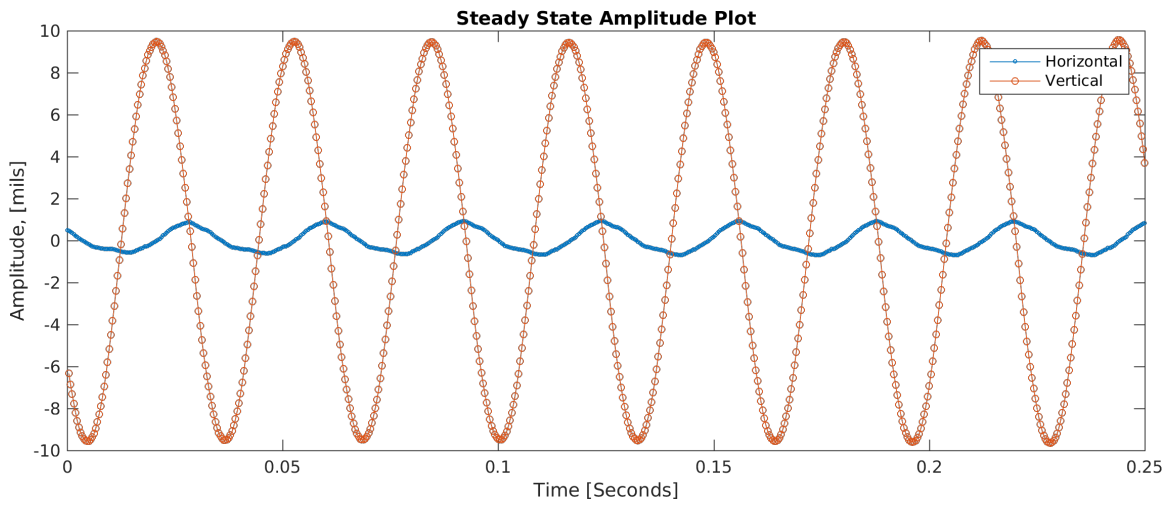


**Figure 2.3:** A window in time of the transient vibration signal in orthogonal directions.

angle of a vector, respectively.

### 2.1.1 Amplitude

Amplitude calculation is fairly straightforward within the window of 2.3. One approach to calculate the peak to peak vibration is to take the  $A_v = \max(v) - \min(v)$  over the whole sample, where  $A$  is the amplitude. Another is to use a peak-finding algorithm to determine the height of each peak and average them all over the sample length.

### 2.1.2 Frequency Spectrum

The frequency spectrum of the signal is calculated inside the window using the Fourier Transform. In MATLAB the Fast Fourier Transform has been preprogrammed allowing easy working between time and frequency domains.

$$Y = \text{fft}(v), \quad \& \quad Z = \text{fft}(w) \quad (2.1)$$

where X and Y must be scaled by the length of v and w to represent amplitude of vibration.

A useful way to represent the data is using complex variable to compact the two orthogonal displacements  $v$  &  $w$  as

$$z = v + iw \quad (2.2)$$

now the frequency spectrum of this complex value represents both equations in one

$$Z = \text{fft}(z) \quad (2.3)$$

Thus far, the frequency spectrum in the real coordinates and in the complex is in terms of samples on the dependent axis. The frequency vector to which the `fft()`

coresponds must be calculated. It is known that the slop of the frequency vector is  $df = Fs/N$ , where  $Fs$  is the sampling rate of the time domain signals. It is also known that the frequency vector is the same length as the time domain signal

$$f = df(0 : N - 1)$$

but the spectrum needs to be centered at 0

$$Q = (N + 1)/2$$

$$f_Q = df(Q - 1)$$

$$f_c = f - f_Q$$

where  $f_c$  is the frequency vector that pairs with the real or complex frequency spectrum.

### 2.1.3 Phase Angle

#### 2.1.3.1 Time Domain Approach

A rather direct way of calculating the phase angle comes from the interpretation of the time domain signal. If some once per turn reference is available, then using either a zero-crossing, peak-finding, or threshold algorithm can be employed to reference a specific angle of the shaft rotation. If the vibration signal is mostly synchronous, that is vibrating at the same frequency as the rotation of the shaft, then a peak-finding or zero-crossing algorithm can be used to determine the number of samples from the shaft reference angle to the peak of the vibration.

$$\beta_i = 2\pi \frac{\#ref_i - \#peak_i}{\#ref_i - \#ref_{i-1}} \quad (2.4)$$

where  $\beta_i$  is the phase lag of the signal of interest from the reference signal at the  $i$ th reference cycle,  $\#ref_i$  is the sample number of the reference trigger, and  $\#peak_i$  is the sample number of the peak of the signal of interest. One large advantage to

this brute force method is that it can run continuously and provide current phase information on just the last rotation of the shaft. In the application to the window of vibration data, fig. 2.3, the measurements of each cycle would be averaged across the window to provide just one phase lag data point to match the one amplitude data point and the one speed data point.

### 2.1.3.2 Frequency Domain Approach

Alternatively, the phase angle can be determined using the frequency domain signals.

If the speed of the rotor is known and the time domain signals  $v$  &  $w$  are known to be synchronous, or filtered to synchronous, then the spectrums of the signals of interest can be used to calculate the phase delay. calculate the fft of the time domain signal of interest and reference signals

$$Y = \text{fft}(v)$$

$$K = \text{fft}(k)$$

where  $K$  and  $k$  are the freq. domain and time domain signals of the reference signal respectively. Now using the speed of synchronous vibration, find the bin that is a peak nearest to that speed. Calculate the angle of the complex number corresponding to that bin for both the reference and signal of interest

$$\varphi_Y = \text{atan2}(Y(\text{max}_\text{bin}))$$

$$\varphi_K = \text{atan2}(K(\text{max}_\text{bin}))$$

and finally, the phase delay  $\beta_y = \varphi_K - \varphi_Y$

## 2.2 Experimental Plots

In the previous section Amplitude, Phase, and frequency spectrum were calculated for the interior of a window on the data as a whole. Each of the data then need to be

indexed on the speed for that window and continue until the entire signal has been exhausted. The Bode, and the Cascade plots can now be formed.

for the visualization of the plots, experimental data from a overhung rotor system with one disk will used to calculate the figures.

### 2.2.1 Bode

The Bode diagram is the stacked plot containing amplitude as a function of speed on top of phase as a function of speed. A Bode plot for the system mentioned in the §2.2 is given in Figure 2.4. Notice how the Vertical plane undergoes a critical speed before the horizontal plane. This is an indication of high anisotropy of stiffness in the system. By observing the phase lag of each the vertical and the horizontal, it is evident that the orbit direction is opposite the spin speed between speeds 1280-1350[RPM]. This is due to the phase angles switching polarity with one another. If normally horizontal lags vertical, as is suggested by the sub-synchronous and super-synchronous range, then during the critical speed the orbit is reversed since vertical begins to lag horizontal.

### 2.2.2 Cascade

The Cascade plot is a cascade, or waterfall of the spectrum at either various spin speeds, or in the case of the waterfall plot, at various times. A Cascade plot is demonstrated with the experimental system described in §2.2, as Figure 2.5. Now using this figure it is easy to detect the portion of the start-up in which the orbit is opposite the spin speed. A sharp dip in positive resonances correlated with a sharp rise in negative ones leads to this phenomena caused by the anisotropy in the stiffness matrix.

The Cascade plot is particularly useful in characterizing non-synchronous vibra-

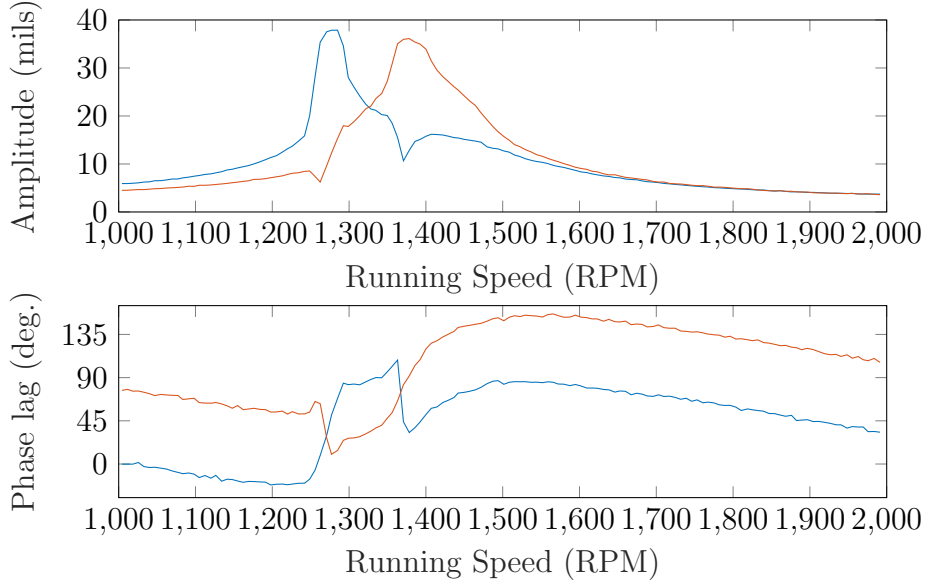


**Figure 2.4: Bode diagram of the experimental system described in §2.2. Red is horizontal plane, and blue is vertical.**

tion. Slightly evident in the example cascade of figure 2.5 is the super-synchronous vibration at twice the spin speed, this is often called the 2X vibration and likewise and other non-synchronous whirl can be referenced as  $nX$ . The cascade plot is an indispensable tool for the analysis of fluid film bearing as they are characterized by sub-synchronous whirl that is difficult to identify in a Bode Diagram.

### 2.2.3 Orbit

Now in the “real” space, the actual orbit or trace of the centerline of the shaft is observed. In this work, the orbit is visualized in two ways; as a path in 2D space at a specific spin speed, or as a 3D orbit with a cascade of orbits as spin speed is increased. The 3D Orbit allows for the visualization of complex phenomena in a unique physical way where the shapes feel more real. Figure 2.6 3D Orbit is given for the experimental example described in §2.2. Appearing, once again is evidence of the negative whirl in the critical speed range. In the 3D orbit a necking of the shape can be seen between the speeds of 1200-1400[RPM] indicating the orbit has reversed its direction.

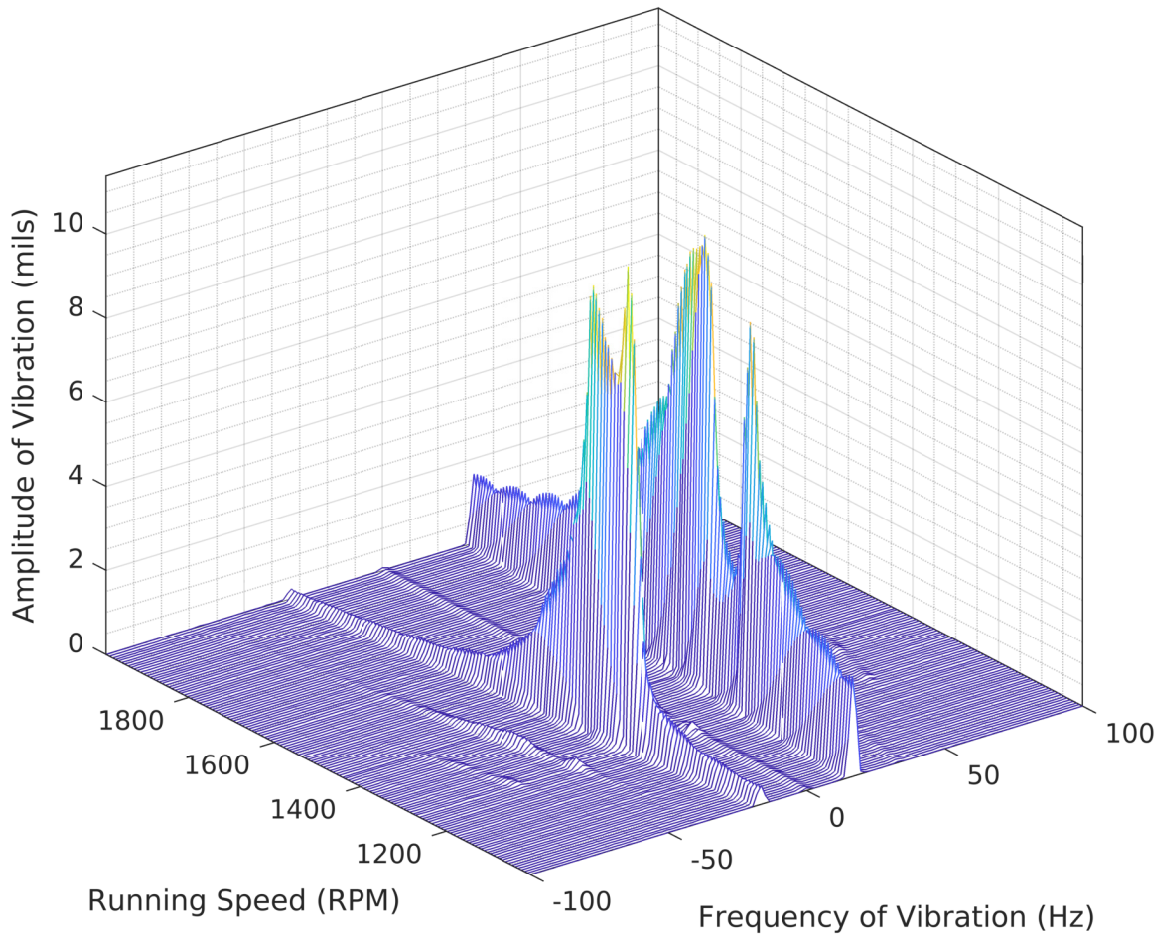


**Figure 2.5:** Cascade of the experimental system described in §2.2.

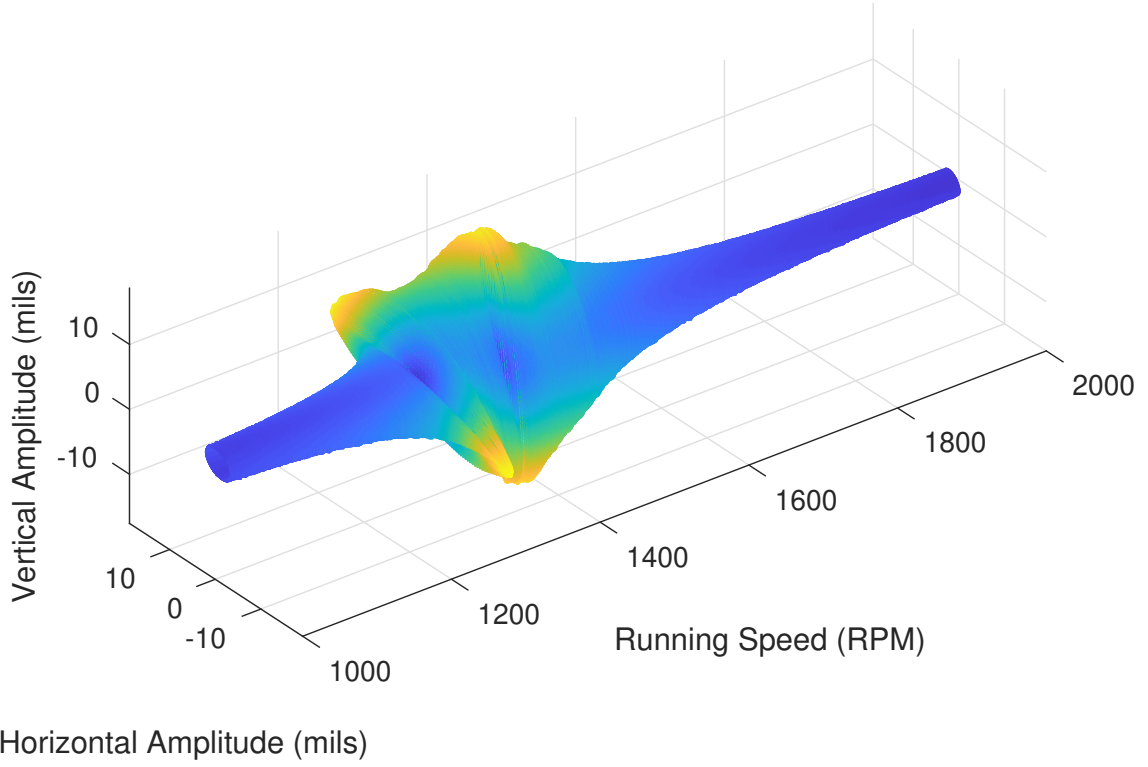


**Figure 2.6: 3DOorbit of the experimental system described in §2.2.**

Looking at independent orbits at specific speeds should explicitly demonstrate the orbit necking and turning negative.

Inspection of the orbits of Figure 2.7 reveals that the orbit is whirling backward between the speeds 1205-1280[RPM].

#### 2.2.4 Filtering

Correlating phase angles between real signals can be extremely difficult due to the noise and harmonic frequencies that may disrupt the measurement. Furthermore, it can be useful to decompose a real signal into specific harmonic components of the spin speed. One such instance is in the analysis of a fluid film bearing. Often the fluid film bearing will cause an unbalance at the subsynchronous frequency of just under 0.5X. Using a filter, the response of the system to this specific frequency can

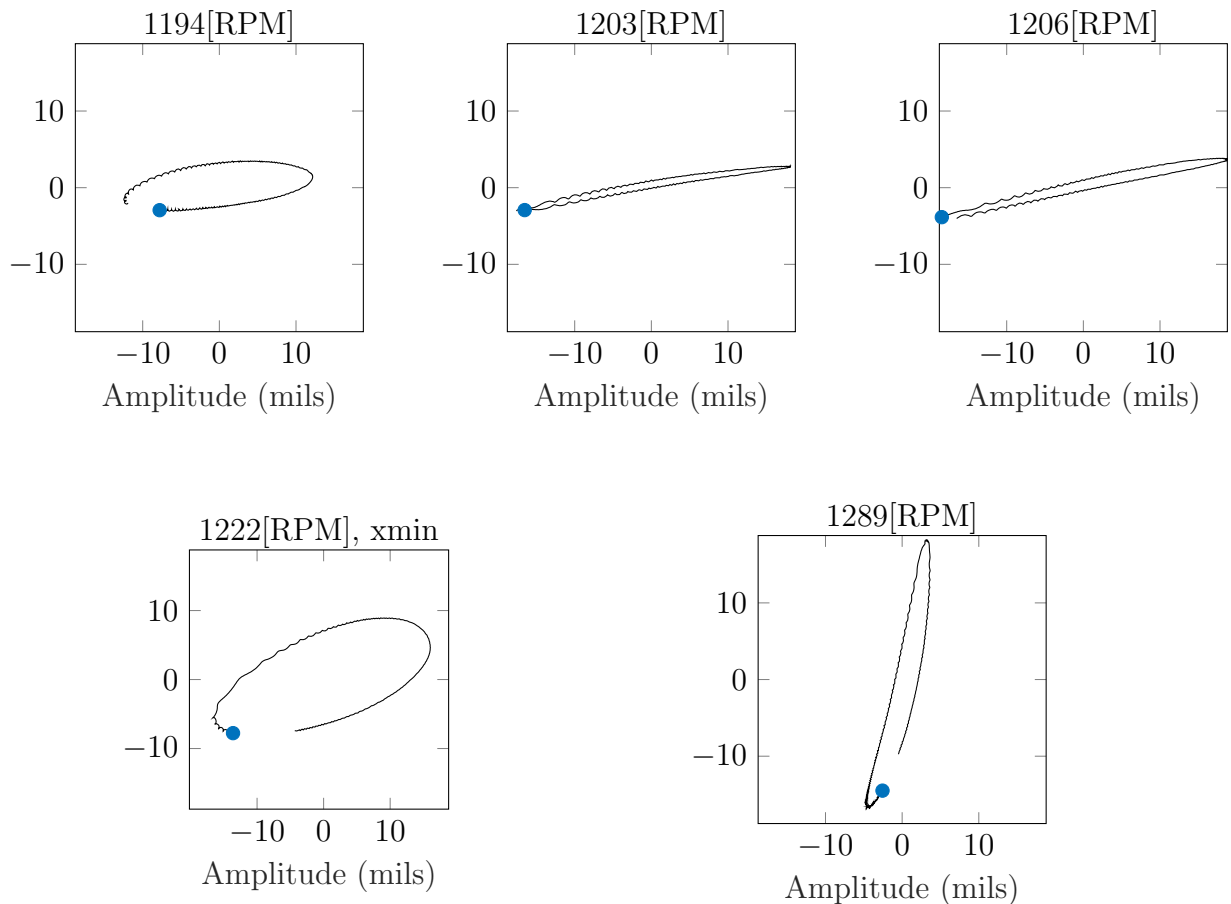


**Figure 2.7:** Orbits of the experimental example. Spin speed is counter-clockwise.

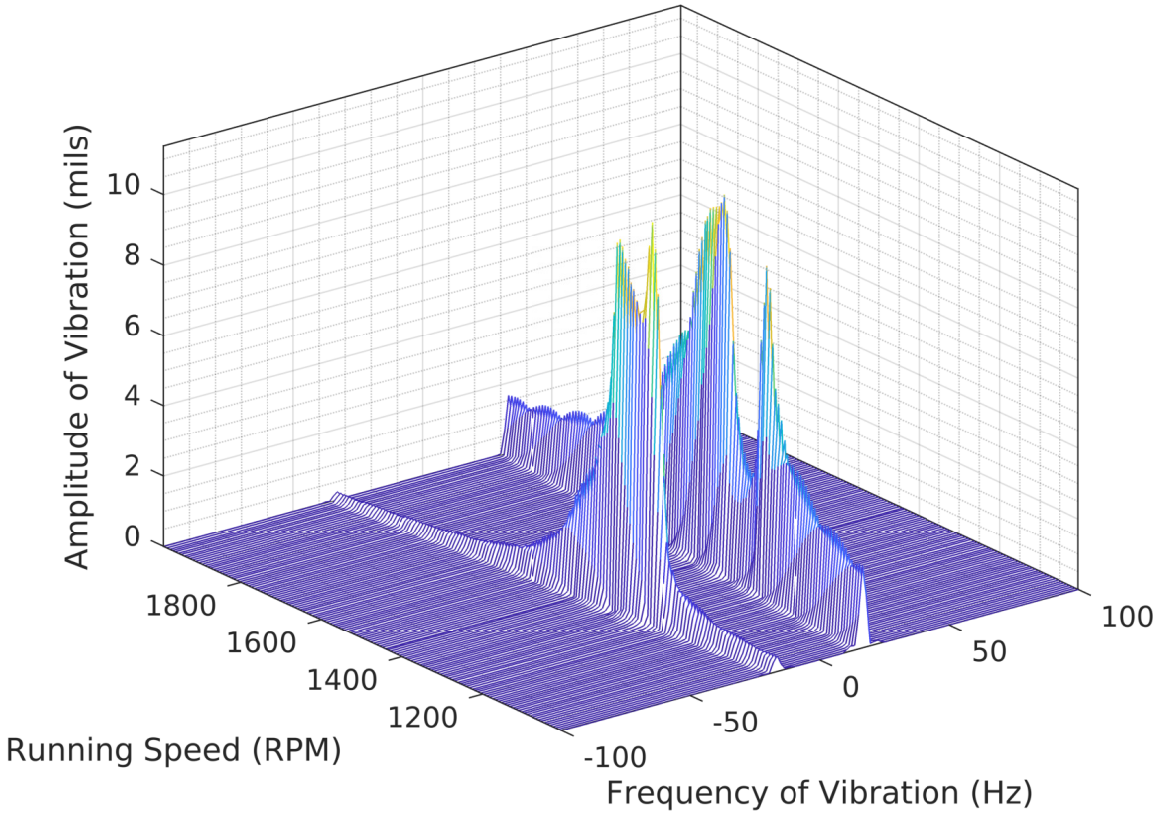


**Figure 2.8: Cascade of the experimental system with a synchronous filter applied.**

be extracted, allowing the analysis of phase angle and amplitude directly due to the influence of interest.

MATLAB has an extensive library of digital filters that can be adjusted to filter specific frequency ranges with no phase delay, and recall the states from the previous window as to not lose dynamic information from one step to the next.

A synchronous filter was applied to the experimental example and the cascade plot is shown in Figure 2.8. All amplitudes of frequencies other than the synchronous frequencies have been eliminated. This system did not have strong super- or sub-synchronous response, so this filtering does not make an appreciable effect to the Bode plot. But, with many real systems filtering will be necessary to analyze the system.

## Chapter 3

### SYNTHESIS IN EXAMPLE OF A MAGNETIC BEARING ON AN OVERHUNG ROTOR

Analysis and modeling techniques of the previous chapters will now be put to use in a practical example. The goal of which will be to reduce vibration on an overhung disk rotor system with the use of an Active Magnetic Bearing(AMB). An experimental test rig, not unlike the system used in the experimental example of §2.2, will be used to calibrate a finite element theoretical model. Then, the theoretical model will be extended to include an AMB near the overhung disk. The model will be evaluated for stability, and parameters of the control algorithm for the AMB will be varied to attempt to eliminate the first natural frequency and stabilize the system.

#### 3.1 Physical System

The rotor system of interest is depicted in Figure 3.1. Geometric parameters are listed in Table 3.1. The springs at nodes 1 & 4 are intended to represent bushings, portion at node 6 is the rotating disk, and nodal numbers are shown as the rotor will be discretized for the finite element model.

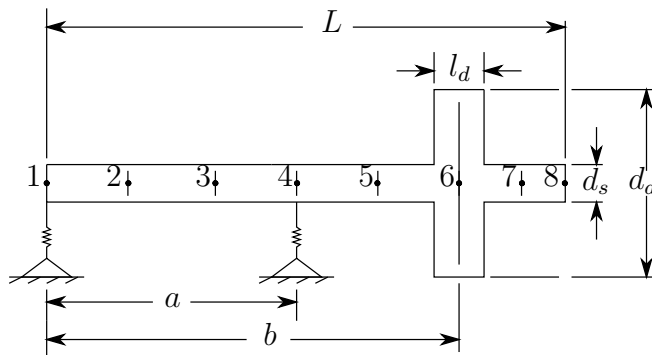
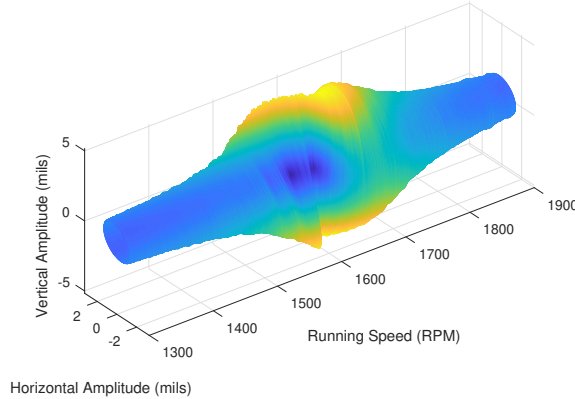


Figure 3.1: Overhung rotor system diagram.

**Table 3.1: Geometric parameters of the overhung rotor system.**

$L[m]$	$a[m]$	$b[m]$	$l_d[m]$	$d_d[m]$	$d_s[m]$
0.5	0.23	0.13	0.025	0.075	0.01



**Figure 3.2: 3D Orbit of the experimental overhung rotor system.**

### 3.2 Experimental Results

The rotor system was tested in a start-up from slow roll to 3000[RPM]. Data shown here is taken from 1000[RPM] to 2000[RPM]. A set of orthogonal eddy current sensors placed near the disk on the outboard side were used to measure the position of the shaft throughout the start-up. Position data was recorded at a sampling rate of 128000[Hz] with no processing applied. The resulting 3D orbit of the start-up is shown in Figure 3.2. Of note is the necking in the 3D orbit that is indicative of high anisotropy inducing a negative whirl during the first natural frequency. Also resulting from the experiment is the full spectrum cascade plot of Figure 3.3, in which it is evident that synchronous vibration dominates the spectra. Though, for the production of the bode diagram (Figure 3.4) there was a benefit in clarity from filtering the data to synchronous speed.

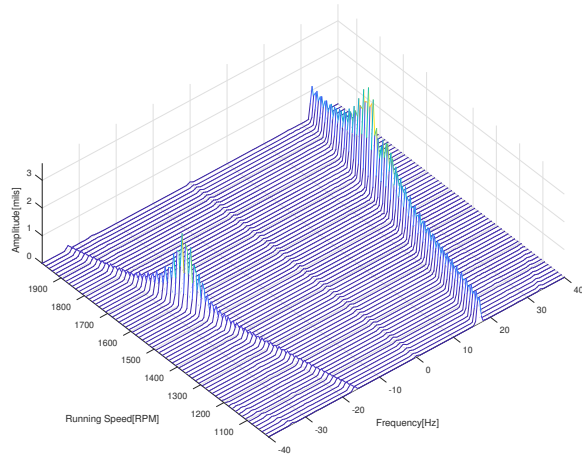


**Figure 3.3:** Cascade of the experimental overhung rotor system.

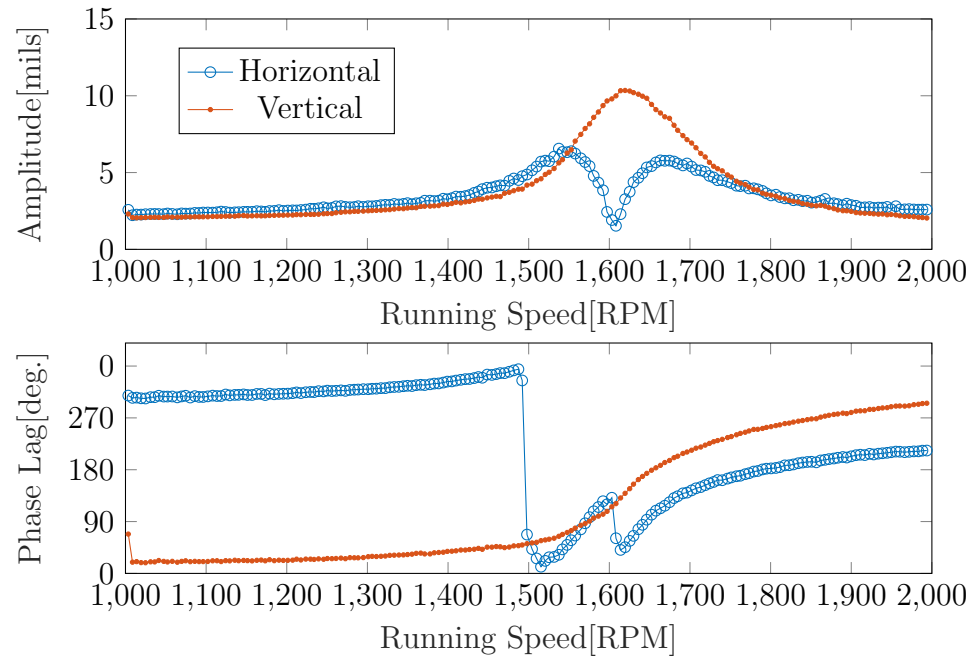


**Figure 3.4:** Bode diagram of the experimental overhung rotor filtered to 1X.

### 3.3 Theoretical Model

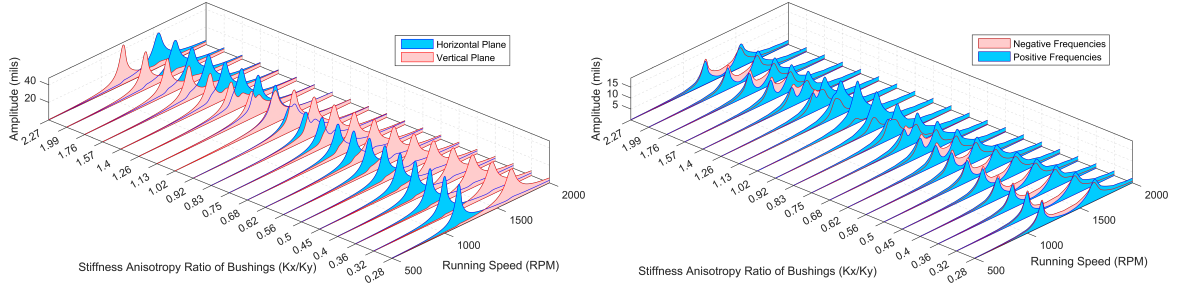
To create a theoretical model for this rotor system. The shaft will be discretized into 7 elements a disk at node 6 and bearings at nodes 1 and 4, as depicted in Figure 3.1. In the experiment, a small length of shaft continued after the overhung disk

**Table 3.2: Properties of disks, shaft elements, and bearings of the theoretical model.**

	$\rho \left[ \frac{kg}{m^3} \right]$	$r[m]$	$\nu$	$E[Pa]$	$\eta_v[s]$	$\eta_h$
<b>Shaft</b>	7850	0.005	0.3	$210 \times 10^9$	0.0002	0
	$\rho \left[ \frac{kg}{m^3} \right]$	$r[m]$	$l[m]$			
<b>Disks</b>	7850	0.0375	0.025			
	$k_y \left[ \frac{N}{m} \right]$	$k_z \left[ \frac{N}{m} \right]$	$c_y \left[ \frac{Ns}{m} \right]$	$c_z \left[ \frac{Ns}{m} \right]$		
<b>Bearing A</b>	$1.7 \times 10^5$	$2.2 \times 10^5$	68	88		
<b>Bearing B</b>	$2.04 \times 10^5$	$2.64 \times 10^5$	81.6	105.6		

and has been included in this model. The AMB will be included as a nodal point element with stiffness and damping to be derived in §3.3.1. Parameter values for the finite element model are provided in Table 3.2. Discovered values such as  $\eta_v$  and the stiffnesses of bearing are listed here, but the process for their determination is discussed. First the model is formed to match the experimental results. Known parameters, such as beam lengths, beam diameters, density of the material, and geometry of the disk and rotor are used to begin construction of the model. Then, guesses are made for the stiffnesses in the rotor bearings. The first natural frequency is calculated with the resulting model and its value compared to the experimentally found natural frequency from the bode diagram (fig.3.4). Stiffness are then adjusted to better match the natural frequency, and this is repeated until the natural frequency of the model matches the experiment. After this process, the stiffness was determined to be around  $2 \times 10^5 \left[ \frac{N}{m} \right]$ .

It is evident by inspection of the Bode diagram for the experimental system (fig.3.4), and the 3D orbit, that there is anisotropy in the system, leading to the dip in amplitude of one plane of vibration. It is also known from inspection of the frequency spectrum in the cascade of figure 3.3 that in this speed range the orbit is in the opposite direction of the rotation—a phenomena only possible with anisotropy



(a) 3D Orbit of the experimental overhung rotor system. (b) 3D Orbit of the experimental overhung rotor system.

of the stiffness. Figures 3.5a&3.5b demonstrate this affect anisotropy has on both the real coordinates, as well as positive and negative whirl amplitudes.

Using the bode diagram, the stiffness anisotropy is adjusted until the shapes of the amplitudes and phases match the experimental results of figure 2.4. Then damping is added to the system to appropriately match the experimental results. The resulting bode diagram is Figure 3.6. Stiffnesses were determined to be  $k_y = 1.7 \times 10^5 [N/m]$  &  $k_z = 2.2 \times 10^5 [N/m]$ . And now the resulting system is further

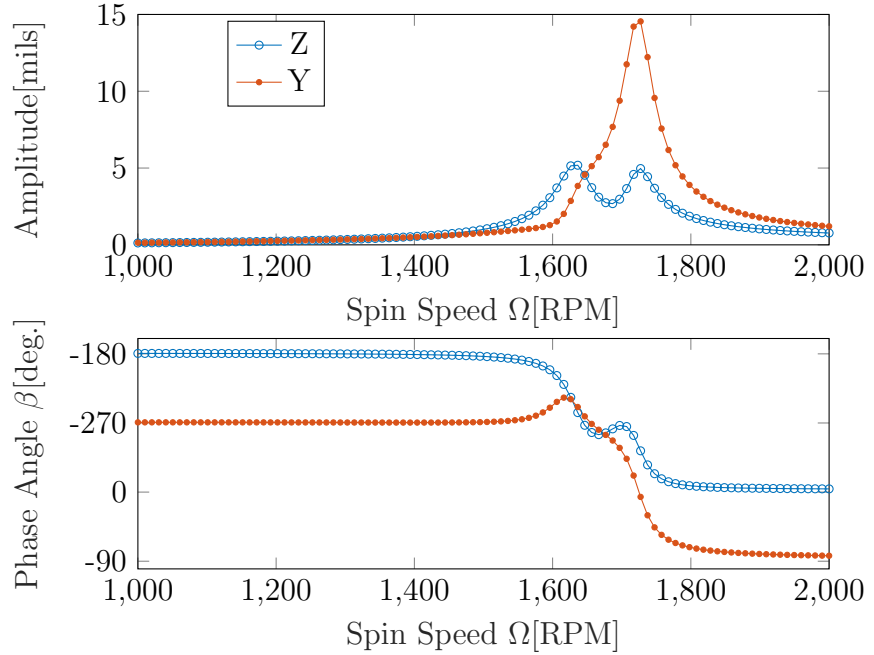


**Figure 3.6: Damping ratio vs. spin speed with indication of threshold of stability.**

described with an expanded speed range of 20000[RPM]. The new Campbell diagram of Figure 3.7, the roots locus of Figure 3.8. Additionally, the first three mode shapes are plotted for this theoretical model (Figures 3.9a, 3.9b, & 3.9c). Note that the first mode is conical in shape, but the disk is far from an antinode at node 6 so it does not experience significant gyroscopic moments. This idea is supported by the campbell diagram, fig. 3.7, as the first mode natural frequency does not change significantly over the speed range. On the other hand, the second mode has its antinode atode 6 so the disk experience maximum gyroscopic moments and the second mode critical speed is much more dependent on speed.

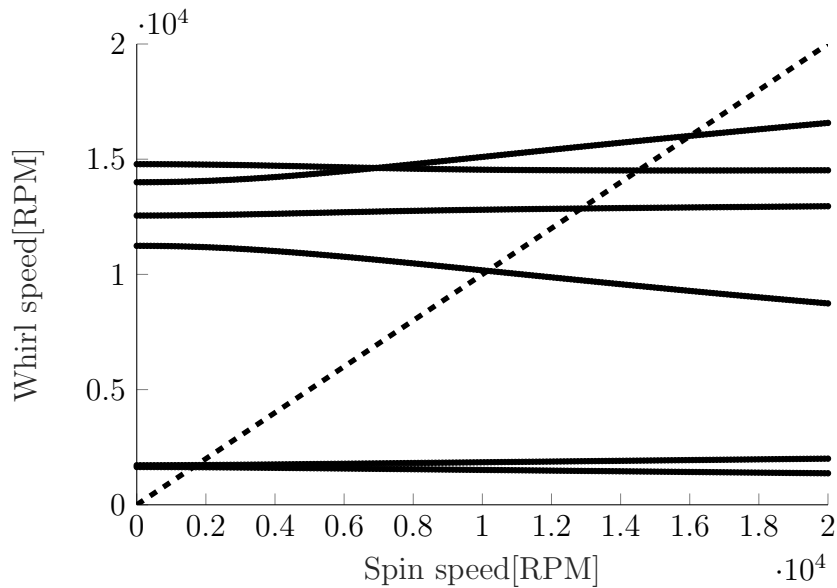


**Figure 3.7: Damping ratio vs. spin speed with indication of threshold of stability.**

### 3.3.1 Active Magnetic Bearing

Magnetic pole-rotor relationship will be derived based on the detailed derivation in [9]. Assumptions made in this model are:

- Air gap between the magnet pole face and the rotor is vanishingly small com-

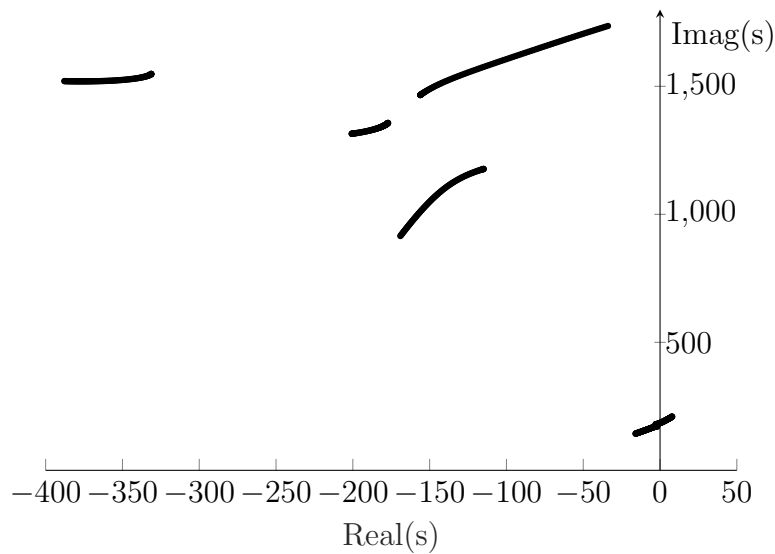


**Figure 3.8: Damping ratio vs. spin speed with indication of threshold of stability.**

pared to the diameter of the shaft.

- Flux leakage from the magnetic pole is negligible.
- Curvature of rotor surface under the pole face is ignored.
- A linear relationship of flux density and magnetic field is assumed.
- Hysteresis of the magnetic field is negligible.

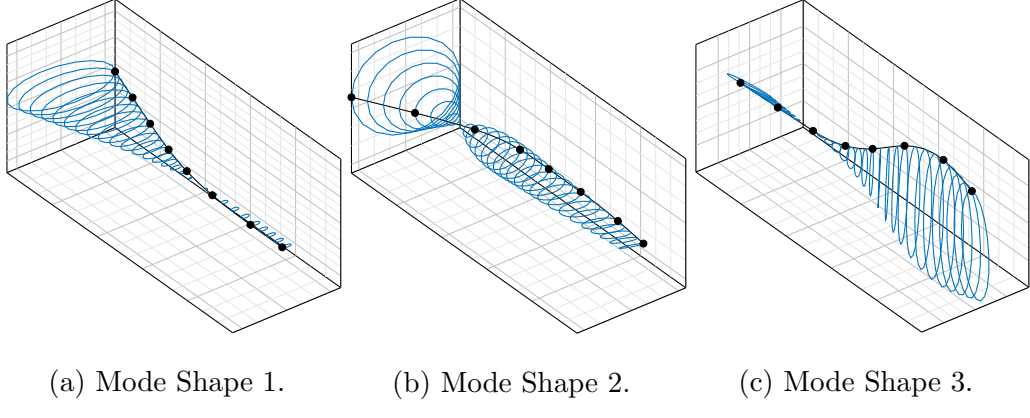
These assumptions lead to a magnetic force due to coil current in the relationship of

$$F_m = \frac{-k_m i^2}{l_g^2} \quad (3.1)$$

where,  $k_m = \frac{\mu_0 A_p N^2}{4}$ , and  $\mu_0 = 4\pi \times 10^{-7}$  is the absolute permeability in free air,  $N$  is the number of coil turns,  $A_p$  is the pole face area,  $i$  is the supplied electrical current, and  $l_g$  is the air gap.

Consider a set of magnetic pole pairs in each the  $y$  &  $z$  directions (i.e. One on the left and one on the right; one on top and one on bottom), where each pole pair has its own electrical circuit. There are 4 total magnets in this model, 2 in each direction,

$\Re(s): -2.6,$	$\Re(s): -1.5e+02,$	$\Re(s): -3.7e+02,$
$\Im(s): 1633[\text{RPM}]$	$\Im(s): 1.015e+04[\text{RPM}]$	$\Im(s): 1.451e+04[\text{RPM}]$
$\Omega: 1633[\text{RPM}]$	$\Omega: 1.015e+04[\text{RPM}]$	$\Omega: 1.451e+04[\text{RPM}]$



and 8 total poles where 2 form a magnet. All poles in the neutral position of the system will have a nominal air gap of  $g_0$  and will be supplied by a bias current of  $i_0$ . Deviations of the current from this bias will be considered as  $i_y$  and  $i_z$ . Deviations of the position from this neutral position are the displacements of the rotor at this beam axis location,  $v$ , &  $w$ . Therefore, total current will be  $(i_0 \pm i_y)$  &  $(i_0 \pm i_z)$  for opposing poles in the  $y$  &  $z$  directions respectively. Similarly, total gaps are given by  $(g_0 \pm v)$  &  $(g_0 \pm w)$ . Using these new definitions for the gap and current, and summing forces in the  $y$  &  $z$  directions leads to the total forces

$$F_y = K_m \left\{ \left( \frac{i_0 + i_y}{g_0 + v} \right)^2 - \left( \frac{i_0 - i_y}{g_0 - v} \right)^2 \right\} \quad \& \quad F_z = K_m \left\{ \left( \frac{i_0 + i_z}{g_0 + w} \right)^2 - \left( \frac{i_0 - i_z}{g_0 - w} \right)^2 \right\} \quad (3.2)$$

where,  $K_m = k_m \cos(\alpha)$ , and  $\alpha$  is half of the angle between the poles of a magnet. Linearizing the magnetic force equations (3.2), while assuming the operating point for the system is where all positions and control currents are zero, results in

$$F_y = k_i i_y + k_y v, \quad \& \quad F_z = k_i i_z + k_z w \quad (3.3)$$

where,  $k_i = 4K_m \frac{i_0}{g_0^2}$  is the current stiffness developed by the bias current, and  $k_y = k_z = k_s = -4K_m \frac{i_0^2}{g_0^3}$ .

### 3.3.1.1 Proportional Derivative Control

A control algorithm is used to control the current sent to each pair of poles based on the position (proportional) and velocity (derivative) of the rotor. It is assumed that each set of pole pairs will receive opposite currents to act as a unit. Current control is given by

$$i_y = -k_g(k_p v + k_v \dot{v}), \quad \& \quad i_z = -k_g(k_p w + k_v \dot{w}) \quad (3.4)$$

where,  $k_g$  is the power amplifier gain,  $k_p$  is the proportional gain, and  $k_v$  is the derivative gain. The total linearized force becomes

$$F_y = -(k_g k_i k_p - k_s)v - k_g k_i k_v \dot{v}, \quad \& \quad F_z = -(k_g k_i k_p - k_s)w - k_g k_i k_v \dot{w} \quad (3.5)$$

so then the stiffness of the AMB is  $k_{mag} = (k_g k_i k_p - k_s)$  and the damping is  $d_{mag} = k_g k_i k_v$ . As an equation of nodal stiffness and damping in the finite element system it can be represented by

$$\underline{\mathbf{D}}^m \dot{\underline{\mathbf{q}}}_k + \underline{\mathbf{K}}^m \vec{\mathbf{q}}_k = 0 \quad (3.6)$$

where,

$$\underline{\mathbf{K}}^m = \begin{bmatrix} k_{mag} & 0 & 0 & 0 & 0 & 0 \\ 0 & k_{mag} & 0 & 0 & 0 & 0 \\ 0 & 0 & 0 & 0 & 0 & 0 \\ 0 & 0 & 0 & 0 & 0 & 0 \\ 0 & 0 & 0 & 0 & 0 & 0 \\ 0 & 0 & 0 & 0 & 0 & 0 \end{bmatrix} \quad \underline{\mathbf{D}}^m = \begin{bmatrix} d_{mag} & 0 & 0 & 0 & 0 & 0 \\ 0 & d_{mag} & 0 & 0 & 0 & 0 \\ 0 & 0 & 0 & 0 & 0 & 0 \\ 0 & 0 & 0 & 0 & 0 & 0 \\ 0 & 0 & 0 & 0 & 0 & 0 \\ 0 & 0 & 0 & 0 & 0 & 0 \end{bmatrix}$$

Knowing that the amplitude of vibration,  $A$ , in the experimental system peaks at about 10 mils, or  $2.54 \times 10^{-4}[m]$ , the greatest possible velocity for synchronous vibration is determined using the simple equation  $v = (A/2)\omega$ , where  $\omega$  is the whirl speed in rad/s. Under the assumption of synchronous vibration,  $\omega$  during the natural frequency is then  $167.6[Rad/s]$ . Leading to a velocity,  $v$ , of  $0.02[m/s]$ . Looking also at the velocity in the upper speed range, knowing that the amplitude of vibration

after the first natural frequency is equal to the eccentricity of the unbalance. With an eccentricity of  $1 \times 10^{-5}$  and an upper speed of 15000[RPM], the velocity is calculated to be 0.008[m/s]. Since the estimated velocity during the natural frequency is higher, it will be used to limit the output of the AMB controller. Since the total voltage supply of most digital to analog converters is limited to 10[V] the control voltage is calculated to be within this range for the given velocity and positions that will be seen under synchronous vibration. This results in a limitation of the term  $k_v$ , which is proportional to the voltage control signal that is sent to the amplifier for conversion to control current. A value of 480[Vs/m] would max the converter, so the value to be determined must be less than this. With a similar, but separate, evaluation of the displacement leads to a cap of 500000[V/m] for  $k_p$ —a value not anticipated to be necessary. The maximum force due to unbalance is  $\epsilon m_d \Omega^2$ , where  $\epsilon$  is the eccentricity, and  $m_d$  is the mass of the disk. At the maximum speed expected of 15000[RPM], the force will be 24[N]. To counteract this force with a single coil would require 1.25[A], or 0.625[A] per coil in a opposing pair. The amplifier gain is assumed to be programmable to  $k_g = 1[A/V]$ , this leads to a reasonable choice of bias current at 0.5[A] to maintain a good resolution on the voltage output of the controller. The voltage should not need to peak above 1.25[V], and will rest at an output of 0.5[V]. Now in the next section, control parameters  $k_v$  &  $k_p$  will be determined to maximize stability of the system while also minimizing vibration.

### 3.4 Addition of Magnetic Bearing to the Rotor Model

In order to measure the effectiveness of the AMB, the Stability of the theoretical model before the addition is shown in Figure 3.10a. The magnetic bearing added is modeled after a magnetic bearing that is currently in the lab at California Polytechnic State University. This theoretical exercise is intended to be followed by experimental

verification not included in this work. The parameters used are listed in 3.3 as well as the control values whose determinations will be evaluated.

First the position of the AMB must be determined. By inspection of the mode shapes, it is evident that in the first mode (the mode we are most concerned about suppressing) a conical mode shape exists with increasing amplitude toward the end of the beam after the second bearing. It is also known that the source of vibration, the rotating disk, is located at nodal index 6. With both these pieces of information, node 7 is chosen as a starting point for the AMB for two reasons: having the AMB closer to the source of vibration reduces the phase lag between the source and the bearing, increasing the effectiveness of control; amplitude of vibration, according to the mode shape, is higher on the outboard side of the disk and placing the AMB on this side will minimize more vibration.

To determine best derivative control, the proportional control was set to zero and the derivative increased until the first mode on the Roots locus( fig. 3.8) moved away from the imaginary axis, becoming more damped. The resulting movement of the Roots on the Roots Locus is given in Figure 3.11. Notice how none of the new modes that appear on the roots locus cross the real plane—this demonstrates the stability of the new system. Stability of the system with the AMB addition is confirmed in the stability plot of Figure 3.10b. In fact from the roots locus with  $k_v = 1$  to the roots locus with  $k_v = 10$  the first mode of vibration is completely relegated to the imaginary axis and not reaching break-away for this entire speed range—this indicates that the first mode has been over-damped.

Proportional control,  $k_p$ , was added after the ideal derivative control was determined, but it did not improve the performance of the controller. It is possible that the stiffness of the bearing inherent to the bias current is sufficient. In any case, proportional control in this scenario is only adding stiffness to the system, and with

**Table 3.3: Active Magnetic Bearing Parameters.**

$\alpha [rad]$	$g_0 [m]$	$i_0 [A]$	$k_p [\frac{V}{m}]$	$k_v [\frac{Vs}{m}]$	$k_g [\frac{A}{V}]$	$N [\#]$	$A_p [m^2]$
$\frac{\pi}{8}$	$2.5 \times 10^{-3}$	0.5	0	10	1	800	$\frac{5}{100*100}$

the objective being to minimize vibration,  $k_p$  does not help. So the optimal control is determined to be with  $k_v = 10[Vs/m]$ . The remaining parameters for this resulting controller are listed in table 3.3. It is worthwhile to note that this optimal control is standing on the basis that the feedback is of synchronous vibration only. In a scenario where there is significant sub or super-synchronous vibrations, this controller may exceed its voltage limit. It is recommended that the feedback signal be filtered to match rotor speed to ensure this scenario does not take place. Furthermore, without at least low-pass filtering of the feedback signal the control would certainly provide out of range signals due to the volatile nature of derivatives of discrete signals.

The frequency spectrum is provided showing the result of the AMB application in the bode diagram of Figure 3.12. Certainly it can be concluded that the AMB is successfully performing the desired task of reducing the vibration while also improving the stability of the system.

Now the result from this synthesis exercise can be implemented on the actual experimental test rig with the AMB set to the control parameters suggested. The power of the finite element method in this application is the ability to move components around with ease. For instance, with the changing of just two parameters in the input file for this model, a new simulation is created for complete levitation of the overhung rotor. The AMB is put in place of bearing b and the resulting frequency spectrum is plotted in Figure 3.13

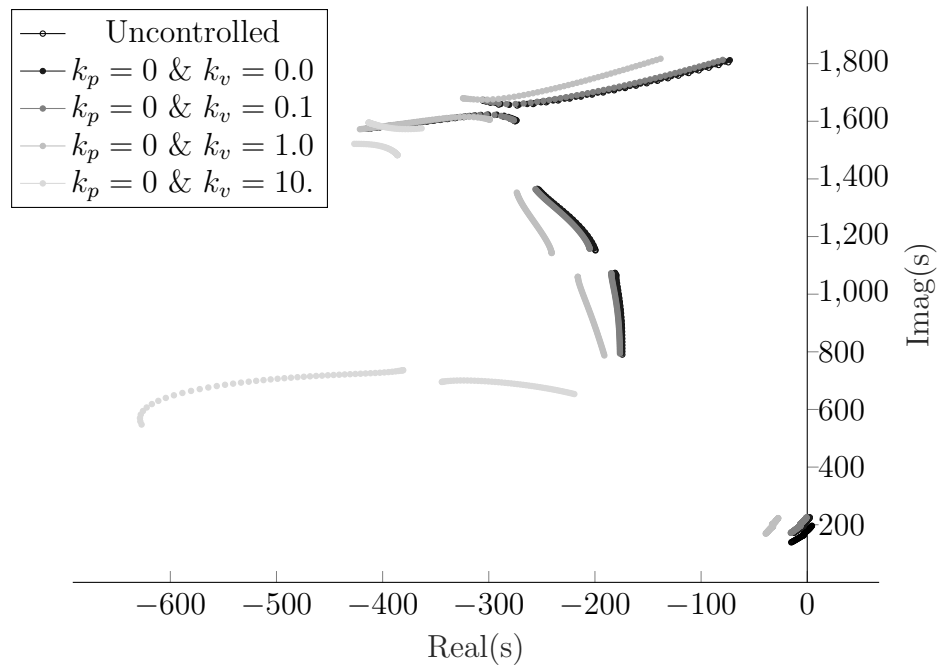
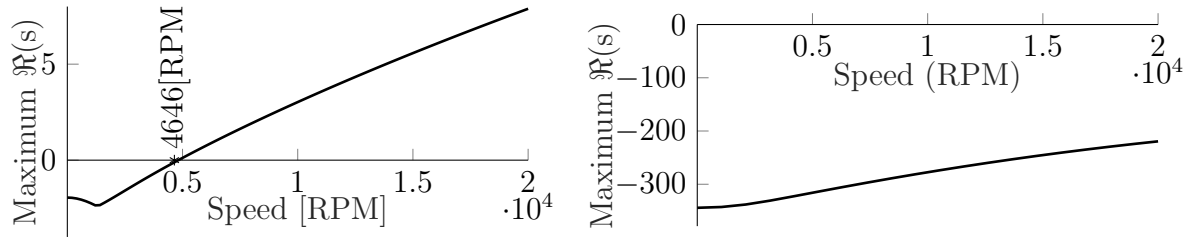


**Figure 3.11:** Roots locus of Overhung rotor system with varying  $k_v$ .

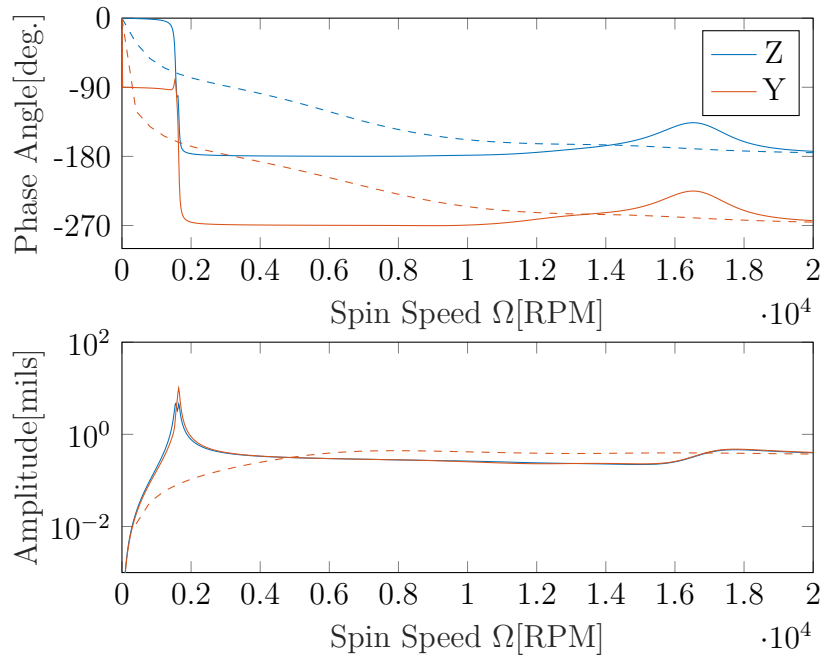


**Figure 3.12:** Bode diagram at node 6 comparing the rotor without AMB(solid) and with AMB(dashed).

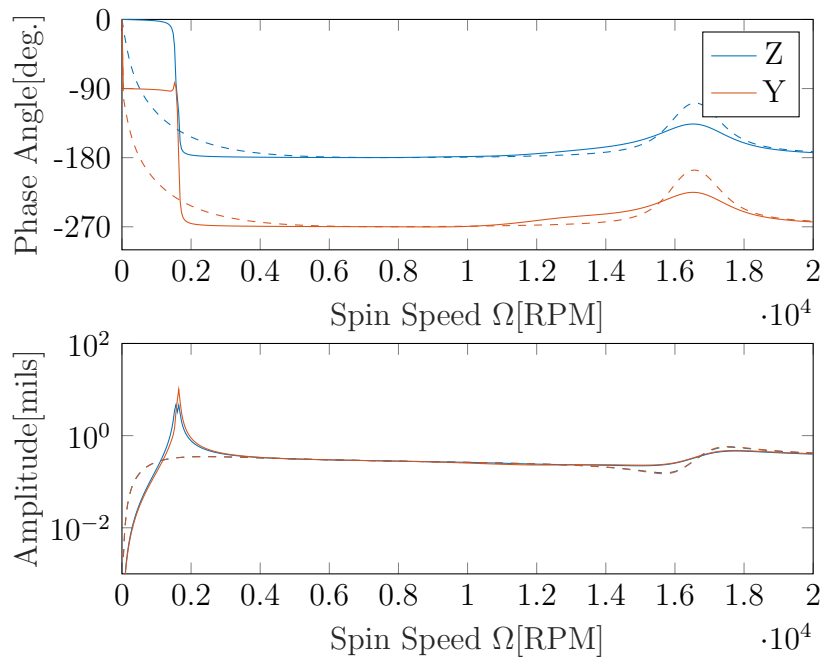


**Figure 3.13:** Bode diagram at node 6 comparing the rotor without AMB(solid) and with AMB(dashed) for complete levitation at node 4.

## BIBLIOGRAPHY

- [1] M. L. Adams. *Rotating machinery vibration: from analysis to troubleshooting*. CRC Press, 2009.
- [2] L. Andersen and S. R. Nielsen. Elastic beams in three dimensions. *Aalborg University*, 2008.
- [3] G. Barbaraci. Axial active magnetic bearing design. *Journal of Vibration and Control*, 22(5):1190–1197, 2016.
- [4] D. E. Bently and T. Hatch'Charles. Fundamentals of rotating machinery diagnostics. *Mechanical Engineering-CIME*, 125(12):53–54, 2003.
- [5] A. Bouaziz, S. Bouaziz, T. Hentati, J. Y. Cholley, and M. Haddar. Vibrations monitoring of high speed spindle with active magnetic bearings in presence of defects. *International Journal of Applied Electromagnetics and Mechanics*, 49(2):207–221, 2015.
- [6] D. W. Childs. *Turbomachinery rotordynamics: phenomena, modeling, and analysis*. John Wiley & Sons, 1993.
- [7] R. R. Craig and A. J. Kurdila. *Fundamentals of structural dynamics*. John Wiley & Sons, 2006.
- [8] S. M. Darbandi, A. Habibollahi, M. Behzad, H. Salarieh, and H. Mehdigholi. Sensor runout compensation in active magnetic bearings via an integral adaptive observer. *Control Engineering Practice*, 48:111–118, 2016.
- [9] A. Das, M. Nighil, J. Dutt, and H. Irretier. Vibration control and stability analysis of rotor-shaft system with electromagnetic exciters. *Mechanism and Machine Theory*, 43(10):1295–1316, 2008.

- [10] A. Dimarogonas and S. Haddad. Vibration for engineers. *VhS^ WI) IN914A R4 22k AWn 22kVAR5£ ilOuF 100k [^ 2k 22k 22k*, page 252, 1993.
- [11] B. Ertas and J. Vance. The influence of same-sign cross-coupled stiffness on rotordynamics. *Journal of Vibration and Acoustics*, 129(1):24–31, 2007.
- [12] M. G. Farmakopoulos, M. D. Thanou, P. G. Nikolakopoulos, C. A. Papadopoulos, and A. P. Tzes. A control model of active magnetic bearings. In *Proceedings of the 3rd International Conference of Engineering Against Failure (ICEAF III)*, pages 26–28, 2013.
- [13] L. Forrai. Stability analysis of symmetrical rotor-bearing systems with internal damping using finite element method. In *International Gas Turbine and AeroB engine Congress and Exhibition, Birmingham, UK*, 1996.
- [14] G. Genta. Consistent matrices in rotor dynamic. *Meccanica*, 20(3):235–248, 1985.
- [15] G. Genta. On a persistent misunderstanding of the role of hysteretic damping in rotordynamics. *TRANSACTIONS-AMERICAN SOCIETY OF MECHANICAL ENGINEERS JOURNAL OF VIBRATION AND ACOUSTICS*, 126(3):459–461, 2004.
- [16] G. Genta. *Dynamics of rotating systems*. Springer Science & Business Media, 2007.
- [17] T. Gmur and J. Rodrigues. Shaft finite elements for rotor dynamics analysis. *Journal of Vibration and Acoustics*, 113(4):482–493, 1991.
- [18] U. Goerguelue. Beam theories the difference between euler-bernoulli and timoschenko. *Lecture Handouts*, 2009.

- [19] P. Goldman and A. Muszynska. Application of full spectrum to rotating machinery diagnostics. *Orbit*, 20(1):17–21, 1999.
- [20] N. Instruments. Ni labview for compactrio developer’s guide. 2013.
- [21] C. Jin, Y. Xu, J. Zhou, and C. Cheng. Active magnetic bearings stiffness and damping identification from frequency characteristics of control system. *Shock and Vibration*, 2016, 2016.
- [22] M. A. Kandil. *On rotor internal damping instability*. PhD thesis, Imperial College London (University of London), 2005.
- [23] B. Kirchgässner. Finite elements in rotordynamics. *Procedia Engineering*, 144:736–750, 2016.
- [24] A. Kuperman. Uncertainty and disturbance estimator-assisted control of a two-axis active magnetic bearing. *Transactions of the Institute of Measurement and Control*, 38(6):764–772, 2016.
- [25] Y. Luo. An efficient 3d timoshenko beam element with consistent shape functions. *Adv. Theor. Appl. Mech*, 1(3):95–106, 2008.
- [26] A. Muszynska. *Rotordynamics*. CRC press, 2005.
- [27] V. Mykhaylyshyn. *Application of Active Magnetic Force Actuator for Control of Flexible Rotor System Vibrations*. PhD thesis, Cleveland State University, 2011.
- [28] H. Nelson and J. McVaugh. The dynamics of rotor-bearing systems using finite elements. *Journal of Engineering for Industry*, 98(2):593–600, 1976.
- [29] H. Roy, A. Das, and J. Dutt. An efficient rotor suspension with active magnetic bearings having viscoelastic control law. *Mechanism and Machine Theory*, 98:48–63, 2016.

- [30] G. Schweitzer. Active magnetic bearings-chances and limitations. In *IFToMM Sixth International Conference on Rotor Dynamics, Sydney, Australia*, volume 1, pages 1–14, 2002.
- [31] E. Swanson, C. D. Powell, and S. Weissman. A practical review of rotating machinery critical speeds and modes. *Sound and vibration*, 39(5):16–17, 2005.
- [32] K. Tammi. *Active vibration control of rotor in desktop test environment*. VTT, 2003.
- [33] J. M. Vance. *Rotordynamics of turbomachinery*. John Wiley & Sons, 1988.
- [34] H. Wettergren and K.-O. Olsson. Dynamic instability of a rotating asymmetric shaft with internal viscous damping supported in anisotropic bearings. *Journal of sound and vibration*, 195(1):75–84, 1996.
- [35] T. Yamamoto and Y. Ishida. *Linear and nonlinear rotordynamics: a modern treatment with applications*, volume 11. John Wiley & Sons, 2001.
- [36] E. Zorzi and H. Nelson. Finite element simulation of rotor-bearing systems with internal damping. *Journal of Engineering for Power*, 99(1):71–76, 1977.

## .1 Bernoulli-Euler Beam equation

Assumptions used to derive the Bernoulli-Euler beam equation are (Complete derivation in [7]):

1. Beam is bending in a plane, in this case in the y-direction, where the x-direction is along the length of the beam.
2. The neutral axis undergoes no deformation in the longitudinal direction.

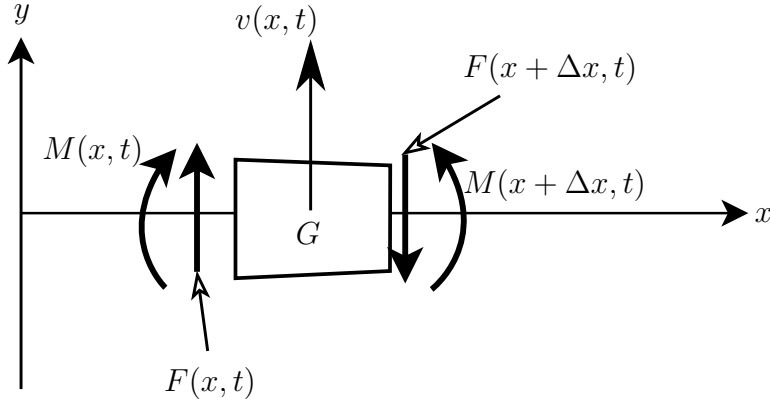


**Figure .14: Free body diagram of a beam section in planar bending.**

3. Cross sections remain plane and perpendicular to the neutral axis.
4. The material is linear-elastic.
5. Stresses in the y and z direction are negligible compared to those in the x direction.
6. Rotary inertial effects are not considered.
7. Mass density is constant at each cross section, so that each mass center is coincident with the centroid of that section.

Using kinematics and assumptions 2 & 3, the strain in the x direction may be related to the curvature of the beam,  $\mu(x, t)$ , and the distance from the neutral axis by

$$\epsilon = -\frac{y}{\mu} \quad (.7)$$

then, with assumption 4 & 7 the relation from curvature to moment is

$$M(x, t) = \frac{EI}{\mu} \quad (.8)$$

where  $E$ , Young's modulus, and  $I$ , area moment of inertia are constant in cross sections. By using Newton's laws and the free body diagram of a single beam element,

see Figure .14, the equations of motion are summarized as:

$$\sum F_y = \Delta m \ddot{v} \quad \& \quad \sum M_G = 0 \quad (.9)$$

Moment equation is represented as moments summarized at the center of mass,  $G$ .

The right hand side of moment equation of EOM (.9) is known to be null due to assumption 6. Applying Newton's equations (.9) to the FBD of Figure .14 results in the force equation

$$F(x, t) - F(x + \Delta x, t) = \rho A \Delta x \frac{\partial^2 v}{\partial t^2} \quad (.10)$$

and moment equation

$$-M(x, t) + M(x + \Delta x, t) + F(x, t) \left( \frac{-\Delta x}{2} \right) + [-F(x + \Delta x, t)] \left( \frac{\Delta x}{2} \right) = 0 \quad (.11)$$

Taking the limit of equations (.10) & (.11) as  $\Delta x \rightarrow 0$  results in equations (.12) & (.13) respectively.

$$\frac{\partial F}{\partial x} = -\rho A \frac{\partial^2 v}{\partial t^2} \quad (.12)$$

$$\frac{\partial M}{\partial x} - F = 0 \quad (.13)$$

Assuming the beam slope,  $\frac{\partial v}{\partial x}$ , remains relatively small, then linearized curvature of the beam is inversely related to  $\frac{\partial^2 v}{\partial x^2}$ . Substituting this linearized curvature in (.8) produces

$$M(x, t) = EI \frac{\partial^2 v}{\partial x^2} \quad (.14)$$

Using linearized moment equation (.14), combined with (.12) & (.13) lends the Euler beam equation

$$\frac{\partial^2}{\partial x^2} \left( EI \frac{\partial^2 v}{\partial x^2} \right) = -\rho A \frac{\partial^2 v}{\partial t^2} \quad (.15)$$

This is the governing differential equation for transverse motion of a slender beam. This equation is not suitable for an application involving lengths that are not much greater than the width of the beam [16].

```

1 classdef RotorFEM< handle
2
3 %MODEL Summary of this class goes here
4 % Detailed explanation goes here
5
6 properties
7     M
8     C
9     K
10    F
11    input_file
12    npos
13 end
14 properties (Access = private)
15
16 end
17 methods
18     function obj = Model(input_filename)
19         if nargin == 1
20             obj.Assem(input_filename);
21             obj.input_file = input_filename;
22         end
23     end
24 end
25
26 end

```

```

1 function Assem(obj , input_file )
2 run( input_file )
3
4 nodes = size( elems ,1 ) +1;
5 npos = zeros( nodes ,1 );
6 for ii = 1: nodes-1
7     npos( ii+1 ) = npos( ii ) + elems( ii ,2 );
8 end
9 obj .npos = npos ;
10
11 K = zeros( nodes*DOF, nodes*DOF ) ;
12 C = zeros( nodes*DOF, nodes*DOF ) ;
13 M = zeros( nodes*DOF, nodes*DOF ) ;
14 F = zeros( nodes*DOF, 1 ) ;
15 for ii = 1:1: size( elems ,1 )
16     E = mate( elems( ii ,1 ),2 );
17     l = elems( ii ,2 );
18     do = elems( ii ,3 );
19     if size( elems( ii ,:) ) <4
20         di=0;
21     else
22         do=elems( ii ,4 );
23     end
24     I = obj .AInert( do , di );
25     A = obj .Area( do , di );
26     rho = mate( elems( ii ,1 ),3 );

```

```

27   nuv = mate( elems( ii ,1) ,4) ;
28   poi = mate( elems( ii ,1) ,5) ;
29   Id = obj . DiaInert( do ,l ,rho ,di ) ;
30   Ip = obj . PolInert( do ,l ,rho ,di ) ;
31   [ kbe , cbe , mbe] = obj . TBeam(E,I,l,A,rho ,Id ,Ip ,nuv ,poi ,DOF
32   );
33   K = obj . Add(K,kbe ,( ii -1)*DOF+1:( ii +1)*DOF) ;
34   C = obj . Add(C,cbe ,( ii -1)*DOF+1:( ii +1)*DOF) ;
35   M = obj . Add(M,mbe ,( ii -1)*DOF+1:( ii +1)*DOF) ;
36
37 if exist( 'disks' , 'var' )
38   for ii = 1:1:size( disks ,1)
39     do = disks( ii ,3) ;
40     l = disks( ii ,2) ;
41     rho = mate( disks( ii ,1) ,3) ;
42     a = disks( ii ,4) ;
43     Ki = disks( ii ,5) ;
44     if size( disks( ii ,:) )<7
45       di=0;
46     else
47       di=disks( ii ,7) ;
48   end
49   md = obj . Mass( do ,l ,rho ,di ) ;
50   Ip = obj . PolInert( do ,l ,rho ,di ) ;
51   Id = obj . DiaInert( do ,l ,rho ,di ) ;
52   [ mi ,gi ,fi ] = obj . Disk(md,Id ,Ip ,a ,Ki ,DOF) ;

```

```

53 M = obj.Add(M, mi,( disks(ii,6)*DOF-DOF+1:disks(ii,6)*
54 DOF));
55 C = obj.Add(C, gi,( disks(ii,6)*DOF-DOF+1:disks(ii,6)*
56 DOF));
57 F = obj.AddVect(F, fi,( disks(ii,6)*DOF-DOF+1:disks(ii
58 ,6)*DOF));
59 end
60
61
62
63
64
65
66
67
68
69
70
71
72
73
74

```

M = obj.Add(M, mi,( disks(ii,6)\*DOF-DOF+1:disks(ii,6)\*  
DOF));  
C = obj.Add(C, gi,( disks(ii,6)\*DOF-DOF+1:disks(ii,6)\*  
DOF));  
F = obj.AddVect(F, fi,( disks(ii,6)\*DOF-DOF+1:disks(ii  
,6)\*DOF));  
end  
for ii = 1:1:size(bears,1)  
kx = beartypes(bears(ii,1),2);  
ky = beartypes(bears(ii,1),3);  
c = beartypes(bears(ii,1),4);  
[ki, ci] = obj.Bear(kx, ky, c, DOF);  
K = obj.Add(K, ki,( bears(ii,2)\*DOF-DOF+1:bears(ii,2)\*DOF))  
;  
C = obj.Add(C, ci,( bears(ii,2)\*DOF-DOF+1:bears(ii,2)\*DOF))  
;  
end  
if exist('mags', 'var')  
for ii = 1:1:size(mags,1)  
olddir = pwd;  
cd(char(magfile(mags(ii,1),2)))  
Magfn = str2func(char(magfile(mags(ii,1),3)));  
[ki, ci] = Magfn();  
cd(olddir)

```

75      K = obj.Add(K, ki ,( mags( ii ,2 ) *DOF-DOF+1:mags( ii ,2 ) *DOF
76                                )) ;
77
78      C = obj.Add(C, ci ,( mags( ii ,2 ) *DOF-DOF+1:mags( ii ,2 ) *DOF
79                                )) ;
80
81      end
82
83      obj.M = M;
84      obj.C = C;
85      obj.K = K;
86      obj.F = F;

```

```

1 function [ K,D,M ] = TBeam( obj , E,I,l,A,rho ,Id ,Ip ,nuv ,poi ,
2 DOF )
3 %TBeam Timoshenko beam element
4 % disp1y disp1z ang1y ang1z disp2y disp2z ang2y ang2z disp1x
5 % ang1x disp2x ang2x
6 %
7 %|
8 %| disp1y
9 %|
10 %| disp1z
11 %|

```

```

8 | ang1y
8 | %
9 | ang1z
9 | %
10 | disp2y
10 | %
11 | disp2z
11 | %
12 | ang2y
12 | %
13 | ang2z
13 | %
13 | ang2x
14 %% Properties %%
15 k = 6*(1+poi)/(7+6*poi);
16 G = E/2/(1+poi);
17 alph = 12*E*I/k/G/A/l^2;
18 %% Variables %%
19 syms x
20 z = x/l;

```

```

21 %% Shape Functions %%
22 N1 = 1-z;
23 N2 = z;
24 Tt1 = (1/(1+alph ))*(2*z^3 - 3*z^2 - alph*z + 1 + alph );
25 Tt2 = (1/(1+alph ))*(-2*z^3+3*z^2+alph*z );
26 Tr1 = (1/(1+alph ))*(z^3 - (2+1/2*alph )*z^2 + (1+1/2*alph )*z );
27 Tr2 = (1/(1+alph ))*(z^3 - (1-1/2*alph )*z^2 - 1/2*alph*z );
28 Rt1 = 6/l*(1/(1+alph ))*(z^2-z);
29 Rt2 = -Rt1;
30 Rr1 = (1/(1+alph ))*(3*z^2 - (4+alph )*z + 1 + alph );
31 Rr2 = (1/(1+alph ))*(3*z^2 - (2-alph )*z );
32 %% Transformation Matrices %%
33 P = [0 0 0 0 0 0;
34     0 0 0 0 0 0;
35     0 -1 0 0 0 0;
36     1 0 0 0 0 0;
37     0 0 0 0 0 0;
38     0 0 0 0 0 0];
39 Di = [12*E*I/alph/l^2          0          0          0          0          0;
40           0          12*E*I/alph/l^2  0          0          0          0;
41           0          0          E*I  0          0          0;
42           0          0          0          E*I  0          0;
43           0          0          0          0          E*A  0;
44           0          0          0          0          0          12*E*I/alph/l^2/A
*2*I ];
45 Mi = diag([rho*A*l , rho*A*l , Id , Id , rho*A*l , Ip]) ./ l ;
46 Gi = kron(diag([0 , 1 , 0]) ,[0 , Ip;-Ip , 0]) ./ l ;

```

```

47 T = kron( diag([1,1,0]) , [0,1;-1,0]) ;
48 N = [ Tt1 0 0 Tr1 Tt2 0 0 Tr2 0 0 0;
49 0 Tt1 Tr1 0 0 Tt2 Tr2 0 0 0 0 0;
50 0 Rt1 Rr1 0 0 Rt2 Rr2 0 0 0 0 0;
51 Rt1 0 0 Rr1 Rt2 0 0 Rr2 0 0 0 0 0;
52 0 0 0 0 0 0 0 0 N1 0 N2 0;
53 0 0 0 0 0 0 0 0 0 N1 0 N2];
54 %% DOF Modifications%%
55 switch DOF
56 case 6
57 I = diag([1,1,-1,1,1,1]);
58 N = I*N*[I, zeros(6); zeros(6), I]; % Adjust for use of
59 -angy,-ang1,2y definitions in shape functions
60 case 4
61 P = P(1:4,1:4);
62 Di = Di(1:4,1:4);
63 Mi = Mi(1:4,1:4);
64 Gi = Gi(1:4,1:4);
65 T = T(1:4,1:4);
66 I = diag([1,1,-1,1]); % Adjust for use of -angy,-ang1
67 ,2y definitions in shape functions
68 N = I*N(1:4,1:8)*[I, zeros(4); zeros(4), I];
69 case 2
70 P = P(2:3,2:3);
71 Di = Di(2:3,2:3);
72 Mi = Mi(2:3,2:3);
73 Gi = Gi(2:3,2:3);

```

```

72      T = T(2:3,2:3);
73      N = N(2:3,[2,3,6,7]);
74 end
75 %% Elemental Integration %%
76 B = diff(N.' ,x) - N.' *P;
77 B = B.' ;
78 K_B = int(B.' *Di*B,x,0,1);
79 K_C = int(B.' *T*Di*B,x,0,1);
80 G = int(N.' *Gi*N,x,0,1);
81 M = int(N.' *Mi*N,x,0,1);
82 %% Case of symbolic Integration %%
83 if isa(l,'sym') || isa(E,'sym') || isa(I,'sym') || isa(nuv,'sym')
84 else
85     K_B = double(K_B);
86     K_C = double(K_C);
87     G = double(G);
88     M = double(M);
89 end
90 K = K_B + nuv.*1i.*K_C;
91 D = nuv.*K_B + 1i.*G;
92
93 end

```

```

1 function [Md,Gd,Fd] = Disk(obj,md,Id,Ip,a,Ki,DOF)
2 %% Creates Disk nodal stiffness matrix in the form:
3 % disp1x disp1y ang1x ang1y

```

```

4 | %-----| disp1x
5 | %-----| disp1y
6 | %-----| ang1x
7 | %-----| ang1y
8 |
9 |
10 %% Begin Function
11 Fx = md*a;
12 Fy = md*a;
13 Mx = (Id-Ip)*Ki;
14 My = (Id-Ip)*Ki;
15 Gi=[0,Ip;-Ip,0];
16 switch DOF
17 case 6
18     Md = diag([md,md,Id,Id,md,Ip]);
19     Gd = 1i*kron(diag([0,1,0]),Gi);
20     Fd = [Fx; Fy; Mx; My; 0; 0];
21 case 4
22     Md = diag([md,md,Id,Id]);
23     Gd = 1i*kron(diag([0,1]),Gi);
24     Fd = [Fx; Fy; Mx; My];
25 case 2
26     Md = diag([md,Id]);
27     Gd = 1i*[0,0;0,Ip];
28     Fd = [Fx; My];
29 end
30 % Fx = md*a*(w^2*cos(theta+phi1)-alph*sin(theta+phi1)); %N,

```

```

Forcing funtion at disk 1
31 % Fy = md*a*(w^2*sin(theta+phi1)+alph*cos(theta+phi1)); %N,
    Forcing funtion at disk 2
32 % Mx = -w^2*(Ip - Id)*Ki*cos(theta+phi2); %N, Forcing funtion
        at disk 1
33 % My = w^2*(Ip - Id)*Ki*sin(theta+phi2); %N, Forcing funtion
        at disk 2;
34 end

```

```

1 function [ Kb,Cb ] = Bear( obj ,kx ,ky ,c ,DOF)
2 %% Creates bearing nodal stiffness matrix in the form:
3 % disp1y disp1z ang1y ang1z disp1x ang1x
4 % -----
5 %| | disp1y
6 %| | disp1z
7 %| | ang1y
8 %| | ang1z
9 %| | disp1x
10 %| ----- | ang1x
11 %% Begin function
12 switch DOF
13     case 6
14         Kb = diag([kx ,ky ,0 ,0 ,0 ,0]);
15         Cb = diag([c*kx ,c*ky ,0 ,0 ,0 ,0]);
16     case 4
17         Kb = diag([kx ,ky ,0 ,0]);
18         Cb = diag([c*kx ,c*ky ,0 ,0]);

```

```

19 case 2
20     k = mean([kx,ky]);
21     Kb = diag([k,k]);
22     Cb = diag([c*k,c*k]);
23 end
24 end

```

```

1 function RootLocus(Model_obj, Omega, plotmodes, ax, linetp,
2 %CAMPBELL Summary of this function goes here
3 % Detailed explanation goes here
4 zci = @(v) find(v(:).*circshift(v(:), [-1 0]) <= 0);
5 if nargin < 6
6     color = [0,0,0];
7     if nargin < 5
8         linetp = '.';
9     end
10    if nargin < 4
11        figure
12        ax = axes;
13    end
14    if nargin < 3
15        plotmodes = 1:2;
16    end
17    if nargin < 2
18        return
19    end

```

```

20
21 end
22
23 for ii = 1:1:length(Omega)
24     w = Omega(ii)/60*2*pi;
25     Mnew = Model_obj.M;
26     Cnew = real(Model_obj.C) + w.*imag(Model_obj.C);
27     Knew = real(Model_obj.K) + w.*imag(Model_obj.K);
28     Zer = zeros(size(Mnew));
29     ey = eye(size(Mnew));
30     A = [-Mnew^-1*Cnew, -Mnew^-1*Knew;
31             ey, Zer];
32     v1=eig(A);
33 %     AA=[Cnew Mnew;Mnew Zer];
34 %     B=[Knew Zer;Zer -Mnew];
35 %     v1=eig(B,-1i*AA);
36     [~, I] = (sort(abs((v1))));
37     eiv(:,ii) = v1((I));
38 end
39 % while min(abs(imag(eiv(1,:)))) == 0
40 %     eiv(1:2,:) = [];
41 % end
42 % eiv = eiv(~any(isnan(eiv) | isnan(eiv), 2),:);
43
44 hold on
45 for jj = 1:1:length(plotmodes)
46

```

```

47 % plot(ax, real(eiv(plotmodes(jj)*4-1,:)),(imag(eiv(
48 % plotmodes(jj)*4-1,:))),linetp,'Color
49 % [0.8500,0.3250,0.0980])
50 % plot(ax, real(eiv(plotmodes(jj)*4-3,:)),(imag(eiv(
51 % plotmodes(jj)*4-3,:))),linetp,'Color',[0,0.4470,0.7410])
52 % plot3(real(eiv(plotmodes(jj)*4-1,:)),abs(imag(eiv(
53 % plotmodes(jj)*4-1,:))),Omega,linetp,'Color',color,
54 % MarkerSize',1);%, 'o','Color',[0.8500,0.3250,0.0980],'
55 % MarkerSize',3)
56 % plot3(real(eiv(plotmodes(jj)*4-3,:)),abs(imag(eiv(
57 % plotmodes(jj)*4-3,:))),Omega,linetp,'Color',color,
58 % MarkerSize',1);%, '.', 'Color',[0,0.4470,0.7410],'
59 % MarkerSize',4)
60 % plot3(real(eiv(plotmodes(jj)*4-0,:)),imag(eiv(plotmodes
61 % (jj)*4-0,:)),Omega,'.','.','Color',[0,0.4470,0.7410])
62 % plot3(real(eiv(plotmodes(jj)*4-2,:)),imag(eiv(plotmodes
63 % (jj)*4-2,:)),Omega,'.','.','Color',[0,0.4470,0.7410])
64 % r(1,:) = real(eiv(plotmodes(jj)*4-1,:));
65 % r(2,:) = real(eiv(plotmodes(jj)*4-3,:));
66 % ZeroCross1 = zci(r(1,:));
67 % ZeroCross2 = zci(r(2,:));
68 % if isempty(ZeroCross1)
69 % else
70 % strcross1 = [num2str(Omega(ZeroCross1(1)),4) '(RPM) '
71 % newline];
72 % text(ax,0,abs(imag(eiv(plotmodes(jj)*4-1,ZeroCross1(1))
73 % )),strcross1,'HorizontalAlignment','right','

```

```

    VerticalAlignment ', ' bottom ', ' FontWeight ', ' bold ');
61 % plot (ax ,0 ,abs( imag( eiv( plotmodes( jj )*4-1,ZeroCross1(1) )
62 % )) ,'*k ');
63 % end
64 % if isempty( ZeroCross2 )
65 % else
66 % strcross2 = [ num2str( Omega( ZeroCross2(1) ) ,4) ' (RPM) '
67 % newline ];
68 % text (ax ,0 ,abs( imag( eiv( plotmodes( jj )*4-3,ZeroCross2(1) )
69 % )) ,strcross2 , ' HorizontalAlignment ', ' right ', '
70 % VerticalAlignment ', ' bottom ', ' FontWeight ', ' bold ');
71 % plot (ax ,0 ,abs( imag( eiv( plotmodes( jj )*4-3,ZeroCross2(1) )
72 % )) ,'*k ');
73 % end
74 end
75 hold off
76 ax.YAxisLocation = ' origin ';
77 axis([-inf ,inf ,0 ,inf ])
78 xlabel(' Real(s) ')
79 ylabel(' Imag(s) ')
80 end

```

```

1 function Campbell(Model_obj ,Omega ,plotmodes ,ax ,linetp )
2 %CAMPBELL Summary of this function goes here
3 % Detailed explanation goes here
4 if nargin < 5
5     if nargin == 2

```

```

6      plotmodes = 1:2;
7      elseif nargin < 2
8          return
9      end
10     linetp = '_.';
11     if nargin < 4
12         ax = [];
13     end
14 end
15 for ii = 1:1:length(Omega)
16     w = Omega(ii)/60*2*pi;
17     Mnew = Model_obj.M;
18     Cnew = real(Model_obj.C) + w.*imag(Model_obj.C);
19     Knew = real(Model_obj.K) + w.*imag(Model_obj.K);
20     Zer = zeros(size(Mnew));
21     ey = eye(size(Mnew));
22     A = [-Mnew^-1*Cnew, -Mnew^-1*Knew;
23           ey, Zer];
24     v1=eig(A);
25     [~, I] = sort(abs((v1)));
26     eiv(:,ii) = v1(I);
27 % eiv(:,ii)=v1;
28 end
29 if isempty(ax)
30     figure
31     ax = axes;
32 end

```

```

33 % while min( abs( imag( eiv( 1,:) ) ) ) == 0
34 %     eiv( 1:2,: ) = [];
35 % end
36 % eiv = eiv( ~any( isnan( eiv ) | isinf( eiv ), 2 ),: );
37
38 hold on
39 for jj = 1:1:length( plotmodes )
40 plot(ax, Omega, abs(imag(eiv(plotmodes(jj)*4-2,:)))/2/pi
41 *60, 'k');%, 'Color',[0,0.4470,0.7410], 'LineWidth',1)
42 plot(ax, Omega, abs(imag(eiv(plotmodes(jj)*4,:)))/2/pi*60,
43 'k');%, 'Color',[0.8500,0.3250,0.0980], 'LineWidth',1,
44 'MarkerSize',4)
45 plot(ax, Omega, (imag(eiv(plotmodes(jj)*4-3,:)))/2/pi
46 *60, linetp, 'Color',[0,0.4470,0.7410], 'LineWidth',1)
47 plot(ax, Omega, (imag(eiv(plotmodes(jj)*4,:)))/2/pi*60, linetp,
48 'Color',[0.8500,0.3250,0.0980], 'LineWidth',1)
49 plot(ax, Omega, imag(eiv(plotmodes(jj),:))/2/pi*60, linetp,
50 'Color',[0,0.4470,0.7410], 'LineWidth',1)
51 xlabel('Spin speed [RPM]')
52 ylabel('Whirl speed [RPM]')
53 title('Campbell Diagram')

```

```
54  
55  
56 end
```

```
1 function Stability( Model_obj , Omega,ax,linetp )  
2 %STABILITY Summary of this function goes here  
3 % Detailed explanation goes here  
4 zci = @(v) find(v(:).*circshift(v(:), [-1 0]) <= 0);  
5 if nargin < 4  
6     linetp = '-';  
7     if nargin < 3  
8         figure  
9         ax = axes;  
10    elseif nargin < 2  
11        return  
12    end  
13  
14 end  
15  
16 for ii = 1:1:length(Omega)  
17     w = Omega(ii)/60*2*pi;  
18     Mnew = Model_obj.M;  
19     Cnew = real(Model_obj.C) + w.*imag(Model_obj.C);  
20     Knew = real(Model_obj.K) + w.*imag(Model_obj.K);  
21  
22     Zer = zeros(size(Mnew));  
23     ey = eye(size(Mnew));
```

```

24 A = [-Mnew^-1*Cnew, -Mnew^-1*Knew;
25     ey ,Zer ];
26 v1=eig (A);
27 eiv (:, i i ) = sort (v1);
28 end
29 while min(abs(imag(eiv(1,:)))) == 0
30     eiv (1:2,:) = [];
31 end
32 eiv = eiv(~any(isnan(eiv) | isnan(eiv), 2), :);
33 hold on
34 plot(Omega,max(real(eiv)), 'LineWidth', 1, 'LineStyle', linetp);
35 ZeroCross = Omega(zci(max(real(eiv))));
36 if ~isempty(ZeroCross)
37     strcross = [ ' Threshold: ' num2str(ZeroCross(1),4) 'RPM'
38 ];
39 text(ZeroCross(1), 0, strcross, 'HorizontalAlignment', 'left'
40       , 'VerticalAlignment', 'middle', 'FontWeight', 'bold',
41       'Rotation', 90);
42 plot(ZeroCross(1), 0, '*k');
43 hold off
44 end
45 ax.XAxisLocation = 'origin';
46 xlabel('Speed (RPM)')
47 ylabel('Maximum \Re(s)')
48 title('Stability region')
49 end

```

1 function Damping(Model\_obj, Omega, plotmodes, ax, linetp, ch)

```

2 %CAMPBELL Summary of this function goes here
3 % Detailed explanation goes here
4 zci = @(v) find(v(:).*circshift(v(:), [-1 0]) <= 0);
5
6 if nargin < 6
7     if nargin == 2
8         plotmodes = 1:2;
9     elseif nargin < 2
10        return
11    end
12    ch = 'dec';
13    if nargin < 5
14        linetp = '-';
15    end
16    if nargin < 4
17        figure
18        ax = axes;
19    end
20 end
21
22 for ii = 1:1:length(Omega)
23     w = Omega(ii)/60*2*pi;
24     Mnew = Model_obj.M;
25     Cnew = real(Model_obj.C) + w.*imag(Model_obj.C);
26     Knew = real(Model_obj.K) + w.*imag(Model_obj.K);
27
28     Zer = zeros(size(Mnew));

```

```

29    ey = eye( size(Mnew) );
30    A = [-Mnew^-1*Cnew, -Mnew^-1*Knew;
31        ey, Zer];
32    v1=eig(A);
33    [~, I] = ( sort( abs((v1)) ) );
34    eiv(:, ii) = v1((I));
35 end
36
37 while min(abs(imag(eiv(1,:)))) == 0
38     eiv(1:2,:) = [];
39 end
40 eiv = eiv(~any(isnan(eiv) | isinf(eiv), 2), :);
41
42 hold on
43 for jj = 1:length(plotmodes)
44     idf = plotmodes(jj)*4-1; %forward mode index location
45     idb = idf - 2; %backward mode index location
46     zeta = -real(eiv([idb, idf], :))/abs(eiv([idb, idf], :));
47 %     delta = 2*pi.*zeta./sqrt(1-zeta.^2); %Logarithmic
48 %     Decrement
49 %     delta = -2*pi*real(eiv([idb, idf], :))/imag(eiv([idb, idf]
50 %     ], :));
50 plot(Omega, zeta(1,:), linetp, 'Color',[0,0.4470,0.7410],
51      'LineWidth',1);
51 plot(Omega, zeta(2,:), linetp, 'Color'
52      ,[0.8500,0.3250,0.0980], 'LineWidth',1);
51 ZeroCross1 = Omega(zci(zeta(1,:)));

```

```

52 ZeroCross2 = Omega( zci( zeta( 2 ,:) ) );
53 if isempty(ZeroCross1)
54 else
55 strcross1 = [ num2str(ZeroCross1(1) ,4) newline ];
56 text(ZeroCross1(1) ,0 ,strcross1 , 'HorizontalAlignment' ,
57      'left' , 'VerticalAlignment' , 'bottom' , 'FontWeight' , 'bold'
58 );
59 plot(ZeroCross1(1) ,0 ,'*k' );
60 end
61 if isempty(ZeroCross2)
62 else
63 strcross2 = [ num2str(ZeroCross2(1) ,4) newline ];
64 text(ZeroCross2(1) ,0 ,strcross2 , 'HorizontalAlignment' ,
65      'left' , 'VerticalAlignment' , 'bottom' , 'FontWeight' , 'bold'
66 );
67 plot(ZeroCross2(1) ,0 ,'*k' );
68 end
69 hold off
70 ax.XAxisLocation = 'origin';
71 xlabel('Speed (RPM)')
72 ylabel('\zeta')
73 title('Damping Characteristics')
74
75
76
77
78
79
80
81
82
83
84
85
86
87
88
89

```

```

1 function Shape( Model_obj ,Omega ,plotmodes ,ax ,linetp )
2 %CAMPBELL Summary of this function goes here
3 % Detailed explanation goes here
4 if nargin < 5
5     if nargin < 2
6         return
7     end
8     linetp = '-';
9     if nargin < 4
10        figure
11        ax = axes;
12    end
13 end
14
15 syms x;
16 l=1;
17 z=x/l;
18 alph=.25;
19 Tt1 = (1/(1+alph))*(2*z^3 - 3*z^2 - alph*z + 1 + alph);
20 Tt2 = (1/(1+alph))*(-2*z^3+3*z^2+alph*z);
21 Tr1 = (1/(1+alph))*(z^3 - (2+1/2*alph)*z^2 + (1+1/2*alph)*z);
22 Tr2 = (1/(1+alph))*(z^3 - (1-1/2*alph)*z^2 - 1/2*alph*z);
23 cpsi = [ Tt1   0       0   Tr1   Tt2   0       0   Tr2;
24           0   Tt1   -Tr1   0       0   Tt2   -Tr2   0];
25 % psi = [1 - 3*(x/l)^2 + 2*(x/l)^3, x - 2*l*(x/l)^2 + l*(x/l)
26 %           ^3, 3*(x/l)^2 - 2*(x/l)^3, -l*(x/l)^2 + l*(x/l)^3];
26 % cpsi = [ psi(1) ,           0 ,           0 ,  psi(2) ,  psi(3) ,           0 ,

```

```

          0,  psi(4) ;
27 %      0,  psi(1), -psi(2),      0,      0,  psi(3), -psi(4),
           0];
28 ipts = 4;
29 d = (0:ipts-1)/ipts;
30 for ii = 1:1:length(d)
31     Nx(ii,:) = subs(cpsi(1,:),x,d(ii));
32     Ny(ii,:) = subs(cpsi(2,:),x,d(ii));
33 end
34 Nx = double(Nx);
35 Ny = double(Ny);
36 w = Omega/60*2*pi;
37 Mnew = Model_obj.M;
38 Cnew = real(Model_obj.C) + w.*imag(Model_obj.C);
39 Knew = real(Model_obj.K) + w.*imag(Model_obj.K);
40 nM = length(Mnew);
41
42 % Zer = zeros(nM);
43 % AA=[Cnew Mnew;Mnew Zer];
44 % B=[Knew Zer;Zer -Mnew];
45     Zer = zeros(size(Mnew));
46     ey = eye(size(Mnew));
47     A = [-Mnew^-1*Cnew, -Mnew^-1*Knew;
48           ey, Zer];
49
50 [V,D] = eig(A, 'vector');
51 % ind=find( (imag(D)>0) & (abs(D)>1e-3) );    % take

```

```

    positive frequencies only

52 % l1=D(ind);
53 % v1=V(nM+1:end ,ind );
54 l1=D;
55 v1=V(nM+1:end ,:) ;
56 % v1=V(1:nM,:) ;
57 [~, I] = sort(abs((l1)));
58 l2 = D(I);
59 v2 = V(:,I);
60 v = v2(:,plotmodes);
61 v=v/norm(v);
62 for ii = 1:1:length(Model_obj.M)/4-1
63     Li = Model_obj.npos(ii+1)-Model_obj.npos(ii);
64     Nxnew = Nx*diag([1 1 1 Li 1 1 1 Li]);
65     Nynew = Ny*diag([1 1 Li 1 1 1 Li 1]);
66     pos( ipts*(ii-1)+1:ipts*(ii-1)+ipts+1) = linspace(
67         Model_obj.npos(ii),Model_obj.npos(ii+1),ipts+1);
68     pos(end)=[];
69     shapex(ipts*(ii-1)+1:ipts*(ii-1)+ipts) = Nxnew*v(4*(ii-1)
70         +1:4*(ii-1)+8);
71     shapey(ipts*(ii-1)+1:ipts*(ii-1)+ipts) = Nynew*v(4*(ii-1)
72         +1:4*(ii-1)+8);
73 end
74 pos = [ pos , Model_obj.npos(end) ];
75 shapex = [ shapex , v(nM-3) ];
76 shapey = [ shapey , v(nM-2) ];
77 plot(ax,[ pos ; pos ]' , real([ shapex; shapey ]) ')

```

```

75 hold on
76 for ii = 1:length(Model_objnpos)
77 plot([Model_objnpos(ii); Model_objnpos(ii)]', real([
78 shapex(ipts*(ii-1)+1); shapey(ipts*(ii-1)+1)])', '.k', '
79 MarkerSize', 8)
80 end
81 hold off
82 figure
83 cpts = 20;
84 theta = linspace(0,2*pi,cpts);
85 for ii =1:length(shapex)
86 xx(:,ii)=real(shapex(ii))*cos(theta) - imag(shapex(ii))*sin(theta);
87 y(:,ii)=real(shapey(ii))*cos(theta) - imag(shapey(ii))*sin(theta);
88 end
89 N = repmat(pos,cpts,1);
90 hold on
91 plot3(real(shapex),pos,real(shapey),'-k')
92
93 plot3(xx,N,y,'Color',[0,0.4470,0.7410])
94 for ii = 1:length(Model_objnpos)
95 plot3(real(shapex(ipts*(ii-1)+1)), Model_objnpos(ii), real(
96 (shapey(ipts*(ii-1)+1)),'.k', 'MarkerSize', 8)
97 end

```

```

97 hold off
98 mx = max([ abs(shapex) ,abs(shapey)]) ;
99 axis([-mx, mx, -inf , inf ,-mx, mx ]) ;
100 disp(['Damping: ' num2str( real(12(plotmodes))) ' . Frequency:
101 ' num2str( imag(12(plotmodes))/2/pi*60) '(RPM)' ])
102 ax=gca;
103 ax.XDir='reverse';
104 ax.Title.String={(['\Re(s): ' num2str( real(12(plotmodes)),2)
105 % [V, D] = eig(Knew, Mnew, 'vector');
106 % D = sqrt(D)*60/2/pi;
107 % [D, ind] = sort(abs(D));
108 % D(plotmodes)
109 % V = V(:,ind);
110 % v2 = (V(:,plotmodes));
111 % v3 = reshape(v2,4,[]);
112 % v4 = bsxfun(@times, v3, 1./sqrt(sum(v3.^2, 2)));
113 % v2 = reshape(v4,1,[]);
114 % for ii = 1:1:length(Model_obj.M)/4-1
115 %     shape(8*(ii-1)+1:8*(ii-1)+8) = N*v2(4*(ii-1)+1:4*(ii-1)
116 %         +8);
117 % end
118 % shape = [shape, v2(end-3)];
119 % plot(real(shape))

```

```

120
121 % if isempty(ax)
122 %     figure
123 %     ax = axes;
124 % end
125 %
126 % hold on
127 % for jj = 1:1:length(plotmodes)
128 %     pv(1,:) = real(eivect(speed,[4.*(1:14)-3],plotmodes(jj))
129 % );
130 %
131 % plot(pv)
132 % end
133 %
134
135 end

```

```

1 function FreqResponse(Model_obj, Omega, node, plottype, fi,
2 linetp)
3 if nargin < 6
4     if nargin == 2
5         node = 1;
6     elseif nargin < 2
7         error('Not enough input arguments.\n Provide: Omega(
8             required), node #s(optional), axes(optional),
9             linetype(optional)', class(Model_obj))

```

```

7    end
8    linetp = '—';
9    if nargin < 5
10       fi = figure;
11       ax = axes( fi );
12       if nargin < 4
13          plottype = 'Bode';
14       end
15       if strcmp( plottype , 'Bode' ) == 1
16          ax(1)=subplot(2,1,1,ax);
17          ax(2)=subplot(2,1,2);
18       end
19    end
20
21 end
22
23 for ii = 1:1:length(Omega)
24    w = Omega( ii )/60*2*pi;
25    Fnew = w^2.* ( Model_obj.F );
26    Mnew = Model_obj.M;
27    Cnew = real( Model_obj.C ) + w.*imag( Model_obj.C );
28    Knew = real( Model_obj.K ) + w.*imag( Model_obj.K );
29    n=length(Mnew);
30    I=kron( eye(n/2) , diag([1,1i]) );
31    Z = I*(Knew + 1i*w.*Cnew - w^2.*Mnew);
32    X(ii,:)=Z^-1*Fnew;
33 end

```

```

34 switch plottype
35   case 'FreqResponse'
36     hold on
37     for jj = 1:1:length(node)
38       ax=fi.Children;
39       plot(ax, Omega,(abs(X(:,node(jj)*4-3))),linetp)
40       plot(ax, Omega,(abs(X(:,node(jj)*4-2))),linetp)
41       ax.YScale = 'log';
42     end
43     hold off
44     ax.XLabel.String='Spin Speed \Omega[RPM]';
45     ax.YLabel.String='Amplitude [m]';
46   case 'Bode'
47     hold on
48     for jj = 1:1:length(node)
49       subplot(211); hold on
50       ax(1)=fi.Children(1);
51 %       plot(Omega,abs(X(:,node(jj)*4-3)),linetp)
52 %       plot(Omega,abs(X(:,node(jj)*4-2)),linetp)
53       plot(ax(1),Omega,abs(39370.1*X(:,node(jj)*4-3)),
54             linetp)
55       plot(ax(1),Omega,abs(39370.1*X(:,node(jj)*4-2)),
56             linetp)
57       ax(1).YScale = 'log';
58       ax(1).XLabel.String='Spin Speed \Omega[RPM]';
59 %       ax(1).YLabel.String='Amplitude [m]';
60       ax(1).YLabel.String='Amplitude [ mils ]';

```

```

59 subplot(212); hold on
60 ax(2)=fi.Children(2);
61 % plot(Omega,unwrap(mod(angle(X(:,node(jj)*4-3))
62 % ,2*pi)),linetp)
63 % plot(Omega,unwrap(mod(angle(X(:,node(jj)*4-2))
64 % ,2*pi)),linetp)
65 plot(ax(2),Omega,180/pi*unwrap(mod(angle(X(:,node
66 % (jj)*4-3)),2*pi)),linetp)
67 plot(ax(2),Omega,180/pi*unwrap(mod(angle(X(:,node
68 % (jj)*4-2)),2*pi)),linetp)
69 ax(2).XLabel.String='Spin Speed \Omega[RPM]';
70 % ax.YLabel.String='Phase Angle [Rad]';
71 ax(2).YLabel.String='Phase Angle [deg.]';
72 % ax.YTick=[-3*pi/2:pi/2:0];
73 % ax.YTickLabel={'-3\pi/2','-\pi','-\pi/2','0'};
74 % ax(2).YTick=[-360:90:0];
75 % ax(2).YTickLabel={'0','-270','-180','-90','0'};
76 end
77 hold off
78
79
80
81
82
83
84
85
86
87
88
89
90
91
92
93
94
95
96
97
98
99
100
101
102
103
104
105
106
107
108
109
110
111
112
113
114
115
116
117
118
119
120
121
122
123
124
125
126
127
128
129
130
131
132
133
134
135
136
137
138
139
140
141
142
143
144
145
146
147
148
149
150
151
152
153
154
155
156
157
158
159
160
161
162
163
164
165
166
167
168
169
170
171
172
173
174
175
176
177
178
179
180
181
182
183
184
185
186
187
188
189
190
191
192
193
194
195
196
197
198
199
200
201
202
203
204
205
206
207
208
209
210
211
212
213
214
215
216
217
218
219
220
221
222
223
224
225
226
227
228
229
230
231
232
233
234
235
236
237
238
239
240
241
242
243
244
245
246
247
248
249
250
251
252
253
254
255
256
257
258
259
260
261
262
263
264
265
266
267
268
269
270
271
272
273
274
275
276
277
278
279
280
281
282
283
284
285
286
287
288
289
290
291
292
293
294
295
296
297
298
299
300
301
302
303
304
305
306
307
308
309
310
311
312
313
314
315
316
317
318
319
320
321
322
323
324
325
326
327
328
329
330
331
332
333
334
335
336
337
338
339
340
341
342
343
344
345
346
347
348
349
350
351
352
353
354
355
356
357
358
359
360
361
362
363
364
365
366
367
368
369
370
371
372
373
374
375
376
377
378
379
380
381
382
383
384
385
386
387
388
389
390
391
392
393
394
395
396
397
398
399
400
401
402
403
404
405
406
407
408
409
410
411
412
413
414
415
416
417
418
419
420
421
422
423
424
425
426
427
428
429
430
431
432
433
434
435
436
437
438
439
440
441
442
443
444
445
446
447
448
449
450
451
452
453
454
455
456
457
458
459
460
461
462
463
464
465
466
467
468
469
470
471
472
473
474
475
476
477
478
479
480
481
482
483
484
485
486
487
488
489
490
491
492
493
494
495
496
497
498
499
500
501
502
503
504
505
506
507
508
509
510
511
512
513
514
515
516
517
518
519
520
521
522
523
524
525
526
527
528
529
530
531
532
533
534
535
536
537
538
539
540
541
542
543
544
545
546
547
548
549
550
551
552
553
554
555
556
557
558
559
559
560
561
562
563
564
565
566
567
568
569
569
570
571
572
573
574
575
576
577
578
579
579
580
581
582
583
584
585
586
587
588
589
589
590
591
592
593
594
595
596
597
598
599
599
600
601
602
603
604
605
606
607
608
609
609
610
611
612
613
614
615
616
617
617
618
619
619
620
621
622
623
624
625
626
627
627
628
629
629
630
631
632
633
634
635
636
637
637
638
639
639
640
641
642
643
644
645
646
647
647
648
649
649
650
651
652
653
654
655
656
657
658
659
659
660
661
662
663
664
665
666
667
668
669
669
670
671
672
673
674
675
676
677
678
679
679
680
681
682
683
684
685
686
687
688
689
689
690
691
692
693
694
695
696
697
698
699
699
700
701
702
703
704
705
706
707
708
709
709
710
711
712
713
714
715
716
717
718
719
719
720
721
722
723
724
725
726
727
728
729
729
730
731
732
733
734
735
736
737
738
739
739
740
741
742
743
744
745
746
747
747
748
749
749
750
751
752
753
754
755
756
757
758
759
759
760
761
762
763
764
765
766
767
767
768
769
769
770
771
772
773
774
775
776
777
778
779
779
780
781
782
783
784
785
786
787
787
788
789
789
790
791
792
793
794
795
796
796
797
798
798
799
799
800
801
802
803
804
805
806
807
808
809
809
810
811
812
813
814
815
816
817
818
819
819
820
821
822
823
824
825
826
827
828
829
829
830
831
832
833
834
835
836
837
838
839
839
840
841
842
843
844
845
846
847
847
848
849
849
850
851
852
853
854
855
856
857
858
859
859
860
861
862
863
864
865
866
867
867
868
869
869
870
871
872
873
874
875
876
877
878
878
879
879
880
881
882
883
884
885
886
887
887
888
889
889
890
891
892
893
894
895
896
896
897
898
898
899
899
900
901
902
903
904
905
906
907
908
909
909
910
911
912
913
914
915
916
917
917
918
919
919
920
921
922
923
924
925
926
927
927
928
929
929
930
931
932
933
934
935
936
937
937
938
939
939
940
941
942
943
944
945
946
946
947
948
948
949
949
950
951
952
953
954
955
956
957
957
958
959
959
960
961
962
963
964
965
966
966
967
968
968
969
969
970
971
972
973
974
975
976
977
977
978
978
979
979
980
981
982
983
984
985
986
986
987
988
988
989
989
990
991
992
993
994
995
996
997
998
999
999
1000
1000
1001
1002
1003
1004
1005
1006
1007
1008
1009
1009
1010
1011
1012
1013
1014
1015
1016
1017
1017
1018
1019
1019
1020
1021
1022
1023
1024
1025
1026
1027
1027
1028
1029
1029
1030
1031
1032
1033
1034
1035
1036
1037
1037
1038
1039
1039
1040
1041
1042
1043
1044
1045
1046
1046
1047
1048
1048
1049
1049
1050
1051
1052
1053
1054
1055
1056
1057
1057
1058
1059
1059
1060
1061
1062
1063
1064
1065
1066
1066
1067
1068
1068
1069
1069
1070
1071
1072
1073
1074
1075
1075
1076
1077
1077
1078
1078
1079
1080
1081
1082
1083
1084
1085
1085
1086
1087
1087
1088
1088
1089
1089
1090
1091
1092
1093
1094
1094
1095
1096
1096
1097
1097
1098
1098
1099
1099
1100
1101
1102
1103
1104
1104
1105
1106
1106
1107
1107
1108
1109
1109
1110
1111
1112
1113
1114
1114
1115
1116
1116
1117
1117
1118
1119
1119
1120
1121
1122
1123
1124
1124
1125
1126
1126
1127
1127
1128
1129
1129
1130
1131
1132
1133
1134
1134
1135
1136
1136
1137
1137
1138
1139
1139
1140
1141
1142
1143
1144
1144
1145
1146
1146
1147
1147
1148
1149
1149
1150
1151
1152
1153
1154
1154
1155
1156
1156
1157
1157
1158
1159
1159
1160
1161
1162
1163
1164
1164
1165
1166
1166
1167
1167
1168
1169
1169
1170
1171
1172
1173
1174
1174
1175
1176
1176
1177
1177
1178
1179
1179
1180
1181
1182
1183
1184
1184
1185
1186
1186
1187
1187
1188
1189
1189
1190
1191
1192
1193
1193
1194
1195
1195
1196
1196
1197
1198
1198
1199
1199
1200
1201
1202
1203
1203
1204
1205
1205
1206
1206
1207
1208
1208
1209
1209
1210
1211
1211
1212
1213
1213
1214
1214
1215
1216
1216
1217
1217
1218
1219
1219
1220
1221
1222
1223
1224
1224
1225
1226
1226
1227
1227
1228
1229
1229
1230
1231
1232
1233
1234
1234
1235
1236
1236
1237
1237
1238
1239
1239
1240
1241
1242
1243
1244
1244
1245
1246
1246
1247
1247
1248
1249
1249
1250
1251
1252
1253
1254
1254
1255
1256
1256
1257
1257
1258
1259
1259
1260
1261
1262
1263
1264
1264
1265
1266
1266
1267
1267
1268
1269
1269
1270
1271
1272
1273
1274
1274
1275
1276
1276
1277
1277
1278
1279
1279
1280
1281
1282
1283
1284
1284
1285
1286
1286
1287
1287
1288
1289
1289
1290
1291
1292
1293
1294
1294
1295
1296
1296
1297
1297
1298
1299
1299
1300
1301
1302
1303
1303
1304
1305
1305
1306
1306
1307
1308
1308
1309
1309
1310
1311
1311
1312
1313
1313
1314
1314
1315
1316
1316
1317
1317
1318
1319
1319
1320
1321
1322
1323
1324
1324
1325
1326
1326
1327
1327
1328
1329
1329
1330
1331
1332
1333
1334
1334
1335
1336
1336
1337
1337
1338
1339
1339
1340
1341
1342
1343
1344
1344
1345
1346
1346
1347
1347
1348
1349
1349
1350
1351
1352
1353
1354
1354
1355
1356
1356
1357
1357
1358
1359
1359
1360
1361
1362
1363
1364
1364
1365
1366
1366
1367
1367
1368
1369
1369
1370
1371
1372
1373
1374
1374
1375
1376
1376
1377
1377
1378
1379
1379
1380
1381
1382
1383
1384
1384
1385
1386
1386
1387
1387
1388
1389
1389
1390
1391
1392
1393
1394
1394
1395
1396
1396
1397
1397
1398
1399
1399
1400
1401
1402
1403
1404
1404
1405
1406
1406
1407
1407
1408
1409
1409
1410
1411
1412
1413
1414
1414
1415
1416
1416
1417
1417
1418
1419
1419
1420
1421
1422
1423
1424
1424
1425
1426
1426
1427
1427
1428
1429
1429
1430
1431
1432
1433
1434
1434
1435
1436
1436
1437
1437
1438
1439
1439
1440
1441
1442
1443
1444
1444
1445
1446
1446
1447
1447
1448
1449
1449
1450
1451
1452
1453
1454
1454
1455
1456
1456
1457
1457
1458
1459
1459
1460
1461
1462
1463
1464
1464
1465
1466
1466
1467
1467
1468
1469
1469
1470
1471
1472
1473
1474
1474
1475
1476
1476
1477
1477
1478
1479
1479
1480
1481
1482
1483
1484
1484
1485
1486
1486
1487
1487
1488
1489
1489
1490
1491
1492
1493
1494
1494
1495
1496
1496
1497
1497
1498
1499
1499
1500
1501
1502
1503
1504
1504
1505
1506
1506
1507
1507
1508
1509
1509
1510
1511
1512
1513
1514
1514
1515
1516
1516
1517
1517
1518
1519
1519
1520
1521
1522
1523
1524
1524
1525
1526
1526
1527
1527
1528
1529
1529
1530
1531
1532
1533
1534
1534
1535
1536
1536
1537
1537
1538
1539
1539
1540
1541
1542
1543
1544
1544
1545
1546
1546
1547
1547
1548
1549
1549
1550
1551
1552
1553
1554
1554
1555
1556
1556
1557
1557
1558
1559
1559
1560
1561
1562
1563
1564
1564
1565
1566
1566
1567
1567
1568
1569
1569
1570
1571
1572
1573
1574
1574
1575
1576
1576
1577
1577
1578
1579
1579
1580
1581
1582
1583
1584
1584
1585
1586
1586
1587
1587
1588
1589
1589
1590
1591
1592
1593
1594
1594
1595
1596
1596
1597
1597
1598
1599
1599
1600
1601
1602
1603
1604
1604
1605
1606
1606
1607
1607
1608
1609
1609
1610
1611
1612
1613
1614
1614
1615
1616
1616
1617
1617
1618
1619
1619
1620
1621
1622
1623
1624
1624
1625
1626
1626
1627
1627
1628
1629
1629
1630
1631
1632
1633
1634
1634
1635
1636
1636
1637
1637
1638
1639
1639
1640
1641
1642
1643
1644
1644
1645
1646
1646
1647
1647
1648
1649
1649
1650
1651
1652
1653
1654
1654
1655
1656
1656
1657
1657
1658
1659
1659
1660
1661
1662
1663
1664
1664
1665
1666
1666
1667
1667
1668
1669
1669
1670
1671
1672
1673
1674
1674
1675
1676
1676
1677
1677
1678
1679
1679
1680
1681
1682
1683
1684
1684
1685
1686
1686
1687
1687
1688
1689
1689
1690
1691
1692
1693
1694
1694
1695
1696
1696
1697
1697
1698
1699
1699
1700
1701
1702
1703
1704
1704
1705
1706
1706
1707
1707
1708
1709
1709
1710
1711
1712
1713
1714
1714
1715
1716
1716
1717
1717
1718
1719
1719
1720
1721
1722
1723
1724
1724
1725
1726
1726
1727
1727
1728
1729
1729
1730
1731
1732
1733
1734
1734
1735
1736
1736
1737
1737
1738
1739
1739
1740
1741
1742
1743
1744
1744
1745
1746
1746
1747
1747
1748
1749
1749
1750
1751
1752
1753
1754
1754
1755
1756
1756
1757
1757
1758
1759
1759
1760
1761
1762
1763
1764
1764
1765
1766
1766
1767
1767
1768
1769
1769
1770
1771
1772
1773
1774
1774
1775
1776
1776
1777
1777
1778
1779
1779
1780
1781
1782
1783
1784
1784
1785
1786
1786
1787
1787
1788
1789
1789
1790
1791
1792
1793
1794
1794
1795
1796
1796
1797
1797
1798
1799
1799
1800
1801
1802
1803
1804
1804
1805
1806
1806
1807
1807
1808
1809
1809
1810
1811
1812
1813
1814
1814
1815
1816
1816
1817
1817
1818
1819
1819
1820
1821
1822
1823
1824
1824
1825
1826
1826
1827
1827
1828
1829
1829
1830
1831
1832
1833
1834
1834
1835
1836
1836
1837
1837
1838
1839
1839
1840
1841
1842
1843
1844
1844
1845
1846
1846
1847
1847
1848
1849
1849
1850
1851
1852
1853
1854
1854
1855
1856
1856
1857
1857
1858
1859
1859
1860
1861
1862
1863
1864
1864
1865
1866
1866
1867
1867
1868
1869
1869
1870
1871
1872
1873
1874
1874
1875
1876
1876
1877
1877
1878
1879
1879
1880
1881
1882
1883
1884
1884
1885
1886
1886
1887
1887
1888
1889
1889
1890
1891
1892
1893
1894
1894
1895
1896
1896
1897
1897
1898
1899
1899
1900
1901
1902
1903
1904
1904
1905
1906
1906
1907
1907
1908
1909
1909
1910
1911
1912
1913
1914
1914
1915
1916
1916
1917
1917
1918
1919
1919
1920
1921
1922
1923
1924
1924
1925
1926
1926
1927
1927
1928
1929
1929
1930
1931
1932
1933
1934
1934
1935
1936
1936
1937
1937
1938
1939
1939
1940
1941
1942
1943
1944
1944
1945
1946
1946
1947
1947
1948
1949
1949
1950
1951
1952
1953
1954
1954
1955
1956
1956
1957
1957
1958
1959
1959
1960
1961
1962
1963
1964
1964
1965
1966
1966
1967
1967
1968
1969
1969
1970
1971
1972
1973
1974
1974
1975
1976
1976
1977
1977
1978
1979
1979
1980
1981
1982
1983
1984
1984
1985
1986
1986
1987
1987
1988
1989
1989
1990
1991
1992
1993
1994
1994
1995
1996
1996
1997
1997
1998
1999
1999
2000
2001
2002
2003
2004
2004
2005
2006
2006
2007
2007
2008
2009
2009
2010
2011
2012
2013
2014
2014
2015
2016
2016
2017
2017
2018
2019
2019
2020
2021
2022
2023
2024
2024
2025
2026
2026
2027
2027
2028
2029
2029
2030
2031
2032
2033
2034
2034
2035
2036
2036
2037
2037
2038
2039
2039
2040
2041
2042
2043
2044
2044
2045
2046
2046
2047
2047
2048
2049
2049
2050
2051
2052
2053
2054
2054
2055
2056
2056
2057
2057
2058
2059
2059
2060
2061
2062
2063
2064
2064
2065
2066
2066
2067
2067
2068
2069
2069
2070
2071
2072
2073
2074
2074
2075
2076
2076
2077
2077
2078
2079
2079
2080
2081
2082
2083
2084
2084
2085
2086
2086
2087
2087
2088
2089
2089
2090
2091
2092
2093
2094
2094
2095
2096
2096
2097
2097
2098
2099
2099
2100
2101
2102
2103
2104
2104
2105
2106
2106
2107
2107
2108
2109
2109
2110
2111
2112
2113
2114
2114
2115
2116
2116
2117
2117
2118
2119
2119
2120
2121
2122
2123
2124
2124
2125
2126
2126
2127
2127
2128
2129
2129
2130
2131
2132
2133
2134
2134
2135
2136
2136
2137
2137
2138
2139
2139
2140
2141
2142
2143
2144
2144
2145
2146
2146
2147
2147
2148
2149
2149
2150
2151
2152
2153
2154
2154
2155
2156
2156
2157
2157
2158
2159
2159
21
```

```
1 | classdef RotorData < handle
```

```

2 properties
3     X %Horizontal Signal
4     Y %Vertical Signal
5     ref %Keyphasor Signal
6     Fs %Sampling Rate (Samp/Sec)
7     Fres %Frequency Resolution
8     n %filter synchronous multiplier: 1X, 2X, 3X, ... nX
9         the running speed
10    end
11 properties (SetAccess = private)
12     Zf %Total Amplitude
13     Phase %Phase
14     Amp %Property that holds X and Y amplitudes
15     Speed %RPM
16 end
17 properties (Access = private)
18     refchop %%%
19     xchop %% Organizes the data arrays into matrices
20         based on windows
21     ychop %%%
22 end
23 properties (Dependent, Access = private)
24     NW %Number of windows
25     freq %Frequency
26     nspw %Number of samples per window
27
28 end

```

```

27 methods
28
29     function obj = RotorData(x, y, r, f, fres)%Fills
30         properties with data
31             if nargin == 5
32                 obj.X = x;
33                 obj.Y = y;
34                 obj.ref = r;
35                 obj.Fs = f;
36                 obj.Fres = fres;
37             end
38         end
39         function set.X(obj, val)
40             obj.X = val;
41         end
42         function set.Y(obj, val)
43             obj.Y = val;
44         end
45         function set.ref(obj, val)
46             obj.ref = val;
47         end
48         function set.Fs(obj, val)
49             obj.Fs = val;
50             if isempty(obj.X) || isempty(obj.Y) || isempty(
51                 obj.ref) || isempty(obj.Fs) || isempty(obj.
52                 Fres)
53             else
54                 obj.update;

```

```

51         end
52     end
53     function set.Fres(obj, val)
54         obj.Fres = val;
55         if isempty(obj.X) || isempty(obj.Y) || isempty(
56             obj.ref) || isempty(obj.Fs) || isempty(obj.
57             Fres)
58     else
59         obj.update;
60     end
61 end
62 function set.n(obj, val)
63     obj.n = val;
64     if isempty(obj.X) || isempty(obj.Y) || isempty(
65         obj.ref) || isempty(obj.Fs) || isempty(obj.
66         Fres)
67     else
68         obj.update;
69     end
70 end
71 function nspw = get.nspw(obj)
72     nspw = ceil(obj.Fs/obj.Fres);
73 end
74 function freq = get.freq(obj)
75     df = obj.Fs/obj.nspw;
76     f = df*(0:obj.nspw-1);
77     Q = ceil((obj.nspw+1)/2); % M/2+1 for M even

```

```

74      fQ = df*(Q-1);
75      freq = f-fQ;
76
77      function NW = get.NW(obj)
78          NW = floor( length(obj.X)/obj.nspw); %Rounds
79              number of windows down to closest integer
80
81      end
82
83      function filter(obj)
84          disp('filtering')
85          for i = 1:1:NW
86              Fpass1 = obj.Speed(i)*obj.n/60-5; %Upper
87                  frequency of bandpass filter
88              Fpass2 = obj.Speed(i)*obj.n/60+5; %Lower
89                  frequency of bandpass filter
90
91              if i == 1
92                  h = fdesign.bandpass('N,Fp1,Fp2,Ast1,Ap,
93                  Ast2', 10, Fpass1, Fpass2, 50, .1, 50,
94                  obj.Fs);
95
96                  Hd(i) = design(h, 'ellip');
97
98                  Hd(i).persistentmemory = true;
99
100                 obj.xchop(:,i) = filter(Hd(i),obj.xchop
101                 (:,i)); %Apply filter to data
102
103                 xf = Hd(i).states;
104
105                 reset(Hd(i));
106
107                 obj.ychop(:,i) = filter(Hd(i),obj.ychop
108                 (:,i)); %|||
109
110                 yf = Hd(i).states;

```

```

94     else
95         h = fdesign.bandpass( 'N,Fp1,Fp2,Ast1,Ap,
96                               Ast2' , 10 , Fpass1 , Fpass2 , 50 , .1 , 50 ,
97                               obj.Fs) ;
98
99         Hd(i) = design(h, 'ellip') ;
100        Hd(i).persistentmemory = true ;
101        Hd(i).states = xf ;
102        obj.xchop(:, i) = filter(Hd(i), obj.xchop
103                                (:, i)); %Apply filter to data
104        xf = Hd(i).states ;
105        Hd(i).states = yf ;
106        obj.ychop(:, i) = filter(Hd(i), obj.ychop
107                                (:, i)); %|||
108        yf = Hd(i).states ;
109
110    end
111
112    end
113
114    function update(obj)
115        obj.xchop = zeros(obj.nspw, obj.NW);
116        obj.ychop = zeros(obj.nspw, obj.NW);
117        obj.refchop = zeros(obj.nspw, obj.NW);
118        obj.Speed = zeros(obj.NW, 1);
119        x = obj.X(1:obj.nspw*obj.NW);
120        y = obj.Y(1:obj.nspw*obj.NW);
121        r = obj.ref(1:obj.nspw*obj.NW);
122        obj.xchop = reshape(x, obj.nspw, obj.NW);
123        obj.ychop = reshape(y, obj.nspw, obj.NW);

```

```

117 obj.refchop = reshape(r,obj.nspw,obj.NW);
118 for i = 1:1:obj.NW
119 pp = pulseperiod(obj.refchop(:,i),obj.Fs,
120 % Tolerance',7);
121 obj.Speed(i) = 1./mean(pp)*60;
122 end
123 if ~isempty(obj.n) && ~obj.n == 0
124 filter(obj)
125 end
126
127 obj.Amp.XAmp = max(obj.xchop) - min(obj.xchop); %
    Calculates Amplitude by subtracting min and
    max from each column
128 obj.Amp.YAmp = max(obj.ychop) - min(obj.ychop); %
    Calculates Amplitude by subtracting min and
    max from each column
129 Zwin = hanning(obj.nspw, 'Periodic');
130 Z = obj.xchop + 1i*obj.ychop;
131 for i = 1:1:obj.NW
132     Z(:,i) = Zwin.*Z(:,i);
133 end
134 obj.Zf = 2*abs(fft(Z)/obj.nspw);
135 obj.Zf = fftshift(obj.Zf',2); %Shifts graph to
    center on the x axis
136
137 obj.Phase.PhaseX = zeros(obj.NW,1);
obj.Phase.PhaseY = zeros(obj.NW,1);

```

```

138     distance = .5*obj.Fs/100;
139     threshold = .5*(max(obj.refchop(:,ceil(end/2))) -
140                           mean(obj.refchop(:,ceil(end/2)))); 
141     for i = 1:1:obj.NW
142         [~, locsref] = findpeaks(obj.refchop(:,i), 'MinPeakHeight', threshold, 'MinPeakDistance',
143                                   distance);
142         [~, locsX] = findpeaks(obj.xchop(:,i), 'MinPeakProminence', 1, 'MinPeakDistance',
143                                   distance);
143         [~, locsY] = findpeaks(obj.ychop(:,i), 'MinPeakProminence', 1, 'MinPeakDistance',
143                                   distance);
144         if length(locsref) < 2 || length(locsX) < 2
145             || length(locsY) < 2
146             obj.Phase.PhaseX(i) = NaN;
146             obj.Phase.PhaseY(i) = NaN;
147         else
148             if length(locsX) ~= length(locsY)
149                 if length(locsX) < length(locsY)
150                     if abs(locsX(1) - locsY(1)) < abs
151                         (locsX(end) - locsY(end))
151                         locsY(end) = [];
152                     else
153                         locsY(1) = [];
154                     end
155                 else

```

```

156           if abs(locsX(1) - locsY(1)) < abs
157             (locsX(end) - locsY(end))
158             locsX(end) = [];
159           else
160             locsX(1) = [];
161           end
162         end
163       if locsref(1) > locsX(1) || locsref(1) >
164         locsY(1)
165         locsX(1) = [];
166         locsY(1) = [];
167       end
168       if length(locsref) > length(locsX)
169         locsref(length(locsX):end) = [];
170       end
171       phx = zeros(length(locsref)-1,1);
172       phy = zeros(length(locsref)-1,1);
173       for j = 1:1:length(locsref)-1
174         phx(j) = mod((locsX(j) - locsref(j))
175                     /(locsref(j+1) - locsref(j))*2*pi
176                     ,2*pi);
177         phy(j) = mod((locsY(j) - locsref(j))
178                     /(locsref(j+1) - locsref(j))*2*pi
179                     ,2*pi);
180       end
181       obj.Phase.PhaseX(i) = 180/mod(mean(phx)

```

```

( : ) ,2*pi);

177      obj . Phase . PhaseY( i ) = 180 / pi *mod( mean( phy
( : ) ,2*pi);

178      clear locsref locsX locsY j

179      end

180      end

181

182      end

183      function acqListener( obj , src , event )

184          obj . newData = [ event . TimeStamps , event . Data ] ' ;

185          obj . ref = [ obj . ref , event . Data( 1 , : ) ];

186          obj . X = [ obj . X , event . Data( 2 , : ) ];

187          obj . Y = [ obj . Y , event . Data( 3 , : ) ];

188          obj . update;

189

190      end

191      %Plotting functions below

192      bode( obj )

193      cascade( obj )

194      obj = downsample( obj , r )

195      orbit3( obj )

196      orbitAnimation( obj )

197      mainplot( obj )

198      end

199 end

```

1    **function** bode( obj )

```

2 figure('Name','Bode Plot')
3 subplot(211)
4 plot(obj.Speed,obj.Amp.XAmp,obj.Speed,obj.Amp.YAmp)
5 xlabel('Running Speed (RPM)');
6 ylabel('Amplitude (mils)');
7 legend('Horizontal Plane','Vertical Plane');
8 subplot(212)
9 plot(obj.Speed,obj.Phase.PhaseX,obj.Speed,obj.Phase.PhaseY)
10 xlabel('Running Speed (RPM)');
11 ylabel('Phase lag (deg.)');
12 set(gca,'ytick',-720:45:720,'YTickLabel',{ '0','45','90','135'
    , '180','225','270','315'})
13 end

```

```

1 function cascade(obj)
2 figure('name','Cascade Plot')
3 waterfall(obj.freq,obj.Speed,obj.Zf)
4 xlabel('Frequency of Vibration (Hz)');
5 ylabel('Running Speed (RPM)');
6 zlabel('Amplitude of Vibration (mils)');
7 axis([-100 100 -inf inf 0 inf])
8 end

```

```

1
2 function orbit3(obj)
3 N = length(obj.X(:));
4 F = (obj.Speed(end) - obj.Speed(1))/N*(0:N-1) + obj.Speed(1);
5 s = fix(sqrt(N));

```

```

6 Xlin = obj.X(1:s^2);
7 Ylin = obj.Y(1:s^2);
8 w = F(1:s^2);
9 x = reshape(Xlin,s,s);
10 y = reshape(Ylin,s,s);
11 o = reshape(w,s,s);
12 C = sqrt(x.^2+y.^2);
13 h = mesh(o,x,y,C);
14 axis([1000 2000 -inf inf -inf inf]);
15 xlabel('Running Speed (RPM)');
16 ylabel('Horizontal Amplitude (mils)');
17 zlabel('Vertical Amplitude (mils)');
18 h.FaceColor = 'none';
19 h.MeshStyle = 'column';
20 end

```

```

1 function orbitAnimation(obj)
2
3 distance = .5*obj.Fs/100;
4 threshold = .5*(max(obj.refchop(:,ceil(end/2))) - mean(obj.
    refchop(:,ceil(end/2))));
5 [~, loc] = findpeaks(obj.ref, 'MinPeakHeight', threshold, 'MinPeakDistance', distance);
6 pksx=obj.X(loc);
7 pksy=obj.Y(loc);
8 Fsh = obj.Fs;
9 maxlm = max(obj.X);

```

```

10 speedarray = ( obj.Speed(end)-obj.Speed(1))/length(pksy)*(0:
11   length(pksy)-1)+obj.Speed(1);
12 for i = 1:1:length(pksx)-1;
13   plot(obj.X(loc(i):loc(i+1)-fix((1/10)*(loc(i+1)-loc(i))), ...
14     ,obj.Y(loc(i):loc(i+1)-fix((1/10)*(loc(i+1)-loc(i))), ...
15     '-k',pksx(i),pksy(i),'.','markersize',15)
16   text = [ ' Running Speed: ',num2str(fix(speedarray(i)),4), ...
17     ' (RPM) '];
18   uicontrol('Style','text',...
19     'String',text,...
20     'Units','normalized',...
21     'Position',[.25 .9 0.5 .05]);
22 axis([-maxlm maxlm -maxlm maxlm]);
23 axis square
24 xlabel('Horizontal Amplitude (mils)');
25 ylabel('Vertical Amplitude (mils)');
26 % pause(1/Fsh)
27 pause
28
29 end
30 end

```